REGULATION OF POSTSYNAPTIC AMPA RECEPTOR TRAFFICKING BY MAPK PATHWAYS IN *Caenorhabditis elegans* NEURONS

by

EUNCHAN PARK

A Dissertation submitted to the

Graduate School-New Brunswick

Rutgers, The State University of New Jersey

and

The Graduate School of Biomedical Sciences

University of Medicine and Dentistry of New Jersey

In partial fulfillment of the requirements

For the degree of

Doctor of Philosophy

Graduate Program in Neuroscience

Written under the direction of

Dr. Christopher Rongo

And approved by

_____

_____

_____

_____

_____

New Brunswick, New Jersey

[January, 2008]

ABSTRACT OF THE DISSERTATION

REGULATION OF POSTSYNAPTIC AMPA RECEPTOR TRAFFICKING BY MAPK PATHWAYS IN *Caenorhabditis elegans* NEURONS

by EUNCHAN PARK

Dissertation Director:

Christopher Rongo

AMPA (a-amino-3-hydroxy-5-methyl-4-isoxazolepropionate)-type glutamate receptors mediate the majority of the rapid ongoing excitatory neurotransmission in the brain. The spatio-temporal regulation of AMPA receptor trafficking, which includes endocytosis and recycling, is a crucial process for synaptic plasticity, and is therefore important for learning and memory. Signaling cascades, including the MAPK pathways, have been implicated in the regulation of synaptic plasticity in mammals. However, little is known about the molecular mechanisms by which MAPK pathways regulate AMPA receptor trafficking. In *C. elegans*, the AMPA receptor subunit GLR-1 is trafficked to synapses within a circuit that regulate locomotion reversal. GLR-1 undergoes clathrin-dependent endocytosis, and its recycling is mediated by the PDZ protein LIN-10; mutations in *lin-10* result in the accumulation of GLR-1 in an internal compartment. From the screening of

genetic modifiers of *lin-10*, we identified mutations in *rpm-1* as an enhancer of *lin-10*. We find that RPM-1, an E3 ubiquitin ligase, negatively regulates PMK-3 (p38 MAPK) activity by decreasing upstream DLK-1(MAPKKK) levels, and that PMK-3 is involved in clathrin-dependent/RAB-5-mediated endocytosis of GLR-1. However, intriguingly, the loss of function mutations of two known components of PMK-3 pathways, *dlk-1(mapkkk)* and *mkk-4 (mapkk)*, do not suppress GLR-1 accumulation, unlike the mutations of *pmk-3*. By examining other known MAPKKs in *C. elegans*, we find that mutations in *jkk-1* suppress the GLR-1 accumulation in *lin-10* mutants, similar to mutations in *pmk-3*. Moreover, we find that mutations in *sek-1*, another MAPKK, result in the accumulation of GLR-1. Finally, by examining the orthologs of Ras family protein known to function upstream of MAPK pathways in mammals, we find that RAP-1 regulates GLR-1 trafficking. Taken together, our results suggest that multiple MAPK pathways regulate AMPA receptor trafficking, sometimes with opposite outcomes. Moreover, our results indicate that there is crosstalk between MAPK pathways, and that factors like RPM-1 act to regulate such crosstalk.

ACKNOWLEDGEMENTS

First of all, I would like to thank God for leading me to here.

I would like to express my deep and sincere gratitude to my advisor, Dr. Christopher Rongo, for his constructive and detailed comments, and for his important support throughout this work.

I would like to express my sincere thanks to my committee, Drs. Bonnie Firestein, Monica Dricoll, Richard Padgett, and Andrew Singson, for their advice and detailed review during the preparation of this thesis.

I would like to thank the Rongo lab members, Doreen Glodowski, Lesley Emtage, Larry Kramer, Reem Hussein, Daiying Chen, Piya Ghose, Gang Liu, Peter Murr, Nora Isaac, Tohru Umemura, Henry Schaefer, Jaegal Shim, Howard Chang, John Lee, and Tricia Wright, for their discussions and help with my work.

I would like to thank my family, my father, my brother, my sister, my father-in-law, and my mother-in-law, for their prayer.

I owe my loving thanks to my wife Hyoung Keun, my daughter Yewon. Without their encouragement and understanding, it would have been impossible for me to finish this work.

DEDICATION

To my father, Rae Ho Park who waited so long for this, my wife, Hyoung Keun whose loving company kept me going, my daughter, Yewon who always smiles my fatigue away, and my mother in heaven, In Sook Yoon whose eternal love and support I feel in my heart and always will...

.

TABLE OF CONTENTS

CHAPTER I

INTRODUCTION

Synaptic Plasticity and AMPA receptor

Dynamic modifications in the efficacy of excitatory synaptic transmission, termed synaptic plasticity, are required for learning and memory, and the development of the brain. Two types of synaptic plasticity have been defined based on their spatial and temporal scale. Hebbian (or associative) forms of plasticity, such as long-term potentiation (LTP) and long-term depression (LTD), are rapid and synapse-specific, whereas homeostatic plasticity, as exemplified by synaptic scaling and the alteration of the threshold for inducing LTP/LTD (or metaplasticity), proceeds over long times periods (Perez-Otano and Ehlers, 2005; Turrigiano and Nelson, 2004). The strength of individual synapses can be modified by Hebbian forms of plasticity. However, Hebbian forms of plasticity tend to destabilize neuronal networks over time if unrestrained potentiation or depression persists (Moser et al., 1998). Therefore, homeostatic forms of plasticity are required to maintain the neuronal network's strength within a functional dynamic range by scaling up or down all synaptic inputs, or altering the threshold for Hebbian forms of plasticity (Abraham and Tate, 1997; Turrigiano et al., 1998; Turrigiano and Nelson, 2004).

AMPA-type glutamate receptors (AMPA receptors) mediate the majority of the rapid ongoing excitatory synaptic transmission in basal neural activity; therefore, they are important for synaptic strength (Isaac et al., 1995; Liao et al., 1995). The trafficking of AMPA receptors is important to regulate both Hebbian forms and homeostatic plasticity (Bredt and Nicoll, 2003; Malenka and Bear, 2004; Malinow and Malenka, 2002; Shepherd et al., 2006; Turrigiano and Nelson, 2004; Wierenga et al., 2005).

Trafficking of AMPA Receptors from Synthesis to Target Membrane (Synapses)

There are four subunits of AMPA receptors: GluR1, GluR2, GluR3, and GluR4. GluR1 or GluR3 always possess long- or short-cytoplasmic C-terminal tails, respectively, but the tails of GluR2 and GluR4 can exist as either long or short forms because of alternative splicing (Bredt and Nicoll, 2003). These subunits are assembled in the ER as heterotetramers to form functional AMPA receptors. In mature hippocampal neurons, the receptors are mainly composed of GluR1/2 (or 4) or GluR2/3 combinations (Bredt and Nicoll, 2003; Wenthold et al., 1996). Interestingly, GluR1/2 heteromers exit the ER rapidly, and traffic to the Golgi compartment, whereas GluR2/3 heteromers are retained longer in the ER. The fact that the ER chaperone BiP extensively colocalizes with GluR2 may explain why there is a delayed retention time of GluR2/3 compared with GluR1/2 because GluR2 in the ER mostly forms a complex with GluR3 rather than GluR1(Greger et al., 2002). SAP97 interacts with a PDZ motif of immature GluR1 while the receptor is still in the ER (Sans et al., 2001). In addition, the PDZ motif protein PICK1, which is known to bind protein kinase C alpha (PKC alpha), is necessary for GluR2 exit from the ER (Dev et al., 1999; Perez et al., 2001; Xia et al., 1999).

Because AMPA receptors are mainly synthesized in the neuronal cell body, they must migrate significant distances to reach their membrane targets. Therefore, for the dendritic transport of AMPA receptors, the activity of motor proteins and the proteins that link AMPA receptors to these motors along the microtubular cytoskeleton are required. Glutamate Receptor Interacting Protein 1/AMPAR Binding Protein (GRIP1/ABP) is a PDZ protein which interacts with the heavy chain of kinesin and binds

to GluR2 and GluR3 via their PDZ motifs. Liprin-α interacts with GRIP/ABP and a kinesin family member, KIF1 (Shin et al., 2003; Wyszynski et al., 2002). GIT1, a multidomain protein with GTPase-activating protein activity for the ADP-ribosylation factor family of small GTPases, interact directly with Liprin-α to form a complex of GIT1-liprin-α-AMPAR–GRIP1 in the brain (Kim et al., 2003; Ko et al., 2003). Interestingly, the cargo proteins sometimes decide the direction of a particular kinesin traveling along a microtubule. For example, the GluR2 interacting protein GRIP1 can direct KIF5 (kinesin1) to dendrites, whereas JSAP1, another kinesin- binding protein, guides KIF5 to axons (Setou et al., 2002).

Since dendritic spines are rich in filamentous actin (F-actin) but lack microtubules, receptors must shift from microtubular tracks to the actin-based cytoskeleton for their final delivery into synapses. A possible adaptor between AMPA receptors and the actin cytoskeleton is protein 4.1. The neuronal isoform 4.1N interacts directly with GluR1 through the juxtamembrane region of its cytoplasmic C-terminal tail (Shen et al., 2000). Upon the arrival at spines, AMPA receptors should be properly inserted at synaptic target membranes for their function. There are two pathways for such AMPA receptor insertion into the synaptic target: a constitutive (continuously cycle in and out of synapses) and a regulated pathway (incorporation to synapses in an activity-dependent manner during plasticity). Receptors with short tails, such as GluR2/3, follow the constitutive pathway (Passafaro et al., 2001; Shi et al., 2001), whereas those with long tails , such as GluR1/2L (or 4), are inserted into the synapses through the regulated pathway (Esteban et al., 2003; Hayashi et al., 2000; Zhu et al., 2000). Therefore, distinct sets of proteins have been identified based on the subunit composition. For

example, GluR2 and GluR3 C-termini bind GRIP/ABP and PICK1. The GluR2 C-terminus also binds to NSF (N-ethylmaleimide-sensitive fusion protein) (Osten et al., 1998; Song et al., 1998) and to the clathrin adaptor AP2 (Lee et al., 2002). The C-terminus of GluR1 binds SAP97 (Synapse-Associated Protein-97), and the C-termini of GluR1 and GluR4 bind the cytoskeletal protein 4.1N (Coleman et al., 2003; Shen et al., 2000). Recently, a family of transmembrane AMPAR regulatory proteins (TARPs) including stargazin, have been identified as being involved in the targeting of AMPA receptors to the synapse. Stargazin overexpression increases the number of extrasynaptic AMPARs. Though Post- synaptic density (PSD)-95 cannot bind to AMPA receptors, it can bind to stargazin, and its overexpression enhances AMPAR-mediated synaptic responses. Therefore, these observations indicate that stargazin may mediate AMPA receptor binding to PSD-95 and also suggest that PSD-95 or related PDZ proteins along with TARPs participate in the synaptic targeting of AMPARs in many neuronal types (Bredt and Nicoll, 2003).

Endocytosis / Recycling of AMPA Receptors

The constitutive cycling of AMPA receptors (the constitutive pathway), mainly GluR2/3, would serve to maintain synaptic strength despite protein turnover, and it might act in a relatively fast manner. In contrast, the regulated pathway might act transiently upon synaptic plasticity induction, leading to LTP. In the regulated pathway, internalization of AMPA receptors can be initiated either by glutamate binding or by activation of other postsynaptic receptors like NMDA or insulin receptors (Beattie et al., 2000; Lin et al.,

2000). AMPA receptor activation without NMDA receptor stimulation results in the receptor degradation; in contrast, NMDA receptor alone or concurrent NMDA/AMPA receptors activation induces recycling of AMPA receptors (Ehlers, 2000b).

Phosphorylation of AMPA receptors is important for LTP and LTD, and therefore for receptor insertion and as well as internalization. There are at least twelve phosphorylation sites in AMPA receptors (Barria et al., 1997; Carvalho et al., 1999; Chung et al., 2000; Mammen et al., 1997; Matsuda et al., 1999; Roche et al., 1996). PKA, PKC, and Ca2+/calmodulin-dependent protein kinase II (CaMKII) are known to be involved in the phosphorylation of AMPA receptors (Song and Huganir, 2002). CaMKII plays a role in LTP by phosphorylating GluR1 subunits at Serine 831 (Lee et al., 2000). Recent studies have revealed that phosphorylation of GluR1 subunits at serine 845 by PKA increases cell-surface expression of AMPA receptors by increasing insertion and decreasing internalization of these receptors. Also, dephosphorylation serine by LTD-inducing NMDA activity increases receptor internalization (Man et al., 2007). Serine 880 of GluR2 is implicated in the interaction of GRIP1 with PICK1, scaffolding protein. Increased phosphorylation of GluR2 at Serine 880 by PKC is observed after LTD induction (Chung et al., 2000; Kim et al., 2001; Malinow and Malenka, 2002; Matsuda et al., 1999).

AMPA receptor endocytosis is regulated by calcium influx through the activation NMDA receptors. Calcineurin (PP2B), clathrin adaptor protein AP-2 stimulation, and PICK1 are known to regulate endocytosis of AMPA receptor through sensing Ca^{2+} from NMDA receptor activation (Beattie et al., 2000; Ehlers, 2000b; Hanley and Henley, 2005; Palmer et al., 2005). Neep21 acts as a sorting protein on early

endosomes that directs AMPA receptors to recycling endosomes through the activity-dependent interaction with GRIP1, which interacts with GluR2 (Alberi et al., 2005; Steiner et al., 2005; Steiner et al., 2002).

Recently, Lu *et al.* demonstrated that an endocytic zone (EZ) is closely localized to the PSD through a physical interaction between the postsynaptic adaptor protein Homer and dynamin-3. Binding of the Dynamin-3-Homer complex to Shank, a PSD scaffold protein, couples the endocytic apparatus to the PSD. This indicates that proximal localization of endocytosis and presumably the recycling machinery together with the PSD acts to retain AMPA receptors in the vicinity of PSD to keep them from drifting away by lateral membrane diffusion (Lu et al., 2007).

Recycling endosomes function as intracellular buffering storage, which supply AMPA receptors for the potentiation of synapses during activity-dependent plasticity. Ehlers and his colleagues found that blocking transport from recycling endosomes reduces the basal level of surface AMPA receptor, and also disrupts the NMDA receptor-dependent delivery of AMPA receptors to the postsynaptic membrane (Park et al., 2004). Rab proteins are also implicated in the activity- dependent synaptic abundance of AMPA receptors in the membrane. Disrupting postsynaptic Rab8, which is known to be involved in trafficking cargo from the TGN to cell surface, and Rab11, a component of the recycling endosome , by expressing dominant-negative versions prevents activity-induced insertion of synaptic molecules into the plasma membrane (Gerges et al., 2004; Gerges et al., 2005; Park et al., 2004; Ullrich et al., 1996).

Rab5 is involved in clathrin dependent endocytosis (Horiuchi et al., 1995; van Delft et al., 1997). Overexpression of Rab5 in neurons, where it localizes to the perimeter

of the PSD as a GTP-bound (active) form after NMDA stimulation, increases endocyosis of AMPA receptors (Brown et al., 2005). However, the endosomal machinery and the intracellular signals that regulate the intracellular AMPA receptors have not been well understood.

Clathrin-Independent AMPA Receptor Trafficking

Endocytosis can also proceed in clathrin-independent pathways. For example, lipid rafts, which are lipid microdomains composed of cholesterol, glycosphingolipids, sphingomyelin, and long-chain unsaturated phospholipids, are known to be responsible for clathrin-independent internalization of plasma membrane proteins (Nichols, 2003).

In cultured hippocampal neurons, lipid rafts are found abundantly in dendrites. Treatment of inhibitors of sphingolipid and cholesterol synthesis for 5-7 days decreases surface AMPA receptors and dendritic spines. Therefore, this result suggests that cholesterol/sphingolipid enriched lipid rafts might function in stabilizing synaptic AMPA receptors (Hering et al., 2003). PSD-95 proteins are associated with lipid rafts (Wong and Schlichter, 2004). However, the roles and mechanisms behind clathrin-indepedent internalization of AMPA receptors are largely unknown.

Ubiquitination and AMPA Receptor Trafficking: Mammals

Ubiquitin, a 76 amino acid polypeptide, is sequentially attached to Lysine residues of target substrates by an E1 ubiquitin activating enzyme, E2 ubiquitin conjugating enzyme,

and E3 ubiquitin ligases and this process, called ubiquitination, is tightly regulated. Of these enzymes for ubiquitination, E3 ubiquitin ligases specifically recognize and directly bind to their substrates and therefore play a key role in modulating the ubiquitination system (DiAntonio and Hicke, 2004). There are four major classes in E3 ubiqutin ligases, HECT domain, RING finger, PHD, and U box (DiAntonio and Hicke, 2004; Pickart, 2001). The HECT domain ubiquitin ligases directly catalyze ubiquitination of substrates by forming a thioester bond with ubiquitin. In contrast, the RING finger, PHD, and U box ubiquitin ligases promote ubiquitination by binding both of the substrate and an E2 ubiquitin conjugating enzyme simultaneously (Huang et al., 1999; Huibregtse et al., 1995; Joazeiro and Weissman, 2000). The conjugation of ubiquitin to a target protein can be achieved by either a single moiety addition (monoubiquination) or polymeric ubiquitin chain addition (polyubiquitination). Mono-ubiquitination is known to regulate protein-protein interactions and protein functions like phosphorylation. By contrast, the Lys48-linked polyubiquitination is known to regulate protein degradation by the 26S proteasome, and the Lys63-linked polyubiquitination mediates other cellular processes (e.g., DNA repair, signal transduction, and endocytosis) (DiAntonio and Hicke, 2004; Glickman and Ciechanover, 2002; Hicke and Dunn, 2003; Hoege et al., 2002; Muratani and Tansey, 2003; Schnell and Hicke, 2003).

Ligands binding to AMPA receptors cause endocytosed receptors to be sorted to late endosomes or lysosomes for degradation, whereas NMDA receptor activation alone leads to AMPA receptor recycling through Ca^{2+}-dependent mechanisms (Ehlers, 2000b). However, in some instances, activity dependent AMPA receptor endocytosis/recycling is also sensitive to proteasomal activity (Colledge et al., 2003; Patrick et al., 2003). Direct

ubiquitination of AMPA receptors in mammals has not been reported. Rather, AMPA receptor internalization by the ubiquitination-mediated degradation of PSD-95, a major scaffolding protein of the postsynaptic density, has been reported (Bingol and Schuman, 2004; Colledge et al., 2003).

MAPK Signal Transduction Pathways and AMPA Receptor Trafficking

The mitogen-activated protein kinase (MAPK) signaling pathways have been studied extensively in synaptic plasticity (Gu and Stornetta, 2007; Haddad, 2005; Thomas and Huganir, 2004). In hippocampal neurons, Ras family proteins, Ras and Rap1, reside upstream of the different MAPK pathways and regulate AMPA receptor trafficking in opposite ways. Upon activation by synaptic activity and NMDA receptor activation, Ras stimulates the extracellular signal-regulated kinase (Erk) 1/2 MAPK cascade to insert AMPA receptors at synapses (LTP), whereas Rap1 triggers the p38 MAPK cascade to remove AMPA receptor from synapses (LTD) (Zhu et al., 2002). Interestingly, the same group also identified that selection of the downstream signaling pathways of Ras depends on the levels of neural activity (e.g., low level for spontaneous neural activity in sleeping animals, high level for the neural activity accompanying neuromodulator (e.g., histamine) release in awake animal). Low levels of activity stimulate the Ras-Erk pathway to induce GluR2L-mediated synaptic insertion of receptors. By contrast, high levels of neural activity additionally stimulate the Ras-PI3K pathway to induce GluR1-mediated synaptic insertion of receptors (Qin et al., 2005).

Ras-Guanine nucleotide-releasing factor (GRF) 2 and Ras-GRF1 activate Ras and Rap1, respectively, mediating NMDA receptor NR2B dependent p38 activation for LTD. Ras-GRF2 mediates NMDA receptors NR2A-dependent Erk1/2 activation for LTP (Li et al., 2006a). Interestingly, exposure of the Ras-GRF1/2 double knockout adolescent mice to an enriched environment (larger cages that include various toys for voluntary physical activities) rescues LTP induction through cAMP mediated p38 activation, implicating p38 MAPK in LTP induction (Li et al., 2006b).

Synaptic Ras GTPase activating protein (GAP) SynGAP is selectively associated with NR2B-containing NMDA receptors in brain, and is required for the inhibition of NMDAR-dependent Erk1/2 activity (Kim et al., 2005). Overexpression of SynGAP results in the loss of synaptic AMPA receptor expression through the regulation of the MAPK pathway, including both the activation of the p38 MAPK pathway and the suppression of the Erk1/2 pathway (Rumbaugh et al., 2006). Moreover, synaptic removal of the long cytoplasmic tail containing AMPA receptors (GluR1 and GluR2L) is important for the depotentiation process. This activity-dependent process is controlled by a Rap2-JNK signaling pathway, which consists of several molecules, including NR2A-containing NMDA receptors (Zhu et al., 2005). The influx of calcium into neurons during the synaptic activity leads to the activation of calcium/calmodulin-regulated phosphatase (calcineurin), which in turn activates myocyte enhancer factor (MEF) 2A,D transcription factors by dephosphorylation. When MEF2 is activated, the number of excitatory synapses decreases. Interestingly, reduction of MEF2 gene by shRNA causes reduction in the mRNA levels of synGAP, implicating MEF2 as a

contributing factor in LTD possibly by regulating the expression of synGAP (Flavell et al., 2006).

LTD induction can also be achieved through metabotropic glutamate receptors (mGluR)-mediated pathways. Activation of the group I mGluR by agonist treatment triggers Rap1-P38 MAPK cascades for inducing LTD in hippocampal neurons (Huang et al., 2004; Rush et al., 2002). Erk1/2 also mediates the group I mGluR dependent LTD induction in hippocampal neurons(Gallagher et al., 2004) and in cerebellar Purkinje cells (Kawasaki et al., 1999a). Summary of these findings are shown in the Figure 1-1,1-2.

Caenorhabditis elegans Glutamate Receptors

Subunits of *C. elegans* Glutamate Receptors

C. elegans has ten putative iGluR subunits. These include eight subunits most similar to the non-NMDA class (GLR-1–GLR-8) and two that belong to the NMDA class (NMR-1 and NMR-2)(Brockie et al., 2001). The large number of receptor subunits suggests that *C. elegans* also expresses a diverse number of hetero-oligomeric ionotropic glutamate receptors. By the expression of the GFP fusion constructs, neurons that express these subunits have been identified. NMR-1,2 (NMDA type) and GLR-1,2,4,5 (non-NMDA type) are expressed in many of the command interneurons such as AVA, AVB, AVC, AVD, AVE, and PVC. GLR-3 and GLR-6 are expressed in the RIA neurons. GLR-7 and GLR-8 are expressed in pharyngeal nervous system. GLR-8 is also expressed in the PLM neurons (Brockie et al., 2001; Hart et al., 1995; Maricq et al., 1995). Among these, GLR-1 and GLR-2, which are homologous to mammalian AMPA receptors, are expressed in overlapping sets of interneurons to form sensory-interneuron and

inter-interneuron synapses (Brockie et al., 2001; Hart et al., 1995; Maricq et al., 1995; Rongo and Kaplan, 1999).

C. elegans AMPA Receptor and Locomotion

Locomotory control circuits were initially identified by laser ablation experiments: AVB and PVC control forward movement, and AVA, AVD, and AVE control backward movement (Chalfie et al., 1985). These command interneurons, except for PVC, make synapses with the presynaptic sensory neurons ASH (White ea al, 1986), which releases glutamate to synapses (Berger et al., 1998). ASH-to-interneuron synapses aversively respond to nose touch through GLR-1; therefore, *glr-1* null mutants have nose-touch mechanosensory defect (Hart et al., 1995; Rongo et al., 1998). *glr-2* null mutants also show a nose-touch mechanosensory defect, although the magnitude of the defects is less severe than *glr-1* null mutants (Mellem et al., 2002).

The homeodomain protein UNC-42 is required for GLR-1 expression in the subsets of command neurons that are responsible for backward movement (AVA, AVD, and AVE). Neurons from these *unc-42* mutants exhibit axon guidance defects. While wild type animals move backward upon anterior tactile stimulation, these mutants move forward (Baran et al., 1999; Brockie et al., 2001). Moreover, the duration of forward movement is longer in *glr-1* null mutants, while shorter in *glr-1* lurcher (expressing a leaky channel) mutants than in wild type animals (Brockie et al., 2001; Glodowski et al., 2007; Mellem et al., 2002; Zheng et al., 1999b). Therefore, the testing of behaviors mediated by the GLR-1 dependent neural circuits is useful means to assay the GLR-1 synaptic activity in *C. elegans.*

C. elegans AMPA Receptor Subunits Can Exist As Homomers or Heteromers

glr-1 and *glr-2* double mutants exhibit similar nose-touch mechanosensory defects as observed in *glr-1* nulls. Also, GLR-1 and GLR-2 subunits tagged with different fluorescent markers are found to both colocalize and exist independently, suggesting GLR-1 can form both hetermeric and homomeric channel (Mellem et al., 2002). Our lab has found that in the absence of endogenous subunits, overexpressed GLR-1 or GLR-2 subunits exist as homomers *in vivo* (Chang and Rongo, 2005).

GLR-1::GFP for Studying GLR-1 Trafficking

GLR-1::GFP chimeras are a very useful marker to follow GLR-1 *in vivo*. GLR-1::GFP localizes to the ventral cord as punctate structures. Alignment of the puncta with presynpatic markers indicates that GLR-1::GFP are localized at synapses and this fusion construct rescues nose touch defects of *glr-1* null mutants, suggesting GLR-1::GFP can form functional channels on synapses (Rongo et al., 1998).

Caenorhabditis elegans AMPA Receptor (GLR-1) Trafficking

Ligand binding and the UPR are needed to exit the ER

For proper synaptic function, the sorting process of receptor proteins in the endoplasmic reticulum (ER) is important. Mutations in GLR-1 that disrupt ligand binding or ion permeability decrease dramatically the level of GLR-1 in neurites, but increase retention of GLR-1 in the ER (Grunwald and Kaplan, 2003). The Unfolded Protein Response (UPR) has a specialized role in GLR-1 trafficking, separate from its role in the ER.

Mutations in components of the UPR signaling pathway, *ire-1* and *xbp-1*, homologues of mammalian IRE1 and XBP1, prevent GLR-1::GFP exit from ER (Shim et al., 2004).

Endocytosis by Clathrin and Receptor Ubiquitination

GLR-1 endocytosis is regulated by clathrin and ubiquitination. Either mutations of clathrin adaptin protein AP180 (UNC-11) or mutations of ubiquitination sites in the GLR-1 cytosolic tail region increase the size of GLR-1:GFP puncta along the ventral nerve cord, and the effect of both mutations is not additive. Overexpression of ubiquitin by the *glr-1* promoter decreases the level of GLR-1::GFP in the neurites. However, GLR-1::GFP puncta amplitude is not changed in *unc-11* mutants by overexpression of ubiquitin. Taken together, these results suggest that UNC-11 and ubiquitination of GLR-1 act together in GLR-1 endocytosis (Burbea et al., 2002).

Recycling of GLR-1 by LIN-10 and RAB-10

LIN-10, a PDZ domain containing protein, functions in GLR-1 localization. In *lin-10* mutant animals, GLR-1::GFP form large accretions. Also, *lin-10* mutants are nose touch defective like *glr-1* null mutants. These results suggest that synaptic GLR-1 levels are reduced and that the accumulation GLR-1::GFP in *lin-10* mutants might be at an intracellular compartment and/or extrasynaptic area. However, a complete mechanistic explanation of LIN-10 function in GLR-1 localization is not clear (Rongo et al., 1998). RAB-10, a small GTPase required for endocytic recycling of intestinal cargo, regulates GLR-1 abundance. Mutant animals are similar in phenotype to *lin-10* mutants. Both *lin-10* and *rab-10* display a decreased frequency of reversals in locomotion, indicating

that the accumulation of GLR-1 might be in endosomal compartments, with the depletion of synaptic GLR-1. *lin-10* and *rab-10* double mutants show larger accumulation of GLR-1 than each of these single mutants, suggesting that *lin-10* and *rab-10* act in parallel pathways. Interestingly, blockade of clathrin-dependent endocytosis by *unc-11* (AP180) or *itsn-1* (Intersectin1) mutations suppresses the *lin-10* but not *rab-10* GLR-1 localization defects, suggesting that the function of LIN-10 occurs downstream of clathrin-dependent endocytosis. By contrast, blocking clathrin-independent endocytosis by depletion of cholesterol suppresses *rab-10* but not *lin-10* GLR-1 localization defects. Taken together, these results suggest that LIN-10 functions after clathrin-dependent endocytosis, whereas RAB-10 functions after clathrin-independent endocytosis (Glodowski et al., 2007).

The Role of E3 Ligases on GLR-1 Trafficking

Mutant worms for subunits of the anaphase promoting complex (APC), a multisubunit E3 ubiquitin ligase, also show accumulation of GLR-1 in the ventral nerve cord. Preventing clathrin-dependent endocytosis blocks the effect of the APC mutations, suggesting that the APC regulates endocytosis or recycling of GLR-1 (Juo and Kaplan, 2004).

LIN-23, the substrate binding subunit of a Skp1/Cullin/F Box (SCF) ubiquitin ligase, regulates the abundance of GLR-1 in neurites. SCF^{LIN-23} ligase does not directly ubiquinate GLR-1 itself. Instead, the increase of GLR-1 in *lin-23* mutant animals is attributable to the regulation of SCF^{LIN-23} ligase of a cytosolic pool of β-catenin BAR-1 that regulates the transcription of Wnt target genes to change postsynaptic properties (Dreier et al., 2005).

The neuronal protein KEL-8, a BTB-Kelch protein, was found to be required for the ubiquitin-mediated turnover of GLR-1 subunits in interneurons. Mutant animals for *kel-8* accumulate GLR-1 in their neurites and show an increased frequency of spontaneous reversals in behavior, suggesting that synaptic GLR-1 levels are increased. KEL-8 binds to CUL-3, a Cullin 3 ubiquitin ligase subunit that also regulates GLR-1 abundance. Therefore, all these findings indicate that KEL-8 is a substrate binding domain for Cullin 3 ubiquitin ligases that is required for GLR-1 receptor turnover (Schaefer and Rongo, 2006).

The Role of Synaptic Activity on GLR-1 trafficking

Calcium-calmodulin dependent protein kinase II (CaMK II) is activated by the calcium influx during synaptic activity and is required for the homeostatic control of synaptic GLR-1 receptor during growth. CaMK II loss-of-function mutants accumulate GLR-1::GFP in cell bodies, with a reduction in GLR-1 puncta density along the ventral cord. However, a gain of function mutation (a mutation that causes constitutively active CaMKII) does not affect receptor trafficking, although it reduces the number of GLR-1 synapses. These findings suggest that CaMKII is required during development for maintaining of GLR-1 synapses by regulation of receptor trafficking from cell bodies. Once the normal synaptic density has been established, CaMKII may function at synapses to regulate GLR-1 density (Rongo and Kaplan, 1999).

Worms lacking a vesicular glutamate transporter (VGLUT; *eat-4*) show accumulation of GLR-1 in the ventral nerve cord. The amplitude of glutamate-evoked currents in the ventral cord interneurons is increased in *eat-4* mutants compared with

wild-type controls. Blocking clathrin-mediated endocytosis occludes the effects of *eat-4* mutants. By contrast, mutations of ubiquitination sites in the GLR-1 cytoplasmic domain did not prevent increased GLR-1 level in the mutants (Grunwald et al., 2004).

Identifying Proteins Involved in *C. elegans* AMPA Receptor (GLR-1) Trafficking

The spatio-temporal regulation of AMPA receptor trafficking, which includes endocytosis and recycling, is a crucial mechanism for synaptic plasticity. Signaling cascades, including MAPK signaling pathways, have been implicated in the modulation of synaptic plasticity. However, little is known as to how the components of the signaling cascades regulate AMPA receptor trafficking, and whether there are interactions and crosstalk between these complex signaling cascades. To address this question, we have employed both forward and reverse genetic approaches to identify regulators of GLR-1 trafficking. We have found that: First, by forward genetic approach, RPM-1, an E3 ubiquitin ligase, negatively regulates DLK-1 (MAPK kinase kinase) levels in PMK-3 (p38 MAPK) pathway and PMK-3, in turn, regulates clathrin-dependent endocytosis of AMPA receptors in *C. elegans* (chapter II and III). Second, as by a reverse genetic approach, we have found that MAPKKs, JKK-1 and SEK-1 function in AMPA receptor trafficking. Moreover, we found that RAP-1(Rap1) might function upstream of PMK-3 to regulate AMPA receptor trafficking in *C. elegans* (chapter IV).

FIGURES

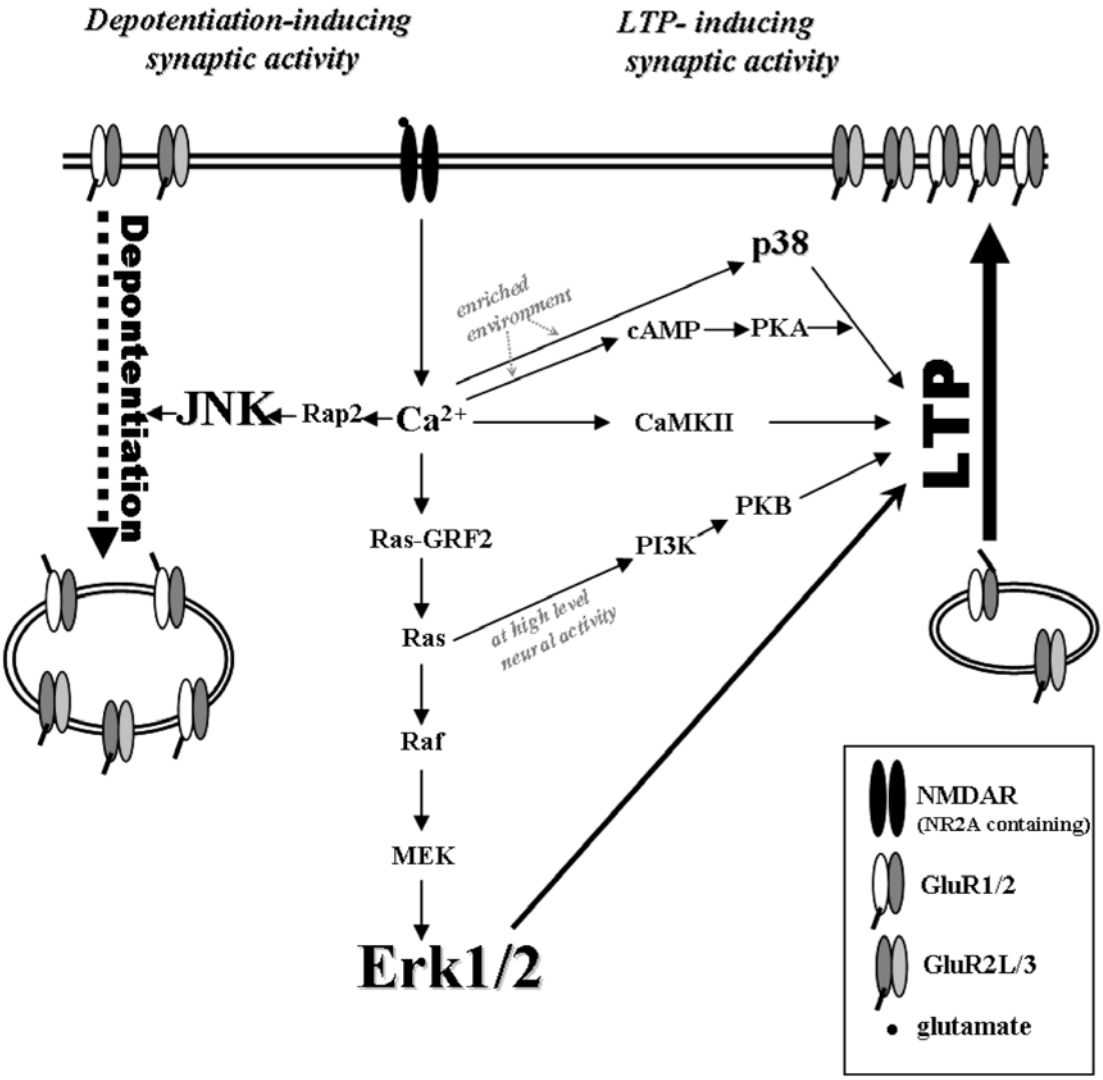

Figure 1-1. Involvement of MAPKs for the AMPA receptors trafficking during LTP or depontentiation.

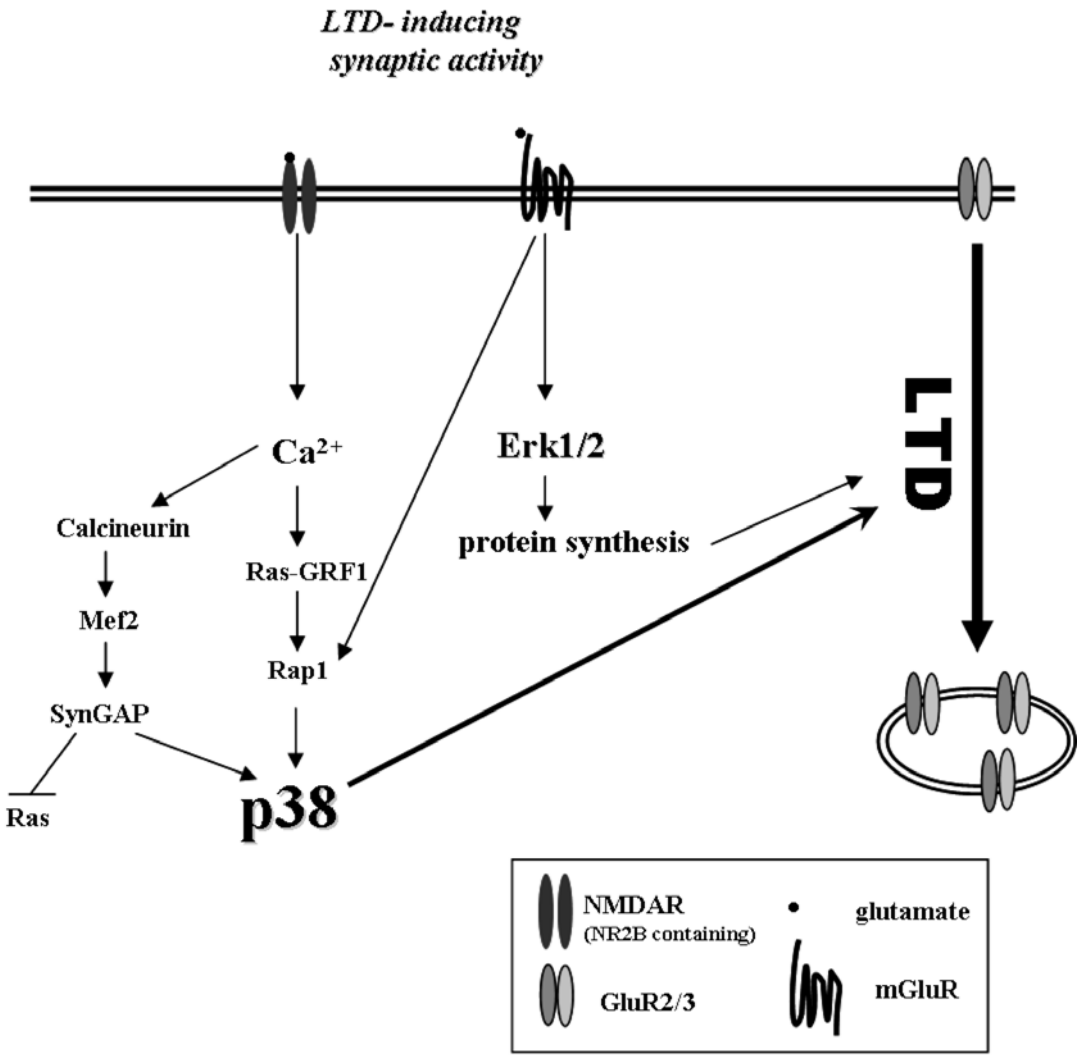

Figure 1-2. Involvement of MAPKs for the AMPA receptors trafficking during LTD.

CHAPTER II

A GENETIC SCREEN FOR SUPPRESSORS AND ENHANCERS OF THE GLR-1 LOCALIZATION DEFECTS IN *lin-10* MUTANTS

ABSTRACT

In *lin-10* mutant neurons, GLR-1 is diffusely distributed throughout the neurites, and accumulates at high levels in these neurites. However, little is known about the role of LIN-10 in postsynaptic GLR-1 localization. In order to gain a better understanding of LIN-10 in GLR-1 localization, we screened for genetic modifiers of *lin-10* in GLR-1 localization. Through screening about 20,000 mutagenized haploid genomes, we isolated 2 mutants (enhancers) that accumulate more GLR-1::GFP than *lin-10* single mutants do, and 18 mutants (suppressors) that display wild-type GLR-1 localization in a *lin-10* mutant background. Through two-point mapping, three-point mapping, and SNP mapping, followed by cosmid rescue experiments, we found that *od14* is a mutation in the *rpm-1* gene. A second enhancer, *od22*, was linked to and failed to complement *od14*. We sequenced *rpm-1* genomic DNA from *od14* and *od22* mutants. *od14* is a missense mutation resulting in a glycine to glutamate change at amino acid 1092, a conserved residue within a PHR domain. For *od22*, we identified a premature stop codon mutation at nucleotide 88 of the predicted *rpm-1* cDNA sequence.

INTRODUCTION

The regulated localization of glutamate receptors to synaptic membranes plays an important role in synaptic plasticity, which is an important mechanism in the learning and

memory process. In *Caenorhabditis elegans*, GLR-1 is an AMPA-type glutamate receptor subunit that is localized to synapses. With chimeric GLR-1 receptors containing green fluorescent protein (GLR-1::GFP), the Rongo lab has focused on identifying factors that regulate GLR-1 localization.

LIN-10 contains two PDZ domains and one PTB (phosphotyrosine-binding) domain, and is homologous to the Mint/X11 family protein. In *C. elegans* epithelial cells, LIN-10 forms herteromultimeric protein complexes with two other PDZ-domain-containing proteins, LIN-2 and LIN-7, and functions in vulval induction through the regulation of basolateral localization of LET-23 (EGF Receptor); therefore, mutant animals have a vulvaless (Vul) phenotype (Kaech et al., 1998; Simske et al., 1996; Whitfield et al., 1999). In the worm interneurons, LIN-10 regulates postsynaptic localization of GLR-1. *lin-10* mutants show the accumulation of GLR-1 in patch-like structures throughout the neurites (Rongo et al., 1998). Intriguingly, LET-23 is not expressed in GLR-1-containing neurons. Moreover, mutant animals of *lin-2* and *lin-7* do not show abnormal GLR-1 localization. These results suggest that there might be different sets of proteins that interact with LIN-10 to regulate postsynaptic GLR-1 localization in neuron (Rongo et al., 1998). To support this hypothesis, our lab showed that distinct domains of LIN-10 are required to regulate GLR-1 localization in neurons and EGFR function in epithelia (Glodowski et al., 2005).

Although our lab recently identified that LIN-10 functions after clathrin-mediated endocytosis (Glodowski et al., 2007), players that modulate the LIN-10 mediated GLR-1 localization have not been identified so far. For a better understanding of the mechanisms of LIN-10 in GLR-1 localization, we decided to identify genetic

modifiers of LIN-10 with regard to GLR-1 localization by an EMS (Ethylmethane Sulphonate) mutagenesis screening. We screened by mutagenizing at a standard rate for *C. elegans* (1 mutation/2,000 genes), for mutants that suppress or enhance GLR-1::GFP accretions in a *lin-10(e1439)* mutant background, which contains Opal stop codon at amino acid 225. We identified two enhancers; both enhancer mutants (*od14* and *od22*) are wild-type for locomotion and show a slight increase of the GLR-1::GFP puncta size by themselves.

By conducting both conventional (two-point and three-point) and SNPs mapping protocols, we have identified novel *rpm-1* mutants alleles *(od14*, *od22).* In this chapter, the entire process of our screening for genetic modifiers of GLR-1 localization defects of *lin-10* mutants, and the methods of mapping and cloning for the identification of *od14* and *od22* will be described.

MATERIALS AND METHODS

Standard methods were used to culture *C. elegans*. Animals were grown at 20^{o}C on standard NGM plates seeded with OP50 *E. coli*. Some strains were provided by the *Caenorhabditis* Genetics Center. The following strains were used: N2, *nuIs25[GLR-1::GFP], lin-10(e1439)nuIs25, dpy-10(e128), lon-1(e185), dpy-20(e1282ts), dpy-11(e224), lon-2(e678), vab-8(gm84), rpm-1(ok364), rpm-1(ju41), rpm-1(js317),* and the CB4856 Hawaiian strain.

Germline Transformation

Transgenic strains were isolated after coinjecting various test plasmids (2-50 ng/μL) and an injection marker *rol-6(dm)* (a gift from C. Mello, UMass).

Fluorescence Microscopy

GFP- and RFP-tagged fluorescent proteins were visualized in nematodes by mounting larvae on 2% agarose pads with 10 mM levamisole. Fluorescent images were observed using a Zeiss Axioplan II. Imaging was done with an ORCA charge-coupled device (CCD) camera (Hamamatsu, Bridgewater, NJ) using IPLab software (Scanalytics, Inc, Fairfax, VA). Exposure times were chosen to fill the 12-bit dynamic range without saturation.

SNP Mapping

For SNP mapping, single worms from each strain of interest were lysed in 3 μl of single-worm lysis buffer (50 mM KCl, 10 mM Tris-HCl pH8.3, 2.5 mM $MgCl_2$, 0.45% NP-40, 0.45% Tween 20, 0.01% gelatine, freshly added 60 μg/ml proteinase K) at 60 ^{o}C for 60 min, followed by 95 ^{o}C for 15 min. PCR was carried out by adding 1 μl of the worm-lysed solution into total 10 μl of PCR reaction mixture. *ExTaq*^{TM} polymerase (Takara) was used for PCR. PCR conditions were as manufacture's protocol provided. The PCR products from SNP primers, 2 μl of the amplified products were digested with

specified enzyme for the primers. RFLPs (restriction fragment length polymorphisms) were analyzed by loading the 2% agarose gel. The chromosomal map position (in parenthesis), sequences, and digestion enzymes for SNP primers were as follows:

pkP5097 (LGV, -1.46)	gtgctaattccagaaatgatcc	tagtgttcatagcatcccattg	DraI
pkP5116 (LGV, 1.51)	aatttcgtcaccctctttgaac	gccgatatctacttgtgtaccg	DraI
pkP5063 (LGV, 1.68)	accacggccttcaaaagagtac	tctgcaagagagtgacaggtc	HinfI
pkP5117 (LGV, 1.92)	agactcccaaaatgctcag	atgcataatgagatgtgactgg	AseI
pkP5064 (LGV, 2.53)	ctcttagataccctttctgcgc	ttcagcgtttggtctgacgtag	DraI

Sequencing *rpm-1* Genomic DNA

Takara *LA Taq*™ was used to amplify *rpm-1* genomic DNA, and PCR conditions were as manufacture's protocol provided. Sequencing reaction mixtures were sent to GENEWIZ, Inc (South Plainfield, NJ) for sequencing. PCR and sequencing primers for *rpm-1* genomic DNA are as follows:

Primers to amplify rpm-1 genomic DNA

5' half	(C01B7.6-1F) ggcgctacgttcaaaatcac	ggaaacagttctcgctacagtca	(rpm-1_m_3)
3' half	(C01B7.6-3F) aacgcggacaactaccatac	gacaatgattctaggttcccga	(C01B7.6-3R)

Sequencing Primers from 5'

C01B7.6-1S aattgacgcctcagagtttc : *od22 mutation is observed by this primer*

C01B7_1-2S	ggagctgatgaagagggaaag	C01B7_1-3S	gcttcgagaagatgcctgtc
C01B7_1-4S	ggaccggcctgaatgaaac	C01B7_1-5S	gcattcattcaagctcgctc

C01B7.6-2S ccctcggtatgtgctcaatg

CO1B7_2-2S ggagccgatggtgattcttc : *od14 mutation is observed by this primer*

CO1B7_2-3S agttgggctgtatggaggac CO1B7_2-4S tggagtcaggaaagagcagg

CO1B7_2-5S tgaggccattttggtcaagg C01B7.6-3S ggtgccgcaataacagaag

CO1B7_3-2S ggttgtcagctaatgcttgtcg CO1B7_3-3S cgtggaggagattcgattgg

CO1B7_3-4S gctgtgaagttaagacgcaagg CO1B7_3-5S gaagtcgtggaaaccagtgtag

CO1B7_4-2S gccaaatgccaaccttgttttc C01B7_4R cgacgaccagaagattgcgaat

CO1B7_4-3S gcgtggattgcatggtaagac CO1B7_4-4S tgcgttcaatctgttcgtcgag

EMS Mutagenesis

lin-10(e1439) nuIs25[GLR-1::GFP], at L4 stage, animals were treated with 47mM ethylmethane sulfonate (EMS) for 4 hours. After washing twice with M9 buffer, animals were transferred with a sterile glass pipette to the edge of OP50 *E. coli.* lawn of NGM plates. 30 minutes later on the plate, healthy-looking late L4 or young adult stage animals were picked and transferred to new plates and were allowed to grow for 24 hours, at which stage animals will be grown to early gravid adults.

Mutants Screening

For the clonal screen (F1 mutant screen), one day after the mutagenesis of *lin-10 nuIs25* animals, 4 gravid P0 animals transferred to a new plate to obtain the designated number of plates for screening. Five days after EMS exposure, transferring of F1 animals at L4

stage were started. A week later, the progenies of F1 (F2) animals were observed for scoring. *lin-10* mutants have vulvaless phenotype; therefore, the progeny hatch in the body at the sacrifice of their mother and only a small number of progeny, about 30, can successfully escape from the dead body and survive. The small number of progeny of *lin-10* mutants made it possible to let animals grow for two generation without depletion of food on the 35mm size culture plates until scoring. This fact inspired us to conduct, alternatively, a non-clonal screen (F2 mutant screen) because we could follow F2 progenies in the same plate from the singled P0 plate. For this screen, one day after the mutagenesis of *lin-10 nuIs25* animals, single P0, instead of F1, animals were transferred to a new plate to obtain the designated number of plates for screening. 12 to 13 days after EMS exposure (after two generation), F2 animals were observed to scoring.

Scoring Mutants

The L4 to young adult stage of F2 animals were scored based upon the GFP intensities of cell body and ventral nerve cord on GFP-filter attached dissection microscope. Selected animals were grown to next generation, and observed by fluorescence compound microscopy by mounting (n=30-50) on 2% agarose pads containing 10mM levamisol to confirm the GLR-1::GFP localization defects. Mutants were further characterized after 4 rounds of backcrossing.

RESULTS

Two Enhancers and Eighteen Suppressors of the GLR-1 Localization Defects in *lin-10* Mutants

1486 F1 (clonal) singled plates were scored to get 1 enhancer and 2 suppressors. From non-clonal method, 269 P0 singled plates were scored to get total 17 mutants (1 enhancer, 16 supressors). Among 17 mutants from the non-clonal screening, 11 mutants were from separate P0 plates, indicating that they might be different mutations. Six suppressor mutants divided by two batches, each of them containing three mutants, were from two P0 plates, indicating that two categorized mutants could possibly contain the same overlapping mutations (Table 2-1). Since the progeny number of *lin-10* is around 30, the number of F1 scored by non-clonal screening might account for approximately 8,000 F1 (269∗30=8,070). As a result, about 10,000 F1 (1486 + 8070) were screened from both clonal and non-clonal screens.

The Mutant Phenotypes from Screening

lin-10 mutant animals show GLR-1::GFP as enlarged and diffused patches, especially at anterior region of ventral nerve cord. Suppressors in *lin-10* mutants background recovered the GLR-1::GFP puncta size comparable to the wild-type phenotype (Figure 2-2). By contrast, enhancers in the *lin-10* mutant background show much larger GLR-1::GFP patches in the anterior region of ventral nerve cord (Figure 2-2). *lin-10* mutants show egg laying defects, resulting from vulvaless phenotype, and also show mild UNC (uncoordinated) phenotype in locomotion behavior. Therefore, in addition to the

GLR-1 GFP phenotype, we checked whether the mutations also suppress or enhance those phenotypes in *lin-10* mutant background. Locomotion and egg laying behavior, and vulval development were observed after mutants were backcrossed to wild type animals to remove any other possible background mutations (Table 2-1). Notably, *od15* (suppressor) animals coiled upon head touch with a platinum wire or on tapping the plates. Two other suppressor mutants, *od21* and *od27*, suppressed the vulvaless phenotype as well as the mild uncoordinated (UNC) phenotypes of *lin-10* mutants. Both *od14* (enhancer) and *od22* (enhancer) animals showed a mild dumpy phenotype. Other mutants did not seem different from *lin-10* mutants in terms of morphological and behavioral phenotype besides GLR-1::GFP localization defects in *lin-10* mutants background (Table 2-1).

Deciding the Mutants for Mapping and Cloning; *od14* and *od22*

Both *lin-10* and *nuIs25* (P_{glr-1}*::glr-1::gfp* fusion construct) are on chromosome I, position at +2.58 and +5~10 (calculated from recombination frequency from our lab experiments), respectively. Therefore, we could judge by segregation frequency of *lin-10* from the mutations whether a mutation is on the same chromosome with *lin-10 nuIs25*. Within the twenty mutants that we found, twelve mutants were identified to be on the same chromosome with *lin-10 nuIs25* (LG I), and eight mutants were identified to be on different chromosomes from *lin-10 nuIs25* (Table 2-1). Mapping and cloning with a mutant that is on the same chromosome with *lin-10 nuIs25* might be very difficult, because lots of recombinants should be generated during mapping and cloning processes. By contrast, it might be convenient to do mapping if the mutants contain distinct

morphological or behavioral phenotypes that could be easily scored directly under dissection microscopy. Therefore, we decided to start doing mapping with two enhancer mutants (*od14* and *od22)*, which were mild dumpy in phenotype. During the backcross analysis, we determined that both mutants were recessive. After four rounds of backcrosses, *od14* and *od22* were analyzed by two-point and three-point mapping (Figure 2-3) and single nucleotide polymorphisms (SNPs) mapping (Wicks et al., 2001) (Figure 2-4) to identify chromosomal location.

_od14_ and _od22_ are on Chromosome V

As *od14* is not linked to chromosome I, we picked several chromosomal markers corresponding to chromosome II, III, IV, V, and X. Markers used were: *dpy-10* (e128, LG II, 0), *lon-1* (e185, LG III, -1.68), *dpy-20* (e1282ts, LG IV, +5.18), *dpy-11* (e224, LG V, 0), and *lon-2* (e678, LG X, -6.17). As the *od14* mutation completely segregated from the *dpy-11* mutation, we concluded that *od14* is on chromosome V. This result was further confirmed by SNP mapping using pkP5097 (map position -1.46 on LG V) primers. We found one recombinant out of twenty F2 animals, suggesting that the mutation is about 5 cM apart from -1.46 LG V. *od14* mutants were segregated by crossing *lin-10 nuIs25;od14* to *dpy-11*. Segregated mutants (*od14*) were confirmed by crossing *od14* males with *lin-10 nuIs25;dpy-11* to regenerate *lin-10 nuIs25;od14*, which was scored by fluorescence compound microscopy. Consistent with prior observation (Table 2-1), *od14* showed a mild-dumpy phenotype on its own. As *od22* has a similar morphological phenotype with *od14*, we directly tested whether it is also on Chromosome V by crossing

with *dpy-11*. We found that *od22* also segregated from *dpy-11*, suggesting *od22* is on chrosome V.

Narrowing-Down Map Position of *od14* Mutation to Between +1.51 and +1.67

Two-factor cross for the narrow-down mapping of od14: The protocol for two-point mapping used is as depicted in Figure 2-5. We singled 79 F2 dumpy (Dpy) animals. At F3 stage, plates were scored on the compound fluorescence microscope to result in 77 plates which lack of recombinants for *dpy-11* and *od14* double, and 2 plates that contain *dpy-11* and *od14* double recombinants. This data indicated that *od14* is approximately 2.53 (2/79*100) cM apart from *dpy-11* (0 on LG V). Previous snip-SNPs mapping suggested that *od14* might be at 5 cM apart from pkP5097 (-1.46 on LG V). Taken together, *od14* might reside on the right arm of chromosome V around +2 region.

***Three-factor cross for the narrow-down mapping of od14 mutation*:** The protocol for three-point mapping used is as depicted in Figure 2-6. Because our two-point mapping result suggested that *od14* might exist at around +2 map position on chromosome V, we selected to use *vab-8* (gm84, LG V, +3.77) to make triple recombinants of *dpy-11 od14 vab-8*. Out of 104 F2 Dpy animals selected, 11 contained *dpy-11* and *vab-8* double recombinants, within which 3 plates showed triple recombinants for *dpy-11 od14 vab-8*. Conversely, out of 58 F2 Vab animals selected, 6 contained *dpy-11* and *vab-8* double recombinants, within which 3 plates showed triple recombinants for *dpy-11 od14 vab-8*. These results suggested that the *od14* mutation is around +1.02~1.88 map position.

***The SNP mapping to further narrow-down the od14 mutation position*:** Strategy for the SNP mapping was as depiced in Figure 2-7. To determine the right side border of *od14*

mutation, triple recombinants for *dpy-11 od14 vab-8* ; *lin-10 nuIs25* were crossed to the CB4856 (Hawaiian, HA) strain. We selected 135 double recombinants of *dpy-11od14* (non Vab-8); *lin-10 nuIs25* to define right side border of *od14* mutation. After restriction digestion with specified enzymes for the PCR products generated by each snip-SNP primer sets, we calculated the location of mutation. From our calculation, the right side border of *od14* mutation was narrowed-down to +1.67. Results are as summarized below. Diagram of calculation is as depicted in Figure 2-8.

pkP5116 (+1.51) → 0 (HA) / 135 : *od14* is on right side of +1.51

pkP5064 (+2.53) → 60 (HA) / 135 : ~1.54 (left side border)

pkP5117 (+1.92) → 16 (HA) / 60(from pkP5064) : ~1.70

pkP5063 (+1.68) → 1 (HA) / 60(from pkP5064) : ~1.67

To determine the left side border of the *od14* mutation, we selected 15 double recombinants of (non Dpy-11) *od14 vab-8*; *lin-10 nuIs25*. After restriction digestion with specified enzymes for the PCR products generated by each snip-SNP primer sets, the left side border of *od14* mutation was narrowed to +1.51. Results are as summarized below.

pkP5117 (+1.92) → 0 (HA)/ 15

pkP5063 (+1.68) → 0 (HA)/ 15

pkP5116 (+1.51) → 2 (HA)/ 15

Candidate Gene Approaches and Complementation Experiments

: *od14* Mutation is in the *rpm-1* Gene

let-340 (+1.52158), *cln-3.3*(+1.5281), *sog-4*(+1.5334), *glr-5*(+1.5464), *tag-117*(+1.5874)

rpm-1 (+1.5974), and *let-467* (+1.6256). Among these genes, *rpm-1* mutants were described as a mild dumpy phenotype in morphology (Nakata et al., 2005; Schaefer et al., 2000) and known to function in presynaptic neurons (described in Chapter III), so we decided to do complementation experiments (Figure 2-9) with three other previously identified alleles of *rpm-1 (js317, ju41, ok364)*. These *rpm-1* mutants failed to complement *od14* mutation. As a parallel experiment, we examined these alleles by making double mutants with *lin-10 nuIs25* and found that all three behaved like *od14* with regard to GLR-1 localization (Figure 2-10). Additionally, injection of cosmid W09B7, which contains the *rpm-1* gene, rescued the GLR-1::GFP localization of *od4;lin-10 nuIs25* back to *lin-10 nuIs25* (Figure 2-11). These results established that *od14* is a mutation in *rpm-1* gene.

od14 is A Missense Mutation in the *rpm-1* Gene

A portion of the *rpm-1* gene, including sequences encoding N-terminal 1951 amino acids, is tandem duplicated (F07B7.X), making recovery of sequence information for that portion of the gene extremely difficult (Schaefer et al., 2000). Because the genomic DNA size of *rpm-1* is 14.54 kb, our initial trial to amplify the whole *rpm-1* gene was not successful. For efficient PCR amplification of *rpm-1* genomic DNA, two primer sets to amplify 5' and 3' halves of genomic DNA (about 7kb each) were chosen. For the exact sequencing of the *rpm-1* gene, the reverse primer for the N-terminal half of *rpm-1* gene was selected beyond the duplication region. The *od14* mutation was finally identified to be a missense mutation altering glycine 1092 to a glutamate (Figure 2-12 A,B). This residue falls within the first PHR domain, and is conserved in all PHR protein family

members, suggesting that glycine 1092 is critical for PHR domain function, and that this domain is required to regulate GLR-1 trafficking.

od22 is a Nonsense Mutation in the *rpm-1* Gene

As mutant animals of *od22* show similar GLR-1::GFP localization patterns (figure 2-10), are mild dumpy like *rpm-1* mutants, and they are on the same chromosome (LGV) with the *rpm-1* gene, we suspected that *od22* might be another *rpm-1* mutation. Therefore, we tested the complementation rescue experiments of o*d22* with *rpm-1* mutants. *od22* did not complement with *rpm-1* alleles. By sequencing of *od22* for the *rpm-1* gene, the *od22* mutation was identified to be a premature stop codon mutation at nucleotide 88 of the predicted *rpm-1* cDNA sequence. The *od22* mutation alters the conceptual translation of RPM-1 protein from arginine to an Opal stop codon at amino acid 30, resulting in a protein lacking all functional domains (Figure 2-12A).

DISCUSSION

Forward genetic screens have been an important tool to identify the genetic modifiers of biological events. We found two suppressors and one enhancer from an F1 (clonal) screen, and sixteen suppressors and one enhancer from an F2 (non-clonal) screen. The advantage of an F1 (clonal) screen over an F2 (non-clonal) screen is that sterile mutants can be isolated. However, the drawback is that lots of F1 animals should be singled to

reach a saturated condition; more than 5,000 F1 animals based upon the Poisson Distribution calculation with the assumption of Sydney Brenner's initial observation. By contrast, an F2 screen, by singling mutagenized P0 animals, could eliminate the process of singling lots of F1 animals for scoring, and potentially a lot of mutants could be found. Therefore, by singling only 269 mutagenized P0 animals, we could get 1 enhancer and 16 suppressors.

For the initial F1 screen, we scored animals by fluorescence compound microscopy by mounting them (n=30-50) from each F1 singled plates on separate 2% agarose pads. During this scoring we noticed that the suppressor and wild type animals show weaker GFP intensities in their nerve ring than *lin-10* mutants, and enhancers show stronger GFP intensities in their nerve cord than *lin-10* mutant alone. Therefore, when F1 or P0 singled animals reached the F2 stage, animals (L4 to young adults stage) were scored directly under the GFP filter attached- dissection microscopy to find enhancers and suppressors. The isolated 20 prospective suppressors and enhancers were observed with fluorescence compound microscopy by putting animals on a slide to confirm the GLR-1::GFP localization defects. Thus, by eliminating the slide making procedure, we could easily isolate 2 enhancers and 18 suppressors.

The *lin-10 e1439* allele was identified to be a nonsense mutation, which introduced the Opal stop codon at amino acid 225. In *C. elegans,* although several Amber suppressors have been identified (Kimble et al., 1982; Kondo et al., 1988; Kondo et al., 1990; Li et al., 1998), Opal and Ochre suppressors have not been identified; therefore, the possibility of non-sense suppression to occur would be lower. However, it is possible that we would isolate mutants for nonsense mediated mRNA decay (NMD) system, another

informational suppression (Hodgkin et al., 1989). This can be tested by examining an endogenous target of NMD, *rpl-7a* (Mitrovich and Anderson, 2000; Updike and Mango, 2007). *rpl-7a* gene generates two mRNAs by alternative splicing: the larger isoform, which introduces a stop codon by alternative splicing of exon 3 region, and the short isoform, which lacks the entire third intron. The larger isoform, therefore, is the target of NMD system, whereas the short one is spared from NMD system. Thus, in animals with NMD system mutations, the larger isoform could be detected by RT-PCR. Notably, several NMD system mutations are found on chromosome I, where *lin-10* and most of the suppressors that we identified are linked.

Traditional mapping methods were dependent on the use of visible phenotypic mutant markers for linkage mapping of mutations (two-factor and three-factor crosses). By this approach, successful cloning usually requires the generation of a lot of recombinants. Also, genetic interaction between markers and mutants for cloning might happen to make positional cloning difficult. However, since the single nucleotide polymorphism (SNP) mapping method has introduced (Wicks et al., 2001), *C. elegans* researchers favor this method for a mapping technique. Because of far denser distribution of SNPs than visible phenotypic markers and lack of genetic interactions, SNP mapping is advantageous, especially for narrowing the candidate region, over conventional linkage mapping methods. By combinatory use of two-point or three-point mapping and SNP mapping methods, we could successfully identify *rpm-1* as a genetic modifier for GLR-1 localization with relationship with *lin-10.*

FIGURES

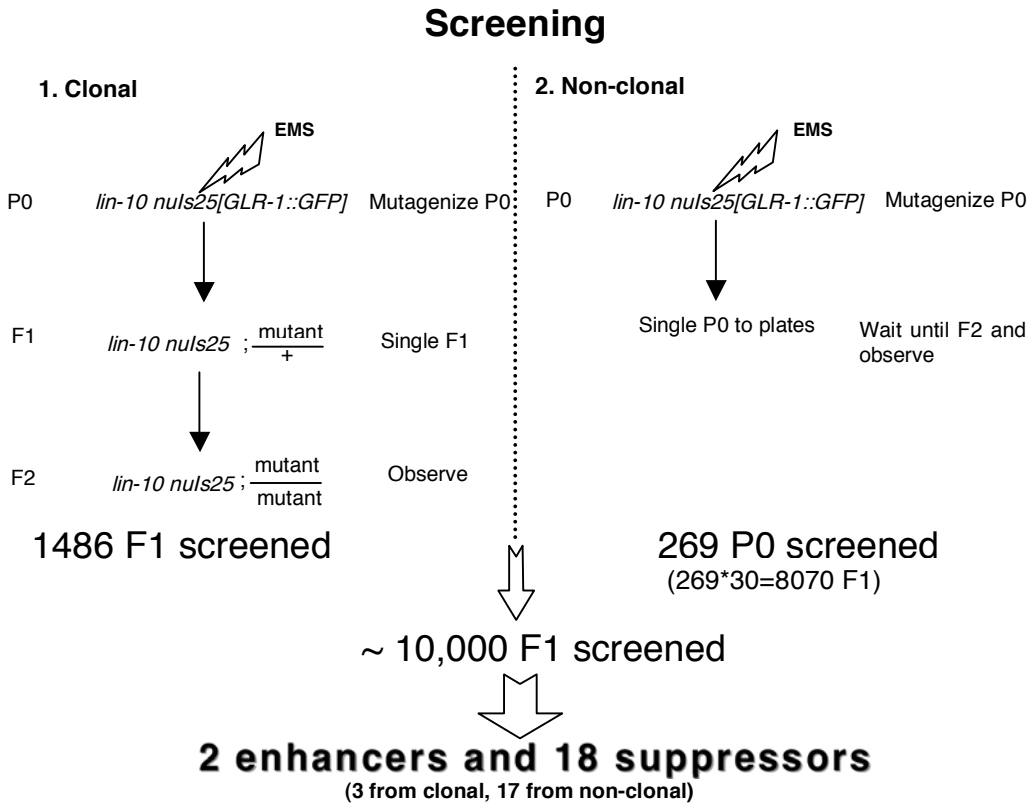

Figure 2-1. Schematic Diagram of Screening Strategy.

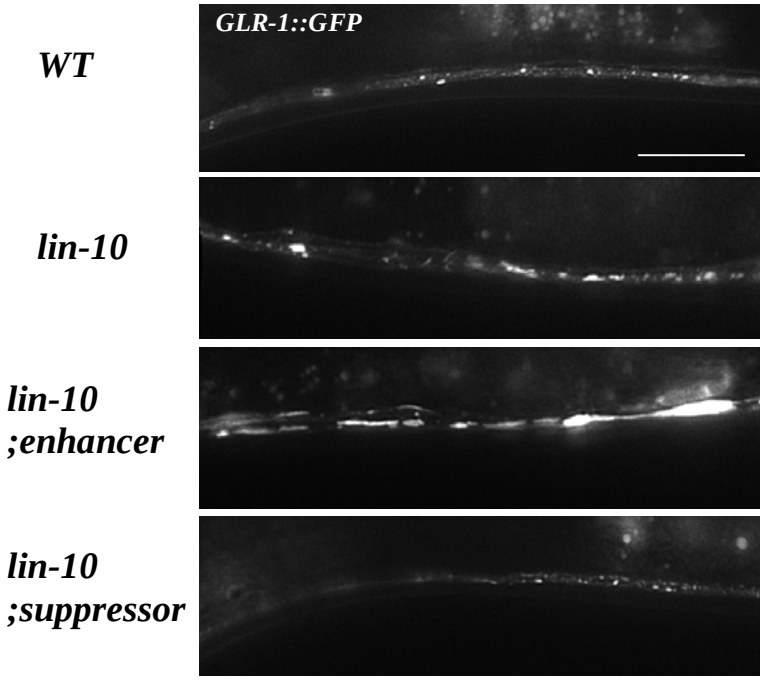

Figure 2-2. GLR-1::GFP phenotypes of mutants. GLR-1::GFP fluorescence was observed along ventral nerve cord of wild-type (*WT*), *lin-10*, *lin-10;enhancer*, and *lin-10;suppressor*. The representative pictures were taken from *od14* as for enhancers, *od15* as for suppressors. od22 (enhancer) and other suppressors in *lin-10* background showed similar GLR-1::GFP phenotype. Bar, 10 μm

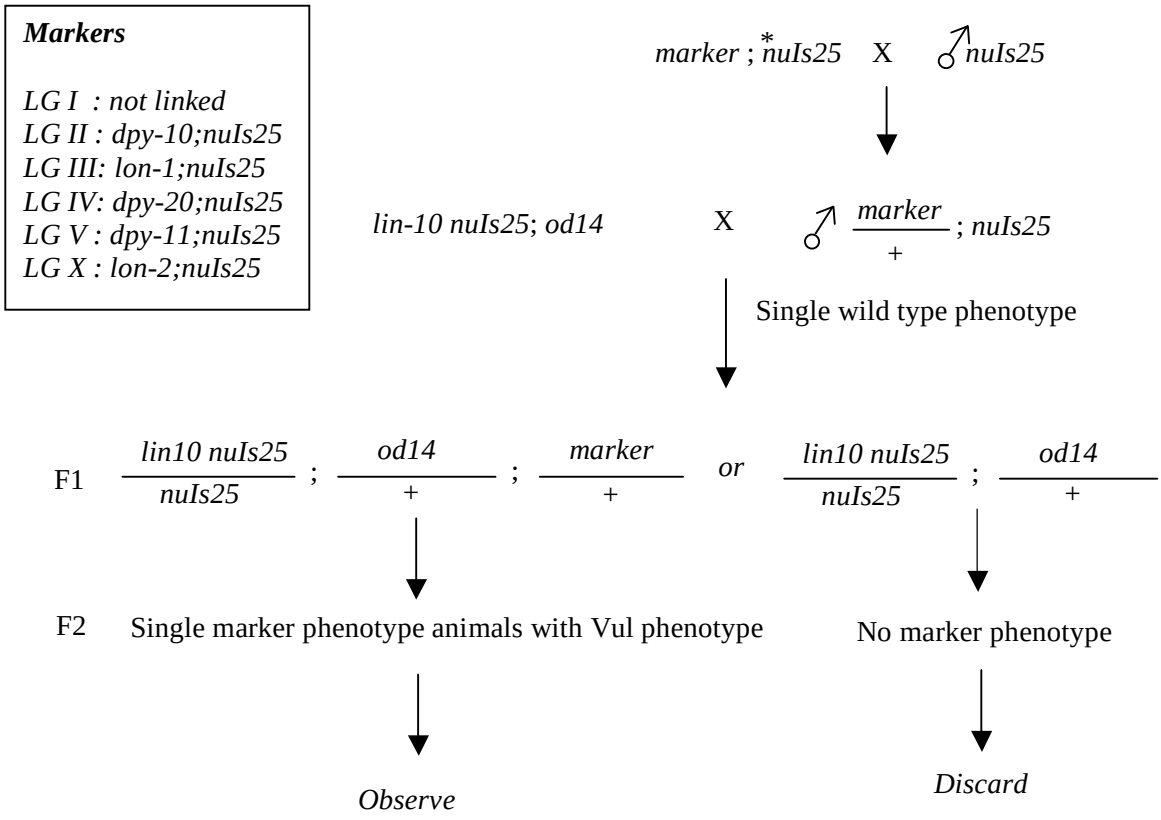

Figure 2-3. Strategy for the chromosomal mapping of *od14*.

nuIs25 is integrated line of *[p_{glr-1}::glr-1::gfp]* construct on chromosome I.

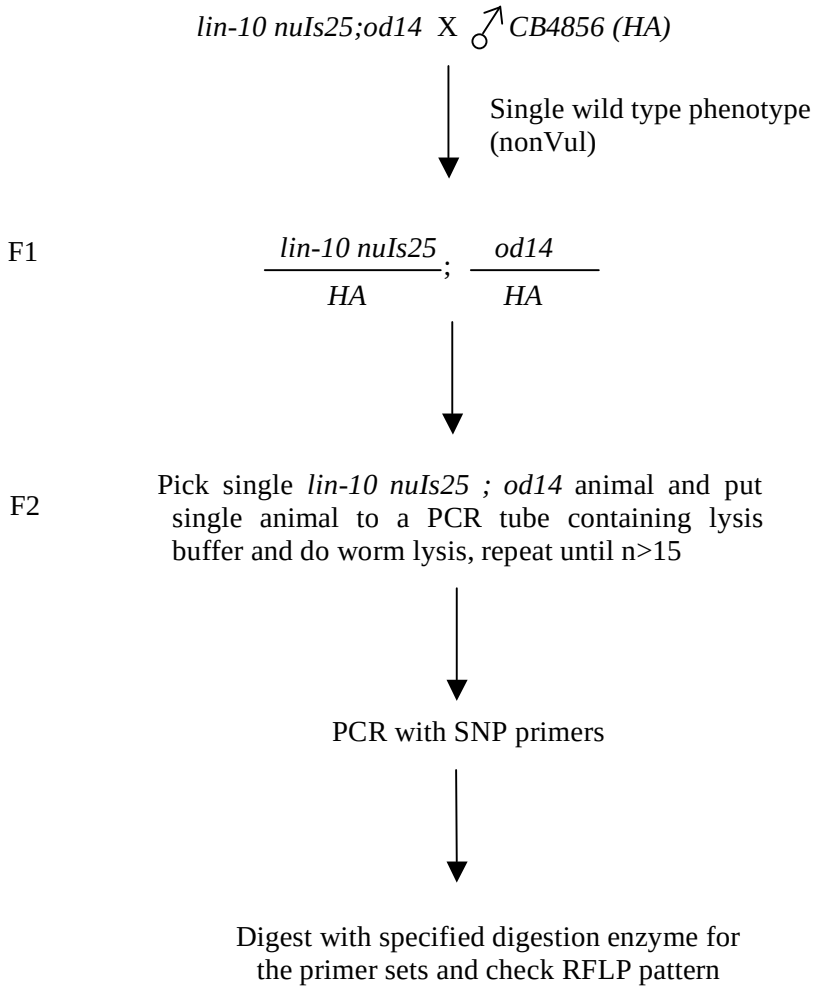

Figure 2-4. Experimental scheme for SNP mapping of *od14*

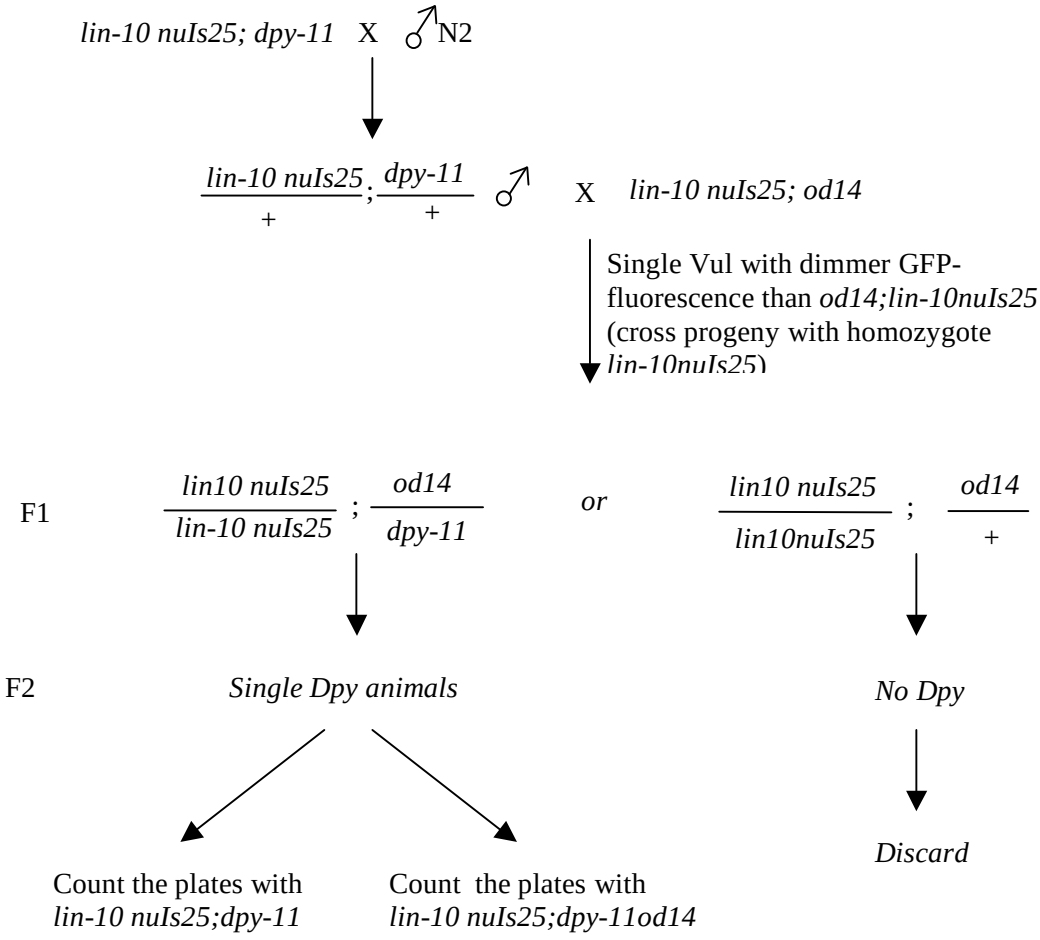

Figure 2-5. Strategy for Two-point mapping of *od14*

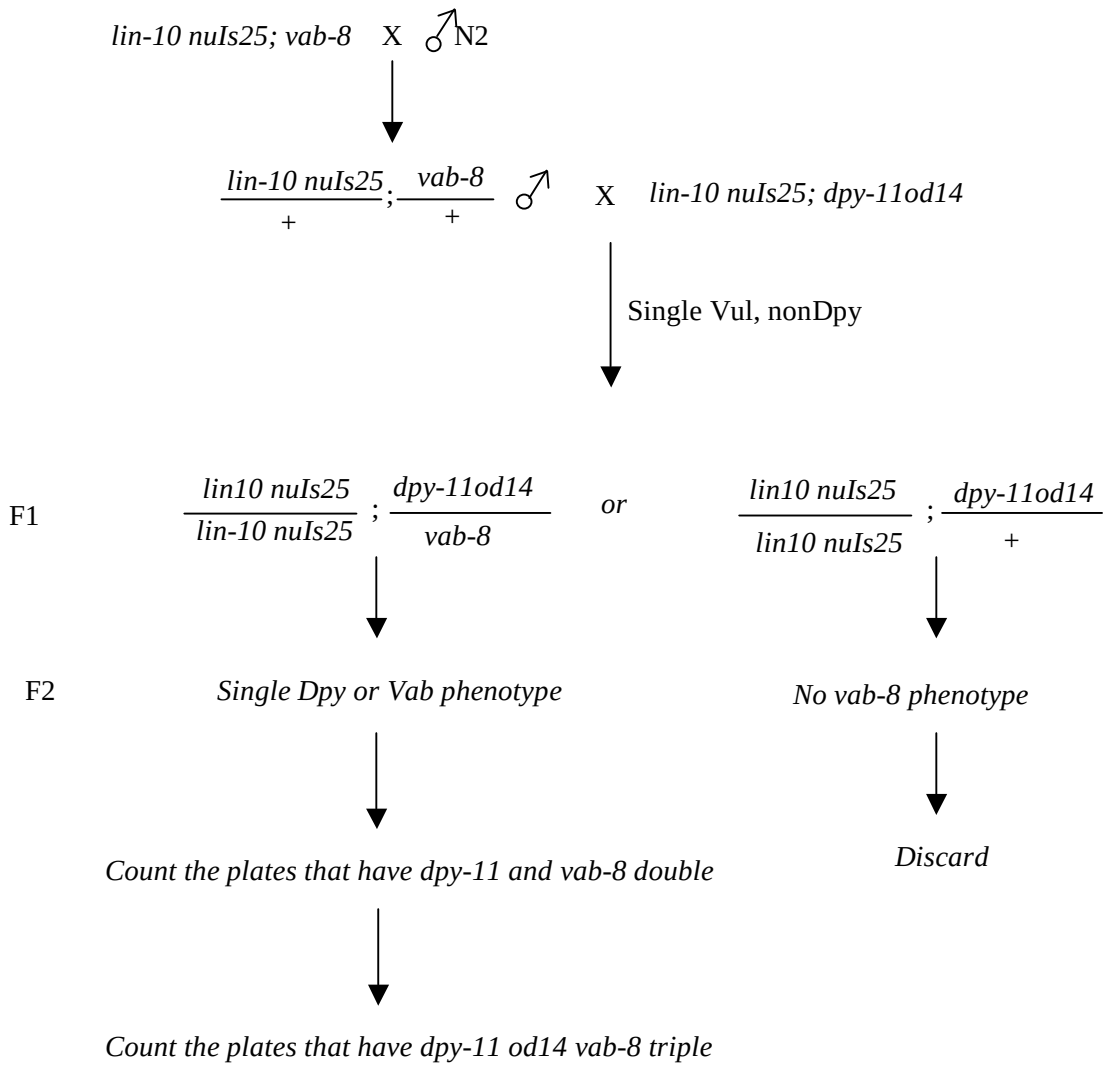

Figure 2-6. Strategy for Three-point mapping of *od14*

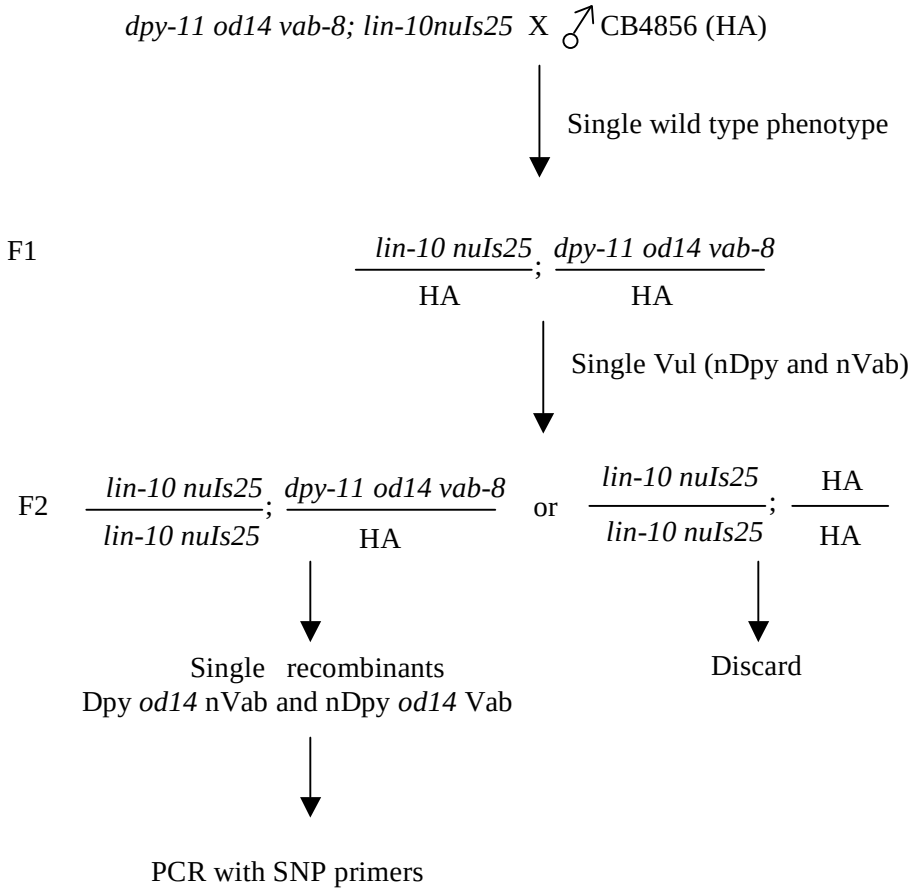

Figure 2-7. Combinatorial method of three-point mapping and SNP mapping to narrow-down the position of *od14* mutaion.

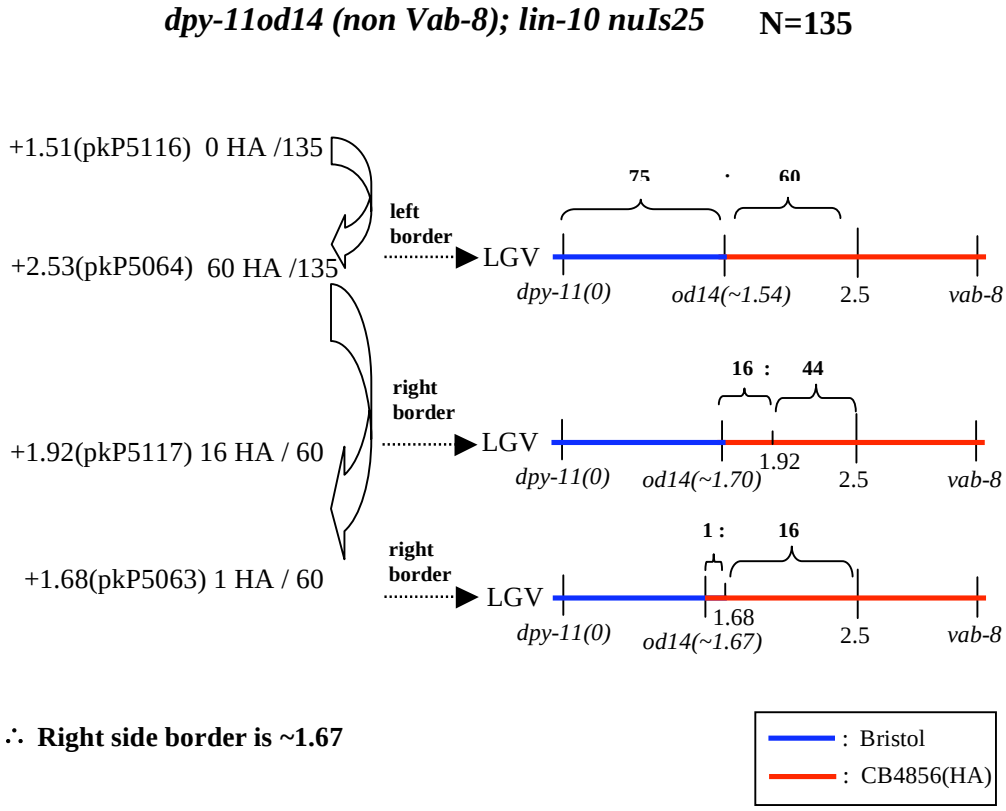

Figure 2-8. Calculation of right side border of *od14* from SNP mapping results

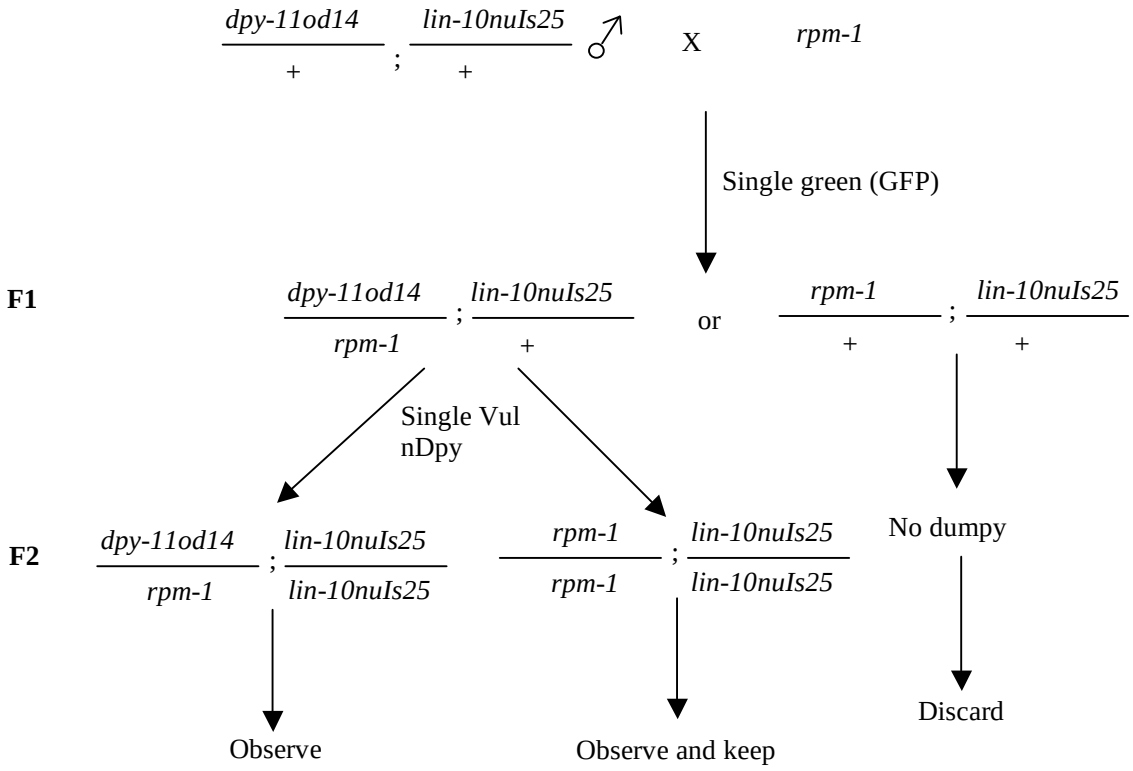

Figure 2-9. Complementation test of *od14* with *rpm-1* mutants and generation of *rpm-1; lin-10 nuIs25* strain.

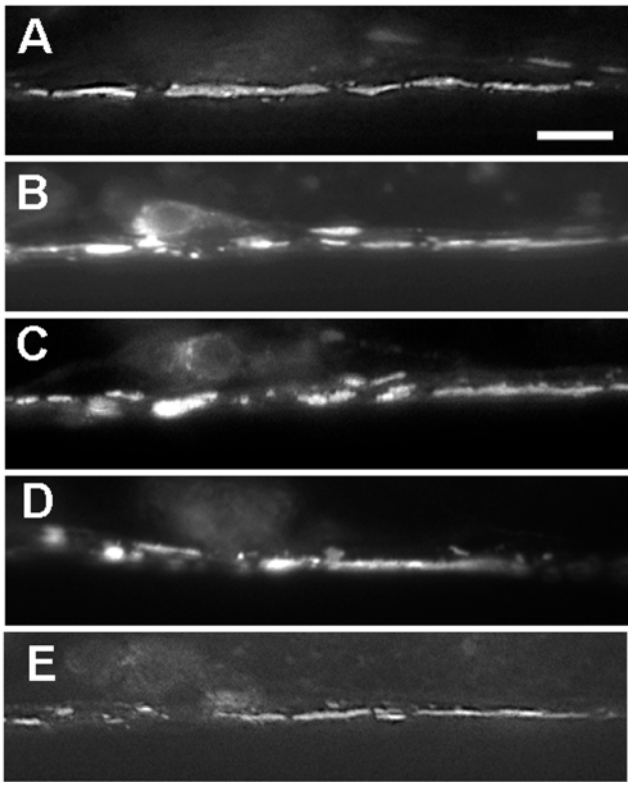

Figure 2-10. GLR-1 localization defects in other alleles of *rpm-1* with *lin-10* mutants and *od14 (or od22) lin-10* mutants. GLR-1::GFP fluorescence was observed along ventral cord dendrites of (A) *od14 lin-10* double , (B) *od22 lin-10*, (C) *rpm-1 (js317) lin-10* (D) *rpm-1(ju41) lin-10* , and (E) *rpm-1(ok364) lin-10* double mutants. Bar, 5 μm.

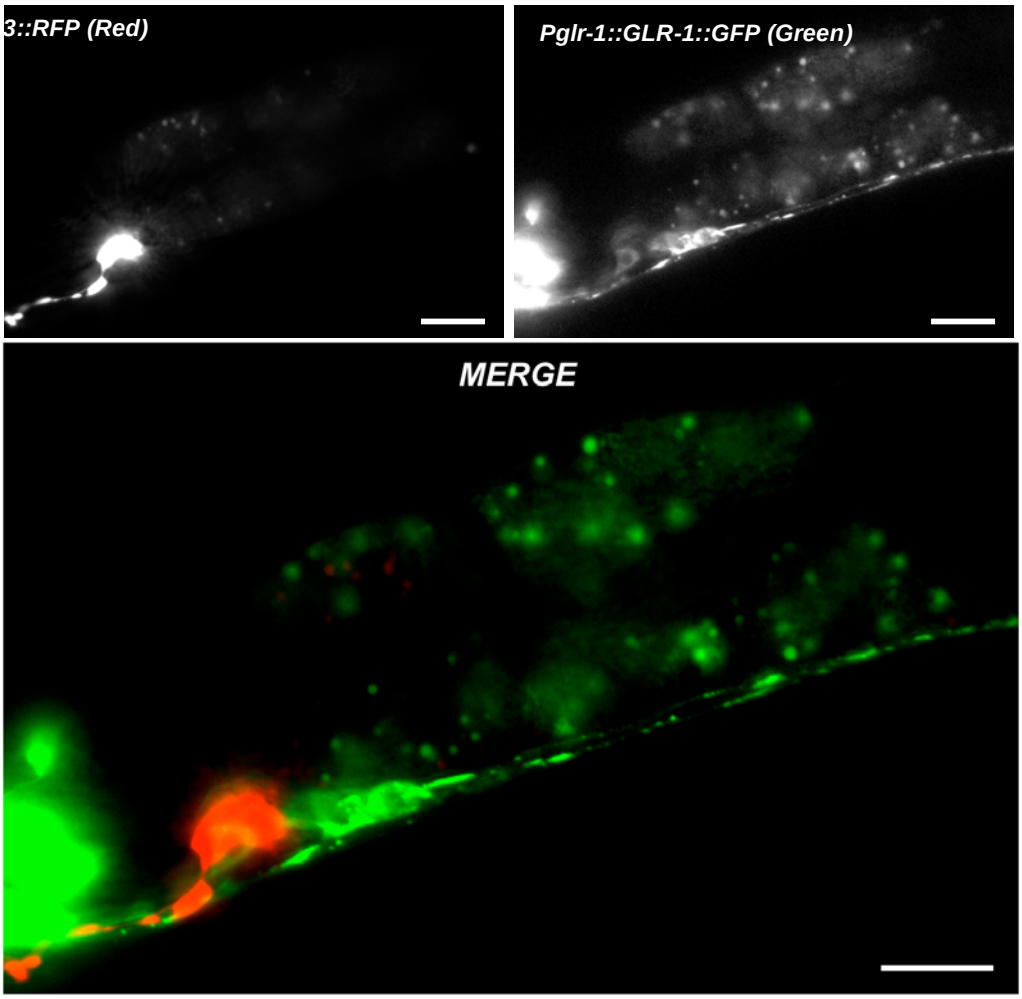

Figure 2-11. Microinjection of cosmid W09B7 reduces the size of GLR-1::GFP accretions observed in *od14; lin-10nuIs25* mutants. Epifluorescence microphotographs (63X) of Coinjection marker, $P_{ttx\text{-}3}$::RFP (upper left), GLR-1::GFP (upper right), and merge (bottom). Bar, 10 μm.

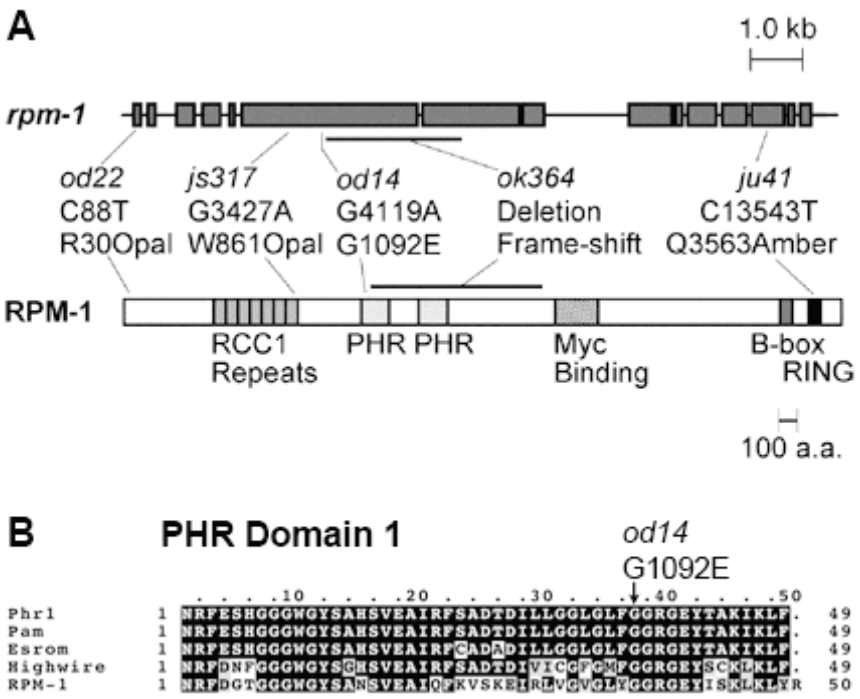

Figure 2-12. Mutations in RPM-1.

(A) The intron/exon gene structure of *rpm-1* (gray boxes) is shown at top. At bottom is the predicted protein domain structure, including the RCC1 repeats, the dual PHR domains, the Myc-bind region, the B-box, and the RING domain. The molecular nature of several known alleles is indicated. (B) Amino acid alignment of mouse Phr1, human Pam, Zebrafish Esrom, Drosophila *highwire*, and *C. elegans* RPM-1. Black highlighting indicates common identities, and gray highlighting indicates similarities. In the *od14* mutation (indicated by the arrow), glycine is replaced with glutamate at a conserved PHR domain residue.

TABLE

	Mutants from Screen		Chromosomal location	BEHAVIOR w/ *lin-10*	EGG LAYING w/ *lin-10*	VULVA phenotype w/ *lin-10*
clonal	od14 (enhancer)		**V**	~lin-10	defective	Vulvaless
	od15		**III**	Dorsal coiler upon tapping	defective	Vulvaless
	od19		**I**	NA	NA	NA
Non-clonal	Same?	od16	**I**	NA	NA	NA
		od17	**I**	~lin-10	defective	Sometimes pVul ~70% rescued
		od18	**I**	~lin-10	defective	Vulvaless
	od20		**I**	NA	NA	NA
	od21		**I**	~WT	some worms bagging but most of the worms lay eggs well	~90% rescued
	od22 (enhancer)		**V**	~lin-10, mild Dpy	defective	Vulvaless
	od23		**I**	~lin-10	defective	Vulvaless
	od24		**NA**	NA	NA	NA
	od25		**I**	~lin-10	Defective	Vulvaless
	od26		**I**	~lin-10	defective	Vulvaless
	od27		**I**	~WT	Lay eggs well	nonVul
	od28		**I**	~lin-10	defective	Vulvaless
	Same?	od29	**NA**	NA	NA	NA
		od30	**NA**	NA	NA	NA
		od31	**NA**	NA	NA	NA
	od32		**I**	~lin-10	defective	Vulvaless
	od33		**I**	~lin-10	defective	Vulvaless

Table 2-1. Summary of phenotypes and linkage analysis

CHAPTER III

THE UBIQUITIN LIGASE RPM-1 AND THE p38 MAPK PMK-3 REGULATE THE ENDOCYTOSIS OF AMPA RECEPTORS

ABSTRACT

Synaptic junctions are specialized in different neuron types, yet the mechanisms underlying synapse variation remain unclear. Here we report that the RPM-1 ubiquitin ligase and the PMK-3 p38 MAPK have differential functions at synapses in two different neuron types *in vivo*. Previous studies demonstrated that RPM-1 and PMK-3 organize presynaptic boutons at neuromuscular junctions in *C. elegans* motorneurons. In contrast, we find that RPM-1 and PMK-3 have a completely novel role in interneurons, where they regulate the postsynaptic trafficking of the AMPA-type glutamate receptor GLR-1. Mutations in *rpm-1* enhance the internal accumulation of GLR-1 observed in animals lacking LIN-10, a PDZ-domain protein that mediates GLR-1 recycling from endosomes. RPM-1 negatively regulates PMK-3, and mutations in *pmk-3* suppress the internal accumulation of GLR-1 observed in both *lin-10* and *rpm-1* mutants. RAB-5(GDP), an inactive mutant of RAB-5 that reduces endocytosis, mimics the effect of *pmk-3* mutations when introduced into wild type, and occlude the effect of *pmk-3* mutations when introduced into *pmk-3* mutants. By contrast, RAB-5(GTP), which increases endocytosis, suppresses *pmk-3* mutations and mimics *rpm-1* mutations when introduced into wild type, and occludes the effect of *rpm-1* mutations when introduced into *rpm-1* mutants. Our findings indicate a novel specialized role for RPM-1 and p38 MAPK in regulating the endocytosis of AMPARs at central synapses.

INTRODUCTION

Synaptic junctions are the sites of cellular communication between presynaptic neurons and their postsynaptic partners. Presynaptic terminals contain multiple synaptic vesicles filled with neurotransmitter. These vesicles are clustered around active zones, which contain the regulated secretory machinery for releasing vesicle contents when the presynaptic neuron is activated (Murthy et al., 2004). On the postsynaptic side of the synapse, neurotransmitter receptors and signaling molecules are assembled, ready to receive and transduce signals from the presynaptic cell. Changes in the localization and regulation of these receptors in turn mediate the changes in synaptic efficacy that occur during learning and memory (Kennedy and Ehlers, 2006). The formation of presynaptic terminals and postsynaptic specializations is coordinated, but requires distinct sets of proteins.

Synapses come in multiple forms. In the central nervous system (CNS), central synapses mediate communication between individual neurons, which often receive thousands of different inputs along a network of dendrites. By contrast, neuromuscular junctions (NMJs) mediate communication between motorneurons and muscles, which often receive a single input at a morphologically specialized motor end plate. These two synapse types differ in form and function, and are likely to be assembled and regulated by different mechanisms.

The formation of presynaptic terminals at NMJs has been well studied, and numerous regulators have been identified. In particular, a conserved family of proteins, the PHR proteins (including vertebrate Phr1 and Pam, *Drosophila* Highwire, and *C. elegans* RPM-1), has been shown to regulate the assembly of presynaptic components at NMJs (Brockie et al., 2001; Burgess et al., 2004; D'Souza et al., 2005; Guo et al., 1998; Lin et al., 2000; Schaefer et al., 2000). PHR proteins contain multiple domains, including several RCC1 repeats, two repeats termed PHR domains, and a RING H2 domain. Physical interactions have been detected between PHR proteins and Myc, adenylate cyclase, tuberin, the co-SMAD Medea, and dual leucine zipper kinases (DLKs) known to regulate the p38 MAP Kinase (MAPK) pathway (Collins et al., 2006; D'Souza et al., 2005; Guo et al., 1998; McCabe et al., 2004; Murthy et al., 2004; Nakata et al., 2005). PHR proteins also have both E3 ubiquitin ligase activity and guanine nucleotide exchange factor (GEF) activity.

A particularly well-studied PHR protein is RPM-1, which regulates the formation of NMJ presynaptic terminals by two parallel mechanisms. First, RPM-1 forms an SCF-like complex with the F-box protein FSN-1, the SKP1 ortholog SKR-1, and the Cullin CUL-1; the resulting ubiquitin ligase facilitates the ubiquitination of DLK-1, an upstream component of a *C. elegans* p38 MAPK pathway (Liao et al., 2004; Nakata et al., 2005). Second, RPM-1 binds to GLO-4, an RCC1-like guanine nucleotide exchange factor that regulates GLO-1, a Rab GTPase (Grill et al., 2007). RPM-1 is thought to positively regulate a Rab GTPase pathway to promote vesicular trafficking via late endosomes, which is critical for the organization of presynaptic terminals. Little is known about the

function of PHR proteins like RPM-1 outside of the presynaptic terminal of NMJs, although they are abundantly expressed in the CNS.

The formation of postsynaptic specializations at excitatory central synapses has also been well studied. Ionotropic glutamate receptors (GluRs) form tetrameric channels on the postsynaptic face of central synapses, where they receive and transduce glutamatergic signals from the presynaptic cell (Dingledine et al., 1999). The regulated trafficking of AMPA-type GluRs (AMPARs) into and out of the postsynaptic membrane is thought to underlie several forms of synaptic plasticity (Beattie et al., 2000; Bredt and Nicoll, 2003; Esteban et al., 2003; Kim et al., 2005). Ubiquitination and endocytosis are key mechanisms that regulate AMPAR postsynaptic accumulation (Burbea et al., 2002; Ehlers, 2000a; Esteban et al., 2003; Gerges et al., 2005; Schaefer and Rongo, 2006; Zhu et al., 2005). However, the specific proteins that mediate the ubiquitin-dependent regulation of AMPARs are not well characterized.

To investigate these processes in a genetic system, we examined the trafficking of the GLR-1 AMPAR subunit in *C. elegans*. GLR-1 is expressed in the command interneurons, where it mediates nose-touch mechanosensation and regulates the frequency of spontaneous reversals in locomotion (Hart et al., 1995; Maricq et al., 1995; Zheng et al., 1999a). Functional GLR-1 receptors, fused with green fluorescent protein (GLR-1::GFP), are localized to punctate clusters at central synapses in the nerve ring (proximal neurites that encircle the pharynx) and along the ventral cord (the fascicle of distal neurites that run along the ventral midline) (Rongo et al., 1998). The synaptic

abundance of GLR-1 is regulated by ubiquitination and endocytosis (Burbea et al., 2002; Dreier et al., 2005; Juo and Kaplan, 2004; Schaefer and Rongo, 2006). GLR-1 synaptic abundance is also controlled by LIN-10, a PDZ-domain protein of the Mint family, which is thought to regulate the membrane recycling of GLR-1 (Borg et al., 1998; Butz et al., 1998; Glodowski et al., 2007; Rongo et al., 1998; Whitfield et al., 1999). Mutants that lack LIN-10 activity have decreased levels of punctate, synaptic GLR-1, and instead accumulate GLR-1 receptors in large, internalized accretions throughout their neurites (Glodowski et al., 2007; Glodowski et al., 2005; Rongo et al., 1998). These mutants have deficits in GLR-1-mediated behaviors.

We screened for genetic modifiers of *lin-10* mutants and identified *rpm-1* as an enhancer of *lin-10* with respect to its GLR-1 trafficking phenotype. Mutations in *rpm-1* enhance the accumulation of GLR-1 in internal accretions that is observed in animals lacking LIN-10. Mutants for *rpm-1* alone also accumulate large accretions of GLR-1, although to a lesser extent than *lin-10* mutants. Whereas *rpm-1* mutants have misorganized presynaptic terminals at motorneuron NMJs, we find that presynaptic terminals at interneuron central synapses are normal at a gross level. We report that RPM-1 functions cell autonomously in postsynaptic interneurons, where it negatively regulates the PMK-3 / p38 MAPK pathway. In addition, our findings point to the regulation of GLR-1 endocytosis as the mechanism for PMK-3 and RPM-1 function. First, mutations in *pmk-3*, like mutations in UNC-11/AP180 and RAB-5, which impede endocytosis, suppress the internal accumulation of GLR-1 in *lin-10* mutants. Second, mutations that impede endocytosis mimic and occlude the effect of *pmk-3* mutations in double mutant

combinations. Finally, mutations that increase GLR-1 endocytosis suppress the effect of *pmk-3* mutations. We propose that p38 MAPK stimulates GLR-1 endocytosis, and that RPM-1 inhibits p38 MAPK signaling, thereby acting to reduce GLR-1 endocytosis and to stabilize GLR-1 at the synapse. Our findings demonstrate a novel function for PHR proteins: the regulation of postsynaptic elements at central synapses.

MATERIALS AND METHODS

Standard methods were used to culture *C. elegans*. Animals were grown at 20^{o}C on standard NGM plates seeded with OP50 *E. coli*. Some strains were provided by the *Caenorhabditis* Genetics Center. The following strains were used: N2, *lin-10(e1439), unc-11(e47), rpm-1(ok364), rpm-1(ju41), rpm-1(js317), pmk-3(ok169), fsn-1(hp1), glo-1(zu391), glo-4(ok623), eea-1(tm933), odIs22[P_{glr-1}::LIN-10::GFP], odIs1[P_{glr-1}::SNB-1::GFP], juIs1[P_{unc-25}::SNB-1::GFP], nuIs89[P_{glr-1}::MUb], nuIs25[GLR-1::GFP], nuIs108[GLR-1(4KR)]*and the CB4856 Hawaiian strain.

Confirming Mutant Strains

Double or triple mutants have been generated to see the genetic interaction of interested genes. To confirm *glo-4(ok623)* strain, a deletion mutant lacking 835bp of *glo-4* gene, primers caatgtctctcacacgaagaggtc (glo-4_5) and gtgtactcaaactcttgttcggcg (glo-4_3) were used for amplification, and size(wild-type 1287bp, mutant 452bp) were checked by running on agarose gel (1%). Because *glo* (gut granule loss) mutants are defective in gut granule biogenesis, these mutant also can be confirmed by fluorescence microscopy by checking lack of birefringent (or autofluorescent) gut granule cells. To confirm *fsn-1(hp1)*, g/a nucleotide change, primers gctcttcactgtgttggctatgttgc (fsn-1_5) and ccaagctgtgctccattgtgc(fsn-1_3) were used for amplification, and PCR products (about 104bp) were sequenced or digested by NlaIII, which cleaves wild-type at half of the PCR product, whereas mutants can't be cleaved, to check RFLP by running on agarose gel

(2%). To confirm *pmk-3(ok169)* strain, a deletion mutant lacking ~1kb deletion, primers cctctcgtttcccatttttcactgcgtc (pmk-3_5) and ggtcgccgacatccccatcaacaa (pmk-3_3) were used for amplification, and size(wild-type ~4kb, mutant ~3kb) were checked by running on agarose gel (1%). To confirm *eea-1(tm933)* strain, a deletion mutant lacking 371bp of *eea-1(tm933)* gene, primers gcttcagcatctctcagctt (tm933_internal_f) and ctaaacaacagtcgaccaag (tm933_internal_b) were used for amplification, and size (wild-type 2074bp, mutant 1703bp) were checked by running on agarose gel (1%).

Transgenes

To express RPM-1 genomic DNA in GLR-1 expressing neurons, we generated $P_{glr\text{-}1}$*::rpm-1*(genomic sequences). The *glr-1* promoter region of pV6 vector (a gift from V. Maricq, University of Utah), a plasmid containing the *glr-1* promoter, was PCR amplified with the primers flanking 5' SmaI and 3' AvrII digestion sequences, gcccgggtgcatgcctgcagcatttttaa (Sma_pglr-1) and gccctaggggatcctctagtcgacttgctttg (Avr_pglr-1_2), respectively. Then PCR products were cloned into the pCR® II (Invitrogen Co., Carlsbad, CA) vector by TA cloning®, following manufacturer's protocols to amplify. After the amplification of *glr-1* promoter containing pCR® II vector, *glr-1* promoter sequences were collected by digestion with SmaI and AvrII, and was transferred into pSAM8 vector (a gift from M. Nonet, Wash. U), RPM-1 genomic clone, of which *rpm-1* promoter region was removed by PmeI and AvrII, by conventional ligation procedure.

To generate P_{glr-1}*::(rfp or gfp)::pmk-3* constructs, we followed the Gateway® Technology (Invitrogen Co.). First, *pmk-3* cDNA including 3'UTR, yk1540e5 (Y. Kohara, National Institute of Genetics, Japan), were amplified with primers ggggacaagtttgtacaaaaaagttgtgatggcgtcagtcccatcgtcatc (Pmk-3_att5) and ggggaccactttgtacaagaaagctgggtcgggtgcaatgacaagaatgacg (Pmk-3UTR_att3) flanking *attB* sites for the Gateway® BP recombination reaction with pDONR221, contains *attP* sites, to generate entry clones, which contains *pmk-3* cDNA sequences that is flanked to *attL* sites. Second, the entry clones were inserted into the destination vector, which contains the *glr-1* promoter upstream of a *ccdB* gene that is flanked by *attR* sites, was generated from pV6 by the Gateway® LR recombination reaction. To generate mRFP(or GFP) N-terminal fusion protein driven by the *glr-1* promoter, the destination vector, which was generated by inserting mRFP(or GFP) coding sequences in between the *glr-1* promoter and *ccdB* gene (by D. Glodowski, Rongo Lab), was used for the Gateway®LR recombination reaction with the entry clones containing *pmk-3* cDNA with 3'UTR sequences.

P_{glr-1}*::(rfp or gfp)::dlk-1* constructs were generated by Gateway® cloning protocol. To acquire complete *dlk-1* cDNA sequences, yk1665e12 and yk1627e8 (Y. Kohara, National Institute of Genetics, Japan) clones, each containing *dlk-1* partial cDNA sequences, were combined by ligation of NcoI and MluI digestion products from each clones. Then *dlk-1* cDNA sequences including 3' UTR were amplified by primers ggggacaagtttgtacaaa aaagcaggcttcatgacatctaccacaatggta(Glodowski et al., 2007) and ggggaccactttgtacaagaaagctgggtcctaggtgttcactgggattcgttct, flanking *attB* sites. The PCR products were cloned into pDONR221 by the Gateway® BP recombination reaction to

generate entry clones. Finally, the entry clones were inserted into the destination vectors, which were used for generating P_{glr-1}*::(mrfp or gfp)::pmk-3,* by the Gateway®LR recombination reaction to generate *glr-1* promoter driven N-terminal mRFP (or GFP) fusion proteins of DLK-1.

The Gateway® entry clones of the *rab-5(GTP)* and *rab-5(GDP)* cDNAs (mutations Q78L and S23N, respectively), were gifts from B. Grant (Rutgers Univ.). P_{glr-1}*::rfp::rab-5(GTP) and* P_{glr-1}*::rfp::rab-5(GDP)* constructs were generated by the Gateway® LR recombination reaction as above(by D. Glodowski, Rongo Lab).

Germline Transformation

Transgenic strains were isolated after coinjecting various test plasmids (2-50 ng/μL) and an injection marker *rol-6dm* (a gift from C. Mello, UMass) or P_{ttx-3}*::mRFP* (monomeric RFP; a gift from R. Tsien, Stanford Univ.) into the gonad (Campbell et al., 2002). All resulting transgenes were introduced into the germline and followed as extrachromosomal arrays. To compare the phenotypes in different genetic backgrounds, transgenic arrays were transferred by intercrossing.

Extraction of total RNA and Real-Time PCR

Total RNAs were extracted with Trizol (Invitrogen Co., Carlsbad, CA). Lysis was done by repeating ten times of freezing (by liquid nitrogen) and thawing (at 37 °C). PCR was performed in a iCycler iQ system (Bio-Rad Laboratories Inc., Hercules, CA) using

iScript™ One-Step RT-PCR Kit With SYBR® Green (Bio-Rad Laboratories Inc., Hercules, CA) in 20 µL reactions with 20 ng of RNA template. Standardized conditions were used for all reactions beginning with an initial RT-PCR step 10 min. at 50 °C followed by 5min at 95°C for denaturation, and then 40 cycles of the following parameters: 95 °C for 30 s, 55 °C for 30 s, and 72 °C for 30 s. At the end of the PCR, the temperature was increased from 55 °C to 90 °C at a rate of 0.5 °C/10 s, and the fluorescence was measured every 10s to get melt curve. Samples were measured three times and average values were used for the calculation of relative fold changes. Relative fold changes were calculated with Pfaffl equation (Pfaffl, 2001), using wild-type *nuIs25* as a control. According to Pfaffl definition, PCR efficiencies (E) for *glr-1* and *dlg-1* primers were 1.83 and 2.03, respectively. The relative levels of *glr-1* mRNA in each preparation were normalized to the levels of *dlg-1* mRNA in each preparation, where the *glr-1*/*dlg-1* ratio in wild-type (*nuIs25* alone) was set to 1.

$$\text{Fold Change} = \frac{(E_{\text{glr-1}})^{\Delta Ct_{\text{glr-1}}(\text{wild type-mutant})}}{(E_{\text{dlg-1}})^{\Delta Ct_{\text{dlg-1}}(\text{wild type-mutant})}}$$

Primers, for *glr-1* tgatacaatgaaagttggagcaaatc and catcgcattgtcctctatcataccac; for *dlg-1*, gacgtgtggttgaacatactggag and gagaatccaaggccggtgtg were used.

Fluorescence Microscopy

GFP- and RFP-tagged fluorescent proteins were visualized in nematodes by mounting larvae on 2% agarose pads with 10 mM levamisole. Fluorescent images were observed

using a Zeiss Axioplan II. A 100X (Numerical Aperture = 1.4) PlanApo objective was used to detect GFP and RFP signal. Imaging was done with an ORCA charge-coupled device (CCD) camera (Hamamatsu, Bridgewater, NJ) using IPLab software (Scanalytics, Inc, Fairfax, VA). Exposure times were chosen to fill the 12-bit dynamic range without saturation. Maximum intensity projections of z-series stacks were obtained and out-of-focus light was removed with a constrained iterative deconvolution algorithm. Cluster outlines were automatically calculated for fluorescent signals that were two standard deviations above the unlocalized baseline by using a macro written for IPLabs. Cluster size was measured as the maximum diameter for each outlined cluster. Cluster number was calculated by counting the average number of clusters per 10 microns of dendrite length. For the quantification of GFP::DLK-1, either mean or maximum intensities of transgenic animals were measured from images of cell bodies (captured by a 20X objective) and ventral cords (captured by a 63X objective) using IPLabs software. For both, background signals were subtracted.

Behavioral Assays

The reversal frequency of individual animals was assayed as previously described, but with some modifications (Zheng et al., 1999b). Single young adult hermaphrodites were placed on NGM plates in the absence of food. The animals were allowed to adjust to the plates for 5 minutes, and the number of spontaneous reversals for each animal was counted over a 5-minute period. Twenty animals were tested for each genotype, and the reported scores reflect the mean number of reversals per minute.

RESULTS

RPM-1 Regulates GLR-1 Trafficking in Neurites

To better understand how GLR-1 is trafficked to synapses, we performed an EMS screen for mutants with defects in GLR-1::GFP localization. To make our direct visual screen more sensitive, we looked for suppressors and enhancers of a *lin-10* loss of function mutation as this mutation results in the internal accumulation of GLR-1 (Glodowski et al., 2007). We identified two mutants, *od14* and *od22*, with an enhanced *lin-10* phenotype. Whereas wild-type animals contain punctate GLR-1::GFP at synapses along neurites (Fig. 1A), mutants for *lin-10* (Figure 3-1B,I) or *rpm-1* (Figure 3-1C,I) accumulate GLR-1 in large accretions found within the neurites. Double mutants for *lin-10* and *rpm-1* have significantly larger accretions of GLR-1 than either single mutant alone (Figure 3-1D,I), and have reduced numbers of small GLR-1 puncta compared to wild type (Figure 3-1J), suggesting that these two genes might act in separate pathways to regulate GLR-1 trafficking.

As RPM-1 forms an E3 ubiquitin ligase complex with the F-box protein FSN-1 and the Cullin CUL-1 (Liao et al., 2004), we tested whether mutations in *fsn-1* resulted in a similar GLR-1 localization phenotype as that in *rpm-1*. The *fsn-1(hp1)* mutation introduces a stop codon before the SPRY domain, resulting in a protein null allele. Like *rpm-1* mutants, *fsn-1* mutants accumulate GLR-1 in large accretions (Figure3-1E,K). Moreover, mutations in *fsn-1* enhance the accumulation of GLR-1 observed in *lin-10* mutants (Figure 3-1F,L) and depress the number of small GLR-1 puncta. Also we observed that the triple mutants of *fsn-1, rpm-1, and lin-10* behave like double mutants of

rpm-1 and *lin-10* or *fsn-1* and *lin-10* with regard to GLR-1 localization (data not shown). These findings suggest that RPM-1 acts with FSN-1 as an E3 ligase to regulate GLR-1 trafficking.

RPM-1 is also known to act via GLO-4, an RCC1-like guanine nucleotide exchange factor that regulates GLO-1, a Rab GTPase (Grill et al., 2007). We tested whether mutations in *glo-1* and *glo-4* resulted in a similar GLR-1 trafficking phenotype as that in *rpm-1*. Unlike mutations in *fsn-1*, mutations in *glo-1* and *glo-4* did not resemble *rpm-1* mutations; no GLR-1 accumulation was observed (Figure 3-1K). In addition, mutations in either *glo-1* or *glo-4* did not enhance *lin-10* mutations (Figure 3-1G,L). These results suggest that, unlike in motorneurons, RPM-1 does not regulate GLR-1 trafficking via GLO-1 and GLO-4.

RPM-1 Does Not Regulate the Organization of Central Synapses

RPM-1 is required for proper presynaptic bouton formation at motorneuron NMJs (Brockie et al., 2001; Schaefer et al., 2000). To determine whether our newly identified *rpm-1* mutations also impair presynaptic bouton formation, we examined the subcellular localization of SNB-1 (synaptobrevin) using *juIs1*, a transgene that expresses a SNB-1::GFP protein fusion in motorneurons. In wild-type animals, SNB-1::GFP is localized to large (1-2 micron) NMJ boutons along both the dorsal and ventral cords (Liao et al., 2004; Nakata et al., 2005; Nonet et al., 1999) (Figure 3-2A). In *rpm-1(od14)* mutants, we observed a decreased number of SNB-1::GFP NMJ boutons and an irregularity in inter-bouton spacing, as was observed for other alleles of *rpm-1* mutants (Figure 3-2C,I). Given the genetic interaction between *rpm-1* and *lin-10* with regard to

GLR-1 localization, we examined SNB-1::GFP at the NMJ boutons of *lin-10* single mutants (Figure 3-2E) and *rpm-1 lin-10* double mutants (Figure 3-2G). NMJ boutons from *lin-10* mutants were indistinguishable from those in wild type, and *rpm-1 lin-10* double mutants were indistinguishable from those in *rpm-1* single mutants. We quantified the total number of the dorsal cord SNB-1::GFP boutons in *rpm-1(od14)* mutants, and found it to be similar to that observed in known alleles of *rpm-1* (Figure 3-2I). As the *od14* mutation alters the first PHR domain, our findings suggest that the PHR domain is critical for RPM-1 function in motorneurons.

The changes in GLR-1 ventral cord accumulation in *rpm-1* mutants could reflect defects in synapse formation at central synapses. To test this possibility, we examined the localization of SNB-1 using *odIs1*, a transgene that expresses a SNB-1::GFP protein fusion in the GLR-1-expressing interneurons of the central nervous system. In wild-type animals, SNB-1::GFP is localized to small (~ 0.5 micron) boutons along the ventral cord (Figure 3-2B). In *rpm-1* mutants, there is no observable difference in SNB-1-labeled bouton number or size at central synapses (Figure 3-2D). We also examined SNB-1-labeled central synapse boutons in *lin-10* single mutants (Figure 3-2F) and *rpm-1 lin-10* double mutants (Figure 3-2H), and found them to be indistinguishable from wild type (Figure 3-2J).

As mutations in *rpm-1* are similar to *lin-10* mutations with regard to their effect on GLR-1 trafficking, we tested whether RPM-1 regulates LIN-10 localization. A LIN-10::GFP chimeric protein is colocalized with GLR-1 in the ventral cord in wild type animals (Glodowski et al., 2005; Rongo et al., 1998). We found that LIN-10::GFP is localized to similar punctate structures in both wild type and *rpm-1* mutants (Figure

3-2K,L). Taken together, our findings indicate that the defects in GLR-1 localization observed in *rpm-1* mutants are unlikely to be due to gross defects in the formation of central synapses. In addition, our findings indicate that RPM-1 has a distinct role in organizing the presynaptic face of NMJ synapses in motorneurons but not central synapses in interneurons.

PMK-3 and DLK-1 Act Downstream of RPM-1

One known target of RPM-1 regulation is the p38 MAPK cascade. To test for a role of p38 MAPK in GLR-1 trafficking, we examined *pmk-3(ok169)* mutants. The *pmk-3(ok169)* mutation is a deletion spanning most of the *pmk-3* coding sequence. Whereas the mutation in *pmk-3* did not affect the number or size of GLR-1 puncta in otherwise wild-type animals (Figure 3-3A), it did suppress the accumulation of GLR-1 observed in both *lin-10* mutants and *rpm-1* mutants (Figure 3-3B,C,G,H). Similarly, *pmk-3* mutations suppressed the exaggerated accumulation observed in *rpm-1 lin-10* double mutants to levels more similar to those observed in *lin-10* single mutants (Figure 3-3D,H). These results indicate that PMK-3 / p38 MAPK function is required for GLR-1 accumulation in *lin-10* and *rpm-1* mutants.

PMK-3 is broadly expressed in many *C. elegans* tissues. To determine if PMK-3 functions in the same cells as GLR-1, we made a transgene, P_{glr-1}*:: pmk-3(+)*, containing *pmk-3* cDNA sequences (with mRFP sequences fused in frame at the PMK-3 N-terminus) under the control of the *glr-1* promoter. We introduced *Pglr-1::pmk-3(+)* into *pmk-3 lin-10* double mutants and found that mutant animals carrying the transgenic array had their GLR-1 localization defects restored (Figure 3-3I), indicating that

RFP::PMK-3 can function cell autonomously. To examine PMK-3 subcellular localization, we introduced $P_{glr\text{-}1}$*::pmk-3(+)* into wild-type animals expressing GLR-1::GFP, and found that RFP::PMK-3 protein was localized to interneuron nuclei (Figure 3-4C) and was present throughout the ventral cord neurites (Figure 3-4D).

Given the nuclear localization of PMK-3, we hypothesized that PMK-3 might regulate the transcription of *glr-1* mRNA. We isolated total mRNA from wild type, *pmk-3* mutants, *rpm-1* mutants, *lin-10* mutants, *pmk-3 lin-10* double mutants, *rpm-1 lin-10* double mutants, and *pmk-3 rpm-1 lin-10* triple mutants. We detected no significant differences among these different genotypes on *nuIs25* background (relative fold change: *pmk-3* 0.92; *rpm-1* 0.83; *lin-10* 0.92; *pmk-3 lin-10* double 1.32; *rpm-1 lin-10 double* 1.53; *pmk-3 rpm-1 lin-10* triple 1.1) . Removing one of the two copies of the *nuIs25[glr-1::gfp]* transgene, which results in two-fold mRNA level differences that are detectable by real time PCR, does not suppress the GLR-1 accumulation observed in *lin-10* mutants (Rongo et al., 1998). Thus, it is unlikely that PMK-3 and RPM-1 regulate GLR-1 trafficking by affecting *glr-1* mRNA expression.

As RPM-1, an ubiquitin ligase, is a negative regulator of the p38 MAPK cascade, the abundance of one or more components of the cascade is likely to be limiting within neurons. To determine if the levels of PMK-3 are limiting, we introduced the *Pglr-1::pmk-3(+)* transgene into animals that also contained both wild-type alleles of the endogenous *pmk-3* locus. The elevation of PMK-3 levels in wild-type animals did not affect GLR-1 localization (data not shown). Also, *lin-10* mutants that contained elevated levels of PMK-3 did not demonstrate the dramatic enhancement observed in *rpm-1 lin-10* double mutants (Figure 3-3E,J). The PMK-3 / p38 MAPK is regulated by DLK-1, an

upstream MAPKKK known to be regulated directly by RPM-1 in motorneurons (Nakata et al., 2005). We generated a transgene, $P_{glr\text{-}1}$*::dlk-1(+)*, containing *dlk-1* cDNA sequences (with mRFP sequences fused in frame at the DLK-1 N-terminus) under the control of the *glr-1* promoter. Unlike animals expressing $P_{glr\text{-}1}$*::pmk-3(+)*, animals expressing $P_{glr\text{-}1}$*::dlk-1(+)* contained GLR-1 accretions in their neurites (data not shown). Moreover, *lin-10* mutants that contained elevated levels of DLK-1 demonstrated a dramatic enhancement in phenotype (Figure 3-3F,J) similar to that observed in *rpm-1 lin-10* double mutants. The removal of PMK-3 activity from *lin-10* $P_{glr\text{-}1}$*::dlk-1(+)* animals blocks the effect of DLK-1 overexpression (Figure 3-3J). Our results indicate that PMK-3 levels are not limiting for GLR-1 localization; rather, DLK-1 levels appear to dictate PMK-3 / p38 MAPK activity in controlling GLR-1 trafficking.

In *C. elegans*, GLR-1 signaling positively regulates spontaneous reversals during forward locomotion as animals forage for food (Mellem et al., 2002; Zheng et al., 2004). Mutants with either reduced GLR-1 activity (e.g., *glr-1* mutants) or reduced levels of GLR-1 receptor at the synaptic membrane surface (e.g., *lin-10* mutants) have a lower frequency of spontaneous reversals (Glodowski et al., 2007). We examined GLR-1-mediated behaviors in wild-type animals and in animals with mutations in *lin-10*, *glr-1*, *rpm-1*, or *pmk-3*. We found that wild-type animals spontaneously reversed about 3.7 times per minute (20 animals, 5 minute trial per animal), whereas *lin-10* and *glr-1* mutants only spontaneously reversed direction about 1.5 and 1.4 times per minute, respectively (Figure 3-3K). Mutants for either *rpm-1* or *pmk-3* spontaneously reversed direction with a frequency similar to wild-type animals. Interestingly, double mutants for *lin-10* and *pmk-3* reversed direction 2.5 times per minute (Figure 3-3L), suggesting that

mutations in *pmk-3* can partially restore GLR-1-mediated reversal behavior to *lin-10* mutants. Thus, the suppression of *lin-10* mutations by *pmk-3* mutations with regard to GLR-1 accumulation correlates with behaviors that indicate restored synaptic strength. These results suggest that PMK-3 helps regulate the abundance of GLR-1 on postsynaptic membranes.

RPM-1 Regulates DLK-1 Abundance in Interneurons

If DLK-1 levels are limiting with regard to the regulation of GLR-1 trafficking, then RPM-1 might regulate DLK-1 levels. To observe changes in DLK-1 protein levels using a more sensitive reporter than our mRFP::DLK-1 chimeria, we generated a transgene, $P_{glr\text{-}1}$*::gfp::dlk-1(+)*, containing GFP sequences fused in frame to *dlk-1* cDNA sequences at the DLK-1 N-terminus, under the control of the *glr-1* promoter. We introduced the transgene into wild-type animals, and found that GFP::DLK-1 protein was present both in neuron cell bodies (near the membrane and excluded from the nucleus; Figure 3-4G,I) and in ventral cord neurites in a punctate pattern (Figure 3-4H,J). We crossed the transgene into *rpm-1* mutants and observed a significant increase in GFP::DLK-1 fluorescence (the same transgenic line is shown in Figure 3-4G,H,I,J). To quantify GFP::DLK-1 fluorescence, we removed background fluorescence from our images, then defined either whole cell bodies or whole ventral cords as single objects. We quantified both the mean fluorescence and the maximum fluorescence for these objects, and found a several fold increase in both mean and peak GFP::DLK-1 fluorescence in *rpm-1* mutants compared to wild type (Figure 3-4K,L; same transgenic line is quantified). These differences were observed in both neuron cell bodies and ventral cords. Our findings

suggest that RPM-1 negatively regulates DLK-1 protein levels in the command interneurons.

RPM-1 is Required for the Ubiquitin-mediated Turnover of GLR-1

GLR-1 trafficking and synaptic abundance are regulated by ubiquitination. Because of a limiting cellular concentration of monoubiquitin, overexpression of Myc epitope-tagged ubiquitin (MUb) by a *nuIs89* transgene has been shown to negatively regulate GLR-1 abundance in neurites (Burbea et al., 2002). While multiple E3 ligases have been shown to be partially required for the turnover of GLR-1 after an overexpression of ubiquitin, mutations in no single E3 ligase have been shown to completely block GLR-1 turnover, suggesting that multiple ligases are involved. To determine if RPM-1 is required for the ubiquitin-mediated turnover of GLR-1, we introduced *nuIs89* into *lin-10* mutants, *rpm-1* mutants, and *rpm-1 lin-10* double mutants. Elevated ubiquitin depresses the number of GLR-1 puncta in wild-type animals (Figure 3-5A,F). Mutations in *lin-10* and *rpm-1* combined block the effect of overexpressed ubiquitin on GLR-1 puncta number (Figure 3-5D,F), indicating that these genes are required for some of the ubiquitin-mediated removal of GLR-1. However, in *lin-10* and *rpm-1* single mutants, as well as in *lin-10 rpm-1* double mutants, elevated ubiquitin can nevertheless still depress the size of GLR-1 accretions (Figure 3-5B,C,D,E), suggesting that the GLR-1 receptors that accumulate internally in these mutants can still be removed in part by other ubiquitin-dependent mechanisms. Thus, RPM-1 is required for part, but not all, of the ubiquitin-mediated degradation of GLR-1.

Ubiquitination of GLR-1 is required for RPM-1 mediated GLR-1 localization

The cytoplasmic tail sequences of GLR-1 have four lysine residues, which are the target of ubiquitination. Previous studies have shown that mutated GLR-1 with all four cytoplasmic lysine residues to arginine, *nuIs108* GLR-1(4KR), localizes to synapses and functional as evidenced by a close apposition to presynpaptic components, synaptobrevin and EAT-4 VGLUT, and nose touch assay (Burbea et al., 2002). However, the size of GLR-1(4KR) puncta are increased, providing additional evidence in support of the involvement of ubiquitination in GLR-1 trafficking (Burbea et al., 2002; Dreier et al., 2005; Juo and Kaplan, 2004)(Figure 3-6A,B,E). We investigated whether changes in GLR-1 ubiquitination are required for RPM-1 and PMK-3 mediated GLR-1 regulation. We couldn't detect significant changes of GLR-1(4KR)::GFP puncta size in *rpm-1* or *pmk-3* mutants (Figure 3-6 B,D,E). Considering that *rpm-1* mutations significantly increase wild type GLR-1 puncta size (Figure 3-1A,C,I), the lack of effect of *rpm-1* on GLR-1(4KR) puncta size indicates that the 4KR mutation occludes the effect of *rpm-1* on GLR-1 localization. Also, since the localization of GLR-1 in *pmk-3* mutants was normal (Figure 3-3A,G), the GLR-1(4KR) puncta size in *pmk-3* mutants was as similar as that of GLR-1(4KR) in wild-type background indicates that the 4KR mutation is epistatic to the *pmk-3* mutation. These results implicate that the ubiquitination of cytoplasmic GLR-1 is required for the RPM-1 mediated GLR-1 localization.

RPM-1 Regulates GLR-1 Endocytosis

Previous studies have shown that p38 MAPK can modulate endocytosis in other systems, raising the possibility that PMK-3 regulates GLR-1 endocytosis (Cavalli et al., 2001;

Huang et al., 2004; Mace et al., 2005). Indeed, the accumulation of GLR-1 receptors in *lin-10* mutants is due to defects in GLR-1 recycling from endosomes to synapses, and can be suppressed by blocking clathrin-mediated endocytosis (Glodowski et al., 2007). Mutations in *unc-11*, a clathrin adaptin protein AP180 ortholog, depress GLR-1 endocytosis. When introduced into *lin-10* mutants, *unc-11* mutations suppress the accumulation of GLR-1 in accretions (Figure 3-7A). Endocytosis is also stimulated by the small GTPase RAB-5, which cycles between an active GTP-bound form and an inactive GDP-bound form (Barbieri et al., 1994; Bucci et al., 1992; Zhu et al., 2002). We generated a transgene, $P_{glr\text{-}1}$*::rfp::rab-5(GDP)*, which contains a mutated form of the *rab-5* cDNA expressed from the *glr-1* promoter. RAB-5(GDP) contains an S23N substitution, locking it in the GDP-bound conformation and depressing endocytosis. Like mutations in *unc-11*, expression of $P_{glr\text{-}1}$*::rfp::rab-5(GDP)* in *lin-10* mutants suppresses the accumulation of GLR-1 in accretions (Figure 3-6A). We also generated $P_{glr\text{-}1}$*::rfp::rab-5(GTP)*, which contains *rab-5* cDNA with the mutation Q78L. RAB-5(GTP) is locked in the GTP-bound conformation and stimulates endocytosis. When we introduced $P_{glr\text{-}1}$*::rfp::rab-5(GTP)* into wild-type animals, we found that GLR-1 accumulated in accretions, similar to those in *lin-10* mutants (Figure 3-6B). Moreover, $P_{glr\text{-}1}$*::rfp::rab-5(GTP)*, when placed into *lin-10* mutants, significantly enhanced the accumulation of GLR-1 (Figure 3-7B). Thus, the net accumulation of GLR-1 in accretions in *lin-10* mutants depends on GLR-1 endocytosis.

To determine whether PMK-3 / p38 MAPK regulates GLR-1 endocytosis, we tested whether suppression of *lin-10* by *pmk-3* mutations and by *unc-11* mutations was additive. We generated *lin-10 pmk-3 unc-11* triple mutants and examined GLR-1

accumulation. We found that *pmk-3* mutations do not enhance *unc-11* mutations (Figure 3-7C), suggesting that mutations in *unc-11* can occlude the effect of mutations in *pmk-3*. Similarly, we depressed endocytosis in *lin-10 pmk-3* double mutants by introducing the P_{glr-1}*::rab-5(GDP)* transgene. We found that the expression of P_{glr-1}*::rab-5(GDP)* occluded the effect of *pmk-3* mutations (Figure 3-7D). In addition, the expression of P_{glr-1}*::rab-5(GDP),* was able to restore GLR-1-mediated spontaneous reversals to *lin-10* mutants to the same extent as the presence of a *pmk-3* mutation (Figure 3-7E). Furthermore, the expression of P_{glr-1}*::rab-5(GDP)* occluded the effect of a *pmk-3* mutation (Figure 3-7E). These results are consistent with RAB-5, UNC-11, and PMK-3 functioning in the same pathway to stimulate GLR-1 endocytosis.

If PMK-3 regulates GLR-1 endocytosis by activating RAB-5, then expression of RAB-5(GTP) should bypass the requirement for PMK-3. To test this idea, we introduced P_{glr-1}*::rab-5(GTP)* into *lin-10 pmk-3* double mutants and observed the effect on GLR-1 accumulation in accretions. We found that P_{glr-1}*::rab-5(GTP)* enhanced the accumulation of GLR-1 in accretions, regardless of the presence of PMK-3 (Figure 3-7F). Expression of P_{glr-1}*::rab-5(GTP)* in *lin-10* mutants also depressed the spontaneous reversal frequency, even in combination with a *pmk-3* mutation (Figure 3-7G). As mutations in *rpm-1* result in elevated PMK-3 / p38 MAPK activity, we tested whether P_{glr-1}*::rab-5(GTP)* would affect GLR-1 accumulation in *rpm-1* mutants. We found that P_{glr-1}*::rab-5(GTP)* did not enhance the accumulation of GLR-1 in accretions in either *rpm-1* single mutants or *lin-10 rpm-1* double mutants, suggesting that mutations in *rpm-1* occlude the effect on GLR-1 endocytosis by RAB-5(GTP) (data not shown). Taken

together, our results suggest that PMK-3 / p38 signaling regulates GLR-1 receptors by stimulating their endocytosis.

Mutation Of *eea-1* Does Not Affect GLR-1 Localization In Both Wild-Type And *lin-10* Mutants

Rab5 function through its effector proteins such as the early endosmal autoantigen 1 (EEA1), Rabenosyn-5 and the Rab GDP dissociation inhibitor (GDI) for receptor endocytosis (Cavalli et al., 2001; Mace et al., 2005; Zwang and Yarden, 2006). EEA1 is one of the best characterized effectors that phosphorylated by p38 MAPK (Mace et al., 2005; Zwang and Yarden, 2006). To determine whether *C. elegans* EEA-1 plays a key role with RAB-5 in GLR-1 endocytosis, we examined GLR-1 localization on *eea-1* alone or with *lin-10* mutants (Figure 3-8). We couldn't detect any distinct differences compared to wild type or *lin-10* mutants, suggesting EEA-1 might not be involved in GLR-1 endocytosis mediated by PMK-3 (p38 MAPK).

DISCUSSION

We identified a novel role for RPM-1 and PMK-3 as regulators of AMPAR endocytosis (Figure 3-9). Previously, the PDZ protein LIN-10 was shown to mediate the recycling of GLR-1 from endosomes back to the synapse (Glodowski et al., 2007). Mutations in *lin-10* result in the accumulation of GLR-1 in endosomes; this accumulation is suppressed by mutations that decrease endocytosis and enhanced by mutations that

increase endocytosis. Several lines of evidence suggest that RPM-1 and PMK-3 regulate the endocytosis of GLR-1 receptors at central synapses, independent of their role in presynaptic differentiation at NMJs. First, animals with mutations in *rpm-1* accumulate GLR-1 receptors in large accretions, and mutations in *rpm-1* enhance the GLR-1 accumulation observed in *lin-10* mutants. Second, while mutations in *rpm-1* result in defective presynaptic boutons at motorneuron NMJs, these same mutations do not appear to alter presynaptic boutons at interneuron central synapses. Third, mutations in PMK-3, a p38 MAPK, suppress the accumulation of GLR-1 in both *lin-10* and *rpm-1* mutants. Moreover, mutations in PMK-3 suppress the behavioral defects of *lin-10* mutants. Fourth, elevated levels of DLK-1, a MAPKKK upstream of PMK-3, result in a GLR-1 accumulation phenotype similar to that of *rpm-1* mutants. Moreover, DLK-1 levels are negatively regulated by RPM-1 in interneurons. Fifth, mutations resulting in decreased GLR-1 endocytosis occlude the effect of *pmk-3* mutations, whereas transgenic manipulations resulting in increased GLR-1 endocytosis bypass the requirement for PMK-3 and occlude the effect of mutations in *rpm-1* (both on GLR-1 accumulation and GLR-1-mediated behaviors). Based on these results, we propose that RPM-1 regulates GLR-1 trafficking by promoting the ubiquitin-mediated degradation of DLK-1, thereby maintaining reduced levels of PMK-3 / p38 MAPK signaling and hence GLR-1 endocytosis.

Mutations in *rpm-1* were originally identified in screens for mutants with aberrant NMJ boutons (Brockie et al., 2001; Schaefer et al., 2000). Wild-type animals contain large, regularly spaced presynaptic boutons, which innervate muscles along the ventral and dorsal midlines. In *rpm-1* mutants, boutons are often missing, smaller in size,

or aberrantly spaced along the dorsal and ventral nerve cords. In Drosophila, mutations in *highwire*, an ortholog of RPM-1, result in a similar phenotype (Lin et al., 2000). RPM-1 is expressed in the central as well as the peripheral nervous system, as are its mammalian orthologs Pam and Phr1, but their function in the CNS is unknown. Surprisingly, we found that RPM-1 is not required to organize presynaptic boutons at central synapses, suggesting that presynaptic elements of central synapses, which are designed for tonic release of synaptic vesicles, are organized by distinct mechanisms compared to presynaptic elements from NMJs, which are designed for a more tetanic release. Instead of a presynaptic role at central synapses, RPM-1 regulates the endocytosis of AMPARs from postsynaptic elements. This is the first postsynaptic function to be identified for a PHR protein.

While we did not observe obvious presynaptic defects at the central synapses of *rpm-1* mutants, we cannot rule out the possibility that there might be subtle presynaptic defects. Nevertheless, the GLR-1 defects observed in *rpm-1* mutants cannot simply be explained based on a presynaptic role for *rpm-1*. First, the GLR-1 trafficking defect observed in *rpm-1* mutants can be rescued by cell-autonomous expression of an *rpm-1* minigene. Second, mutants for *unc-104* (KIF1A), which lack most synaptic vesicles from central synapse terminals, do not have the gross GLR-1 localization defects observed in *rpm-1* mutants. In addition, mutants for *unc-18* (Munc18/Sec1), which are deficient in synaptic vesicle release, also are not similar to *rpm-1* mutants (Rongo and Kaplan, 1999; Rongo et al., 1998).

How does RPM-1 function presynaptically in one neuron type and postsynaptically in another? Interestingly, p38 MAPK signaling is the target of RPM-1

regulation at both central synapses and NMJs, suggesting that these genes function as a signaling cassette. One difference for RPM-1 function is the requirement for the GEF GLO-4 and the small GTPase GLO-1 (Grill et al., 2007). In motorneurons, RPM-1 acts as an E3 ubiquitin ligase via FSN-1 and as an activator of the GLO-1 Rab via the GLO-4 GEF. Mutations in either *fsn-1* or *glo-4* alone yield mild presynaptic defects, whereas mutations in both are similar to mutations in *rpm-1*, suggesting that RPM-1 relies on both of these factors in parallel to organize NMJ presynaptic boutons. By contrast, mutations in *fsn-1* alone yield the same postsynaptic defects with regard to the trafficking of GLR-1 as do *rpm-1* mutations. Mutations in *glo-1* and *glo-4* appear to have no major postsynaptic defects, suggesting that, in interneurons, RPM-1 acts primarily as an E3 ubiquitin ligase to conduct its postsynaptic function. Thus, the nature of the effector molecules that associate with RPM-1 in each neuron type might dictate the role of RPM-1 in that neuron.

Two additional critical issues will need to be addressed in order to understand the disparate roles of RPM-1. First, the mechanisms that differentially localize the RPM-1 / p38 MAPK cassette to presynaptic elements in motorneurons and postsynaptic elements in interneurons will need to be elucidated. Second, the targets of p38 MAPK in each neuron type will need to be identified. In mammals, p38 MAPK regulates endocytosis by phosphorylating components of the endocytosis machinery, including the Rab5 effectors EEA1 and Rabenosyn-5. It also phosphorylates guanyl nucleotide dissociation inhibitor (GDI), stimulating the formation of the GDI:Rab5 complex so that Rab5 can recycle back to the location of endocytosis (Cavalli et al., 2001; Huang et al., 2004; Mace et al., 2005). The net effect of these p38-dependent events is increased

endocytosis. Similarly, our findings suggest that PMK-3 stimulates GLR-1 endocytosis, perhaps via the activation of RAB-5. However, unlike the *pmk-3* loss of function mutants, the *eea-1* loss of function mutants did not suppress the GLR-1 localization defects of *lin-10* mutants, suggesting that EEA-1 might not be the target of PMK-3 for GLR-1. It is necessary to examine other RAB-5 effectors such as *rabs-5* (Rabenosyn-5 ortholog) or *gdi-1*(GDI ortholog) to find the target of PMK-3 for promoting GLR-1 endocytosis.

FIGURES

Figure 3-1. RPM-1 regulates GLR-1 trafficking.

GLR-1::GFP fluorescence was observed along ventral cord dendrites of (A) wild-type animals, (B) *lin-10* mutants, (C) *rpm-1* mutants, (D) *rpm-1 lin-10* double mutants, (E) *fsn-1* mutants, (F) *fsn-1 lin-10* double mutants, (G) *glo-4 lin-10* double mutants, or (H) *rpm-1 lin-10* double mutants that express a wild-type *rpm-1* minigene using the *glr-1* promoter. Arrowheads indicate the accumulation of GLR-1::GFP in large accretions in *lin-10*, *rpm-1*, and *fsn-1* mutants. Arrows indicate the exaggerated accumulation of GLR-1::GFP in very large accretions in *rpm-1 lin-10* double mutants and *fsn-1 lin-10* double mutants. The mean size (H,K,L) and the mean number (J) of fluorescent structures (including puncta and accretions) are plotted for adult nematodes of the given genotype. Bar, 5 μm. Error bars are SEM. N=15-20 animals for each genotype. *P<0.01, **P<0.001 by ANOVA followed by Dunnett's Multiple Comparison to (I,J,K) wild type or to (L) *lin-10* mutants.

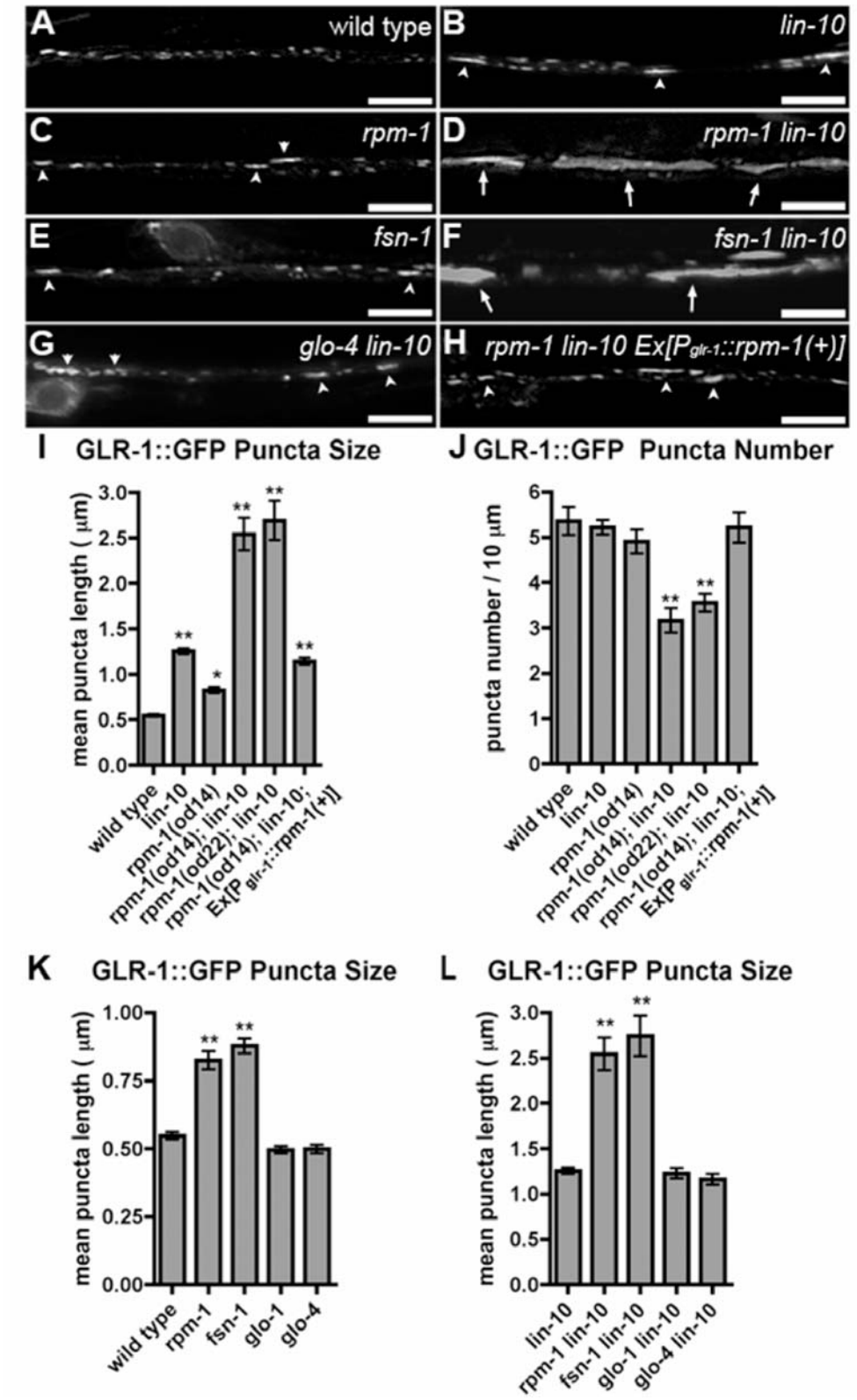
A wild type
B lin-10
C rpm-1
D rpm-1 lin-10
E fsn-1
F fsn-1 lin-10
G glo-4 lin-10
H rpm-1 lin-10 Ex[Pglr-1::rpm-1(+)]
I GLR-1::GFP Puncta Size
mean puncta length (μm)
3.0
2.5
2.0
1.5
1.0
0.5
0.0
wild type
lin-10
rpm-1(od14)
rpm-1(od14); lin-10
rpm-1(od22); lin-10
rpm-1(od14); lin-10; Ex[Pglr-1::rpm-1(+)]
J GLR-1::GFP Puncta Number
puncta number / 10 μm
6
5
4
3
2
1
0
K GLR-1::GFP Puncta Size
mean puncta length (μm)
1.00
0.75
0.50
0.25
0.00
wild type
rpm-1
fsn-1
glo-1
glo-4
L GLR-1::GFP Puncta Size
mean puncta length (μm)
3.0
2.5
2.0
1.5
1.0
0.5
0.0
lin-10
rpm-1 lin-10
fsn-1 lin-10
glo-1 lin-10
glo-4 lin-10

Figure 3-2. Differential requirements for RPM-1 at NMJs versus central synapses. SNB-1::GFP fluorescence was observed along the ventral cord of animals either (A,C,E,G) expressing the reporter at motorneuron NMJs via the *unc-25* promoter, or (B,D,F,H) expressing the reporter at interneuron central synapses via the *glr-1* promoter. SNB-1::GFP localization was observed in (A,B) wild-type animals, (C,D) *rpm-1* mutants, (E,F) *lin-10* mutants, or (G,H) *rpm-1 lin-10* double mutants. (I) The number of fluorescent structures (puncta) is plotted for motorneuron NMJs. (J) The mean number of puncta is plotted for interneuron central synapses. The fluorescence of LIN-10::GFP, expressed from the *glr-1* promoter, was also observed along the ventral cord of (K) wild-type animals and (L) *rpm-1* mutants. Bar, 5 μm. Error bars are SEM. N=15-20 animals for each genotype. ***P<0.001 by ANOVA followed by Dunnett's Multiple Comparison to wild type.

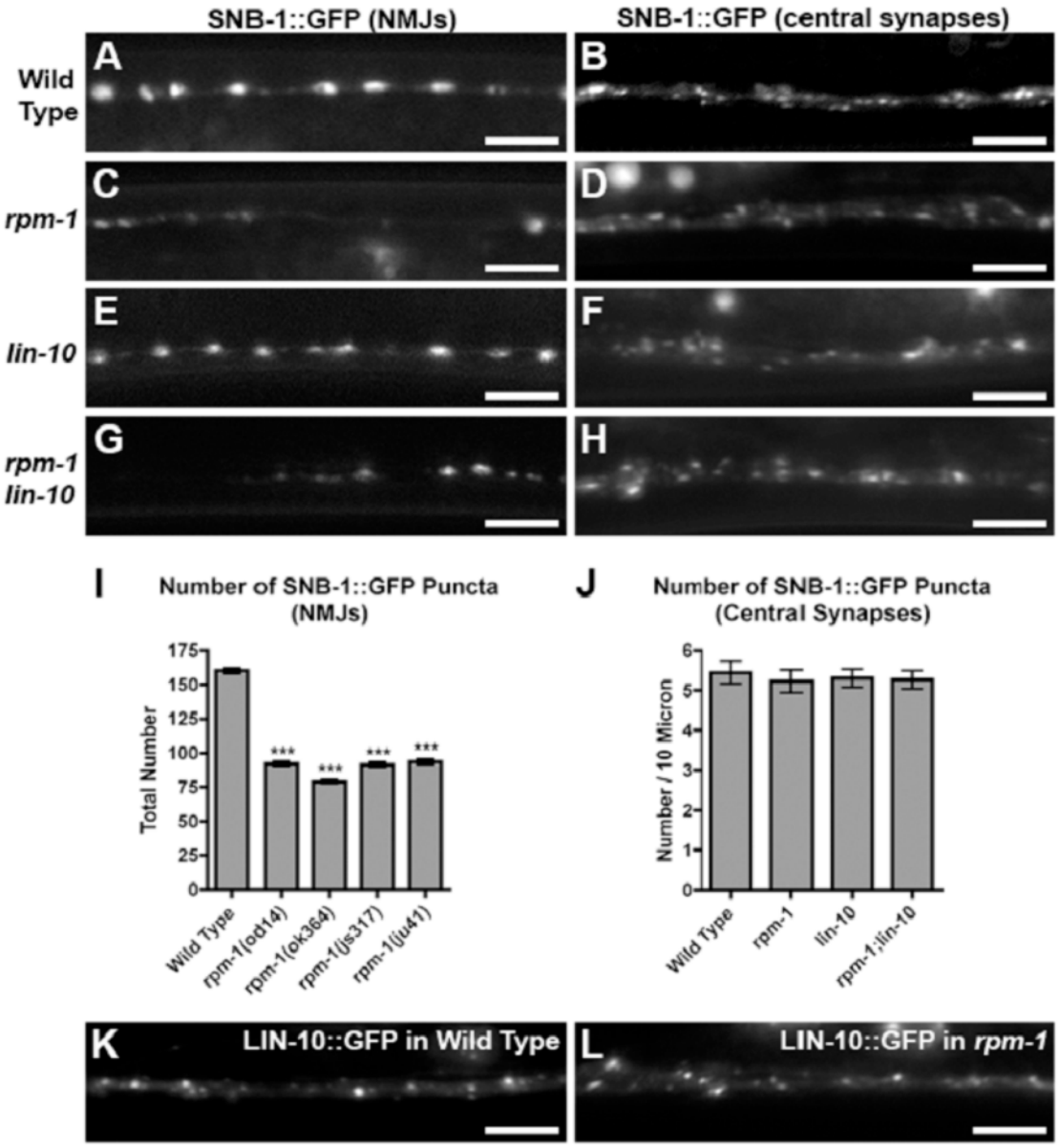
SNB-1::GFP (NMJs)
SNB-1::GFP (central synapses)
Wild Type
rpm-1
lin-10
rpm-1 lin-10
A
B
C
D
E
F
G
H
I
Number of SNB-1::GFP Puncta (NMJs)
Total Number
175
150
125
100
75
50
25
0
***
***
***
Wild Type
rpm-1(ed14)
rpm-1(ok364)
rpm-1(js317)
rpm-1(ju41)
J
Number of SNB-1::GFP Puncta (Central Synapses)
Number / 10 Micron
6
5
4
3
2
1
0
Wild Type
rpm-1
lin-10
rpm-1;lin-10
K
LIN-10::GFP in Wild Type
L
LIN-10::GFP in rpm-1

Figure 3-3. The PMK-3 / p38 MAPK pathway modulates GLR-1 trafficking.

GLR-1::GFP fluorescence was observed along ventral cord dendrites of (A) *pmk-3* mutants, (B) *pmk-3 lin-10* double mutants, (C) *pmk-3 rpm-1* double mutants, (D) *pmk-3 rpm-1 lin-10* triple mutants, (E) *lin-10* mutants that express a wild-type *pmk-3* cDNA using the *glr-1* promoter, or (F) *lin-10* mutants that express a wild-type *dlk-1* cDNA using the *glr-1* promoter. Arrowheads indicate the accumulation of GLR-1::GFP in small accretions. Arrows indicate accumulation in large accretions (similar to those found in *lin-10 rpm-1* double mutants). (G,H,I,J) The mean size of fluorescent structures (puncta) is plotted for adult nematodes of the given genotype. (K,L) The mean number of spontaneous reversals of locomotion for adult animals is plotted for the given genotype. Bar, 5 μm. Error bars are SEM. N=15-20 animals for each genotype. ***P<0.001 by ANOVA followed by a Bonferroni Multiple Comparison test (indicated by line).

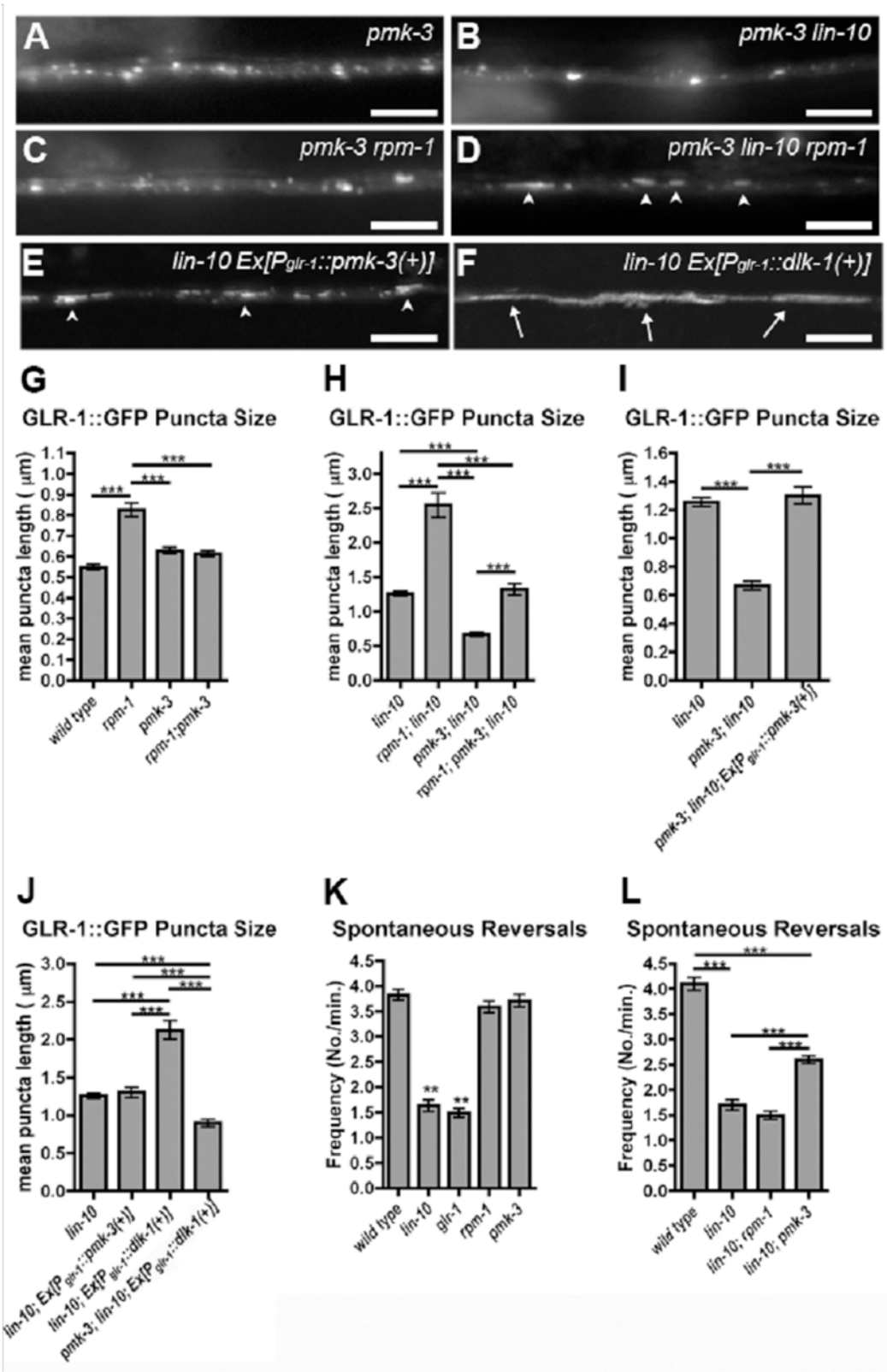
A
pmk-3
B
pmk-3 lin-10
C
pmk-3 rpm-1
D
pmk-3 lin-10 rpm-1
E
lin-10 Ex[Pglr-1::pmk-3(+)]
F
lin-10 Ex[Pglr-1::dlk-1(+)]
G
GLR-1::GFP Puncta Size
mean puncta length (μm)
wild type
rpm-1
pmk-3
rpm-1;pmk-3
H
GLR-1::GFP Puncta Size
mean puncta length (μm)
lin-10
rpm-1; lin-10
pmk-3; lin-10
rpm-1; pmk-3; lin-10
I
GLR-1::GFP Puncta Size
mean puncta length (μm)
lin-10
pmk-3; lin-10
pmk-3; lin-10; Ex[Pglr-1::pmk-3(+)]
J
GLR-1::GFP Puncta Size
mean puncta length (μm)
lin-10
lin-10; Ex[Pglr-1::pmk-3(+)]
lin-10; Ex[Pglr-1::dlk-1(+)]
pmk-3; lin-10; Ex[Pglr-1::dlk-1(+)]
K
Spontaneous Reversals
Frequency (No./min.)
wild type
lin-10
glr-1
rpm-1
pmk-3
L
Spontaneous Reversals
Frequency (No./min.)
wild type
lin-10
lin-10; rpm-1
lin-10; pmk-3

Figure 3-4. RPM-1 regulates DLK-1 levels in interneurons.

(A,B) GLR-1::GFP or (C,D) RFP::PMK-3 fluorescence was observed in (A,C) the neuron cell bodies and (B,D) the ventral cord neurites of wild-type animals. (E,F) Merge images. GFP::DLK-1 fluorescence from the same transgenic line was observed in (G,I) the neuron cell bodies and (H,J) the ventral cord neurites of (G,H) wild-type animals and (I,J) *rpm-1* mutants. Arrows indicate puncta of GFP::DLK-1. The mean (white bars) and maximum (gray bars) GFP::DLK-1 fluorescence intensity for (K) neuron cell bodies and (L) ventral cord neurites is plotted for adult nematodes of the indicated genotype. Error bars are SEM. N=20-25 animals for each genotype. ***P<0.0001 by t test, comparing *rpm-1* mutants to wild type for either mean or maximum intensity values.

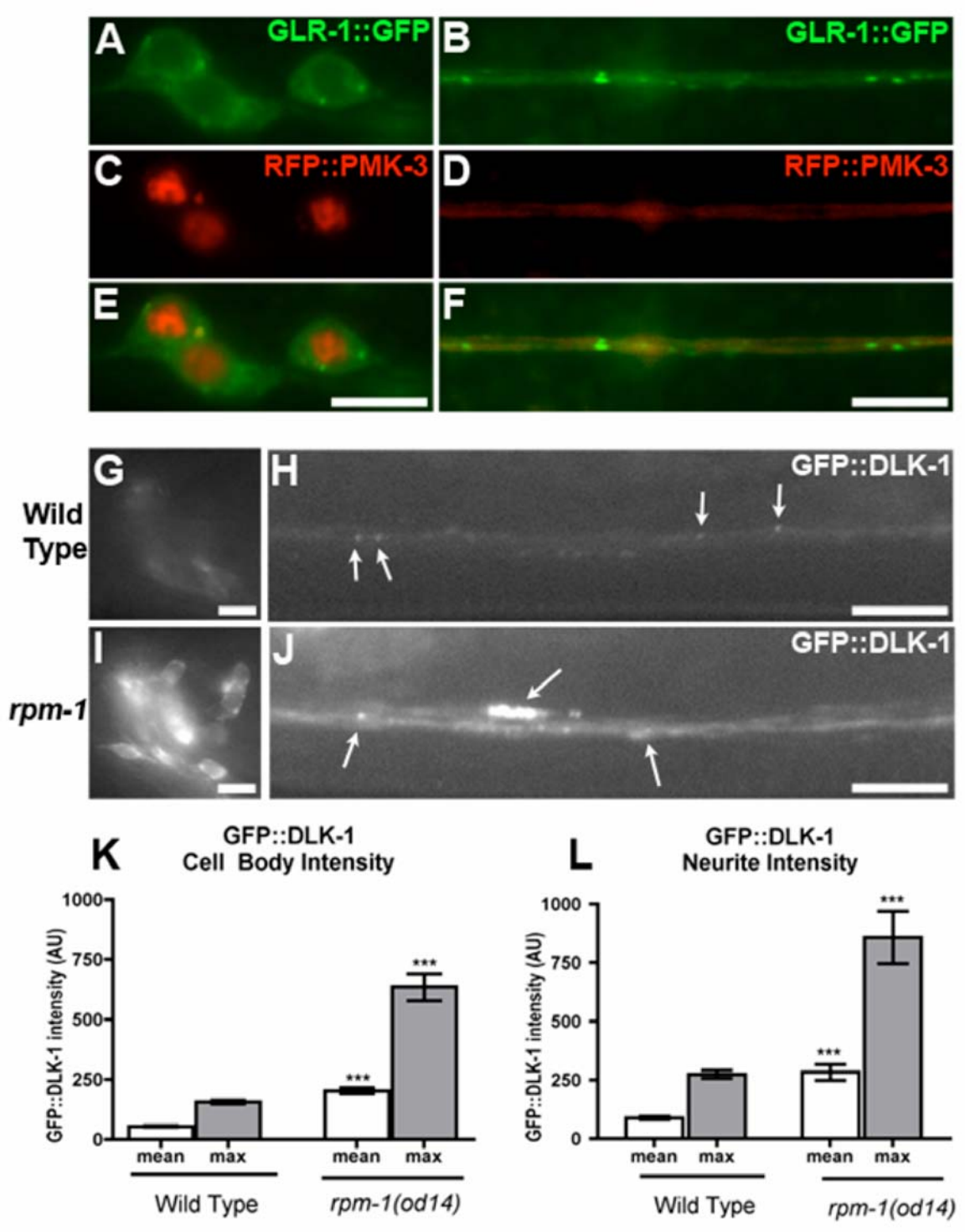
A
GLR-1::GFP
B
GLR-1::GFP
C
RFP::PMK-3
D
RFP::PMK-3
E
F
Wild Type
G
H
GFP::DLK-1
rpm-1
I
J
GFP::DLK-1
K
GFP::DLK-1
Cell Body Intensity
GFP::DLK-1 intensity (AU)
1000
750
500
250
0
***
***
mean
max
mean
max
Wild Type
rpm-1(od14)
L
GFP::DLK-1
Neurite Intensity
GFP::DLK-1 intensity (AU)
1000
750
500
250
0
***
***
mean
max
mean
max
Wild Type
rpm-1(od14)

Figure 3-5. RPM-1 is required for the ubiquitin-mediated turnover of GLR-1.

GLR-1::GFP fluorescence was observed along ventral cord dendrites of (A) wild-type animals, (B) *lin-10* mutants, (C) *rpm-1* mutants, or (D) *rpm-1 lin-10* double mutants, all of which also express ubiquitin from the *nuIs89* transgene. The mean size (E) and the mean number (F) of fluorescent structures (puncta) are plotted for adult nematodes of the given genotype. Bar, 5 μm. Error bars are SEM. N=15-20 animals for each genotype. *P<0.05, ***P<0.001 by ANOVA followed by a Bonferroni Multiple Comparison test (indicated by line). ##P<0.001 by ANOVA followed by Dunnett's Multiple Comparison to wild type.

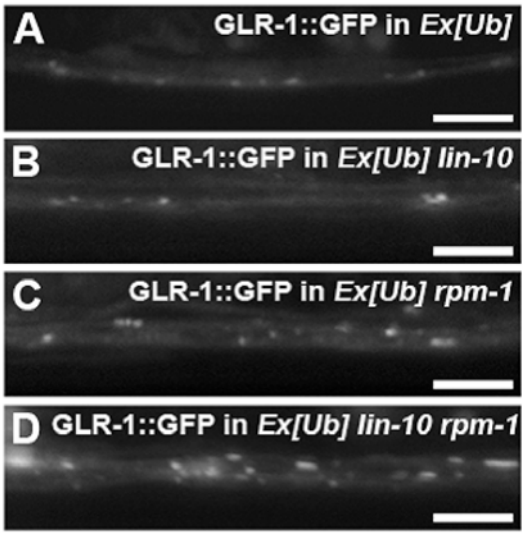
A
GLR-1::GFP in Ex[Ub]
B
GLR-1::GFP in Ex[Ub] lin-10
C
GLR-1::GFP in Ex[Ub] rpm-1
D
GLR-1::GFP in Ex[Ub] lin-10 rpm-1

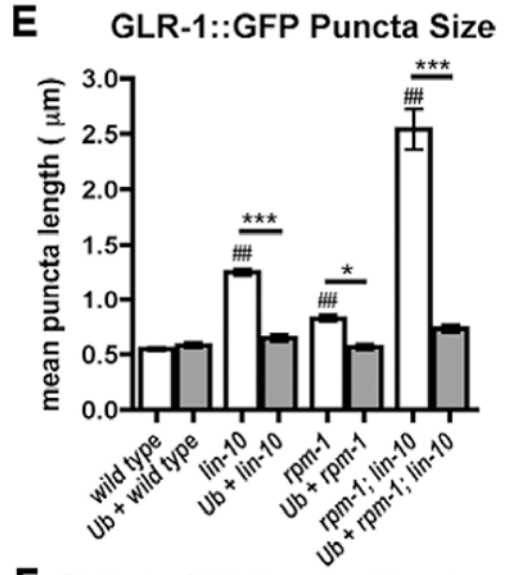
E
GLR-1::GFP Puncta Size
mean puncta length (μm)
3.0
2.5
2.0
1.5
1.0
0.5
0.0
***
##
*
wild type
Ub + wild type
lin-10
Ub + lin-10
rpm-1
Ub + rpm-1
rpm-1; lin-10
Ub + rpm-1; lin-10

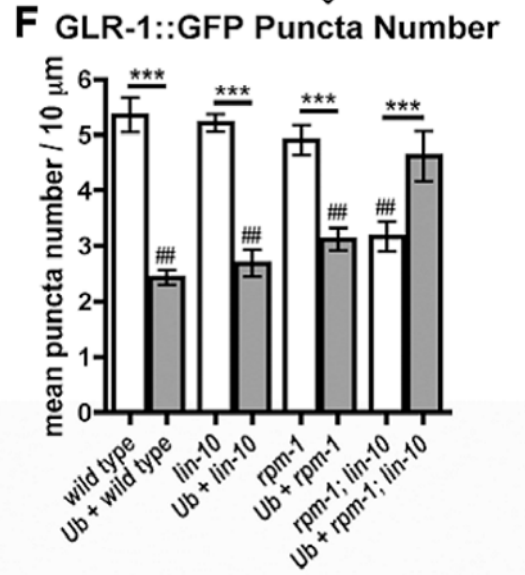
F
GLR-1::GFP Puncta Number
mean puncta number / 10 μm
6
5
4
3
2
1
0
***
##
wild type
Ub + wild type
lin-10
Ub + lin-10
rpm-1
Ub + rpm-1
rpm-1; lin-10
Ub + rpm-1; lin-10

Figure 3-6. **GLR-1(4KR) occludes the effect of RPM-1 on GLR-1 localization**

GLR-1::GFP fluorescence was observed along ventral cord dendrites of (A) wild-type animals, (B) *GLR-1(4KR)*, (C) *rpm-1 GLR-1(4KR)* mutants, or (D) *pmk-3 GLR-1(4KR)* mutants. The mean size of fluorescent structures (puncta) are plotted for L4 or young adult nematodes of the given genotype (E). Arrow heads denote GLR-1 accretion. Bar, 10 μm. Error bars are SEM. N=15-18 animals for each genotype. ANOVA followed by a Bonferroni Multiple Comparison test (indicated by solid line).

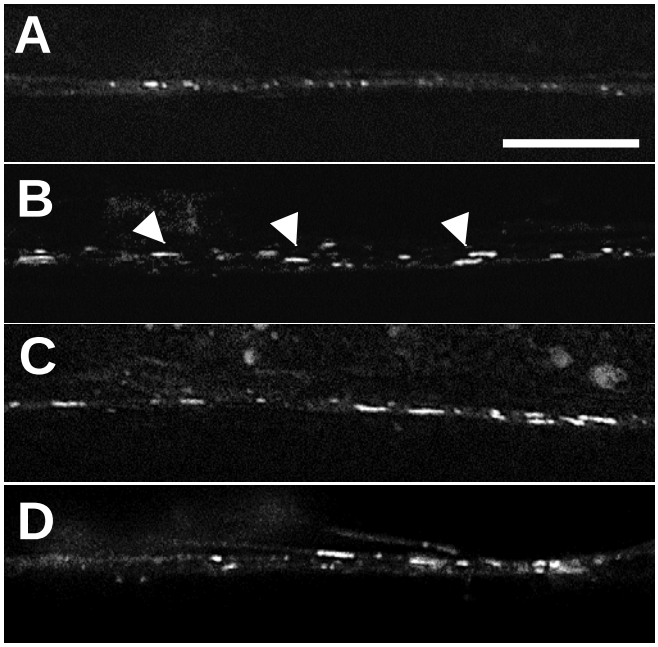
A
B
C
D

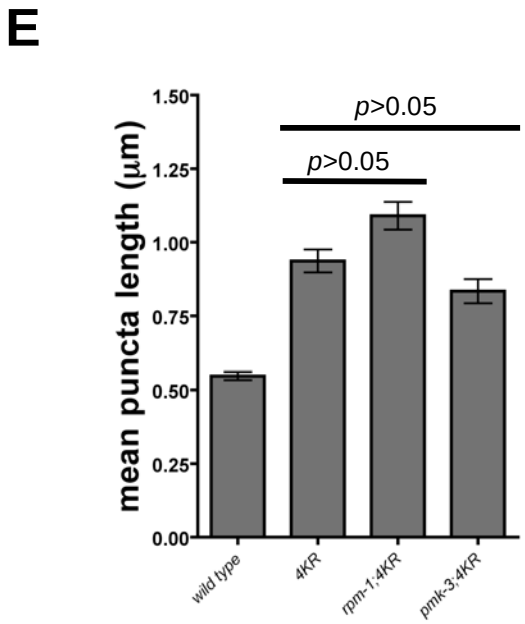
E
mean puncta length (μm)
1.50
1.25
1.00
0.75
0.50
0.25
0.00
p>0.05
p>0.05
wild type
4KR
rpm-1;4KR
pmk-3;4KR

Figure 3-7. RPM-1 regulates GLR-1 endocytosis.

(A,B,C,D,F) The mean size of fluorescent structures (puncta and accretions) and (E,G) the mean reversal frequency is plotted for adult nematodes of the given genotype. (A) Decreased or (B) increased endocytosis suppresses or enhances the accumulation of GLR-1 in *lin-10* mutants, respectively. Decreased endocytosis, either by (C) *unc-11* mutation or (D,E) expression of *rab-5(GDP)*, can both mimic and occlude the effect of *pmk-3* mutations on GLR-1 trafficking. (F,G) Expression of *rab-5(GTP)* can block the effect of *pmk-3* mutations, thus bypassing the requirement for PMK-3. Error bars are SEM. N=15-20 animals for each genotype. **P<0.01, ***P<0.001 by ANOVA followed by a Bonferroni Multiple Comparison test (indicated by solid line). Not all comparisons to the "wild type" genotype are shown on the graphs due to space restrictions.

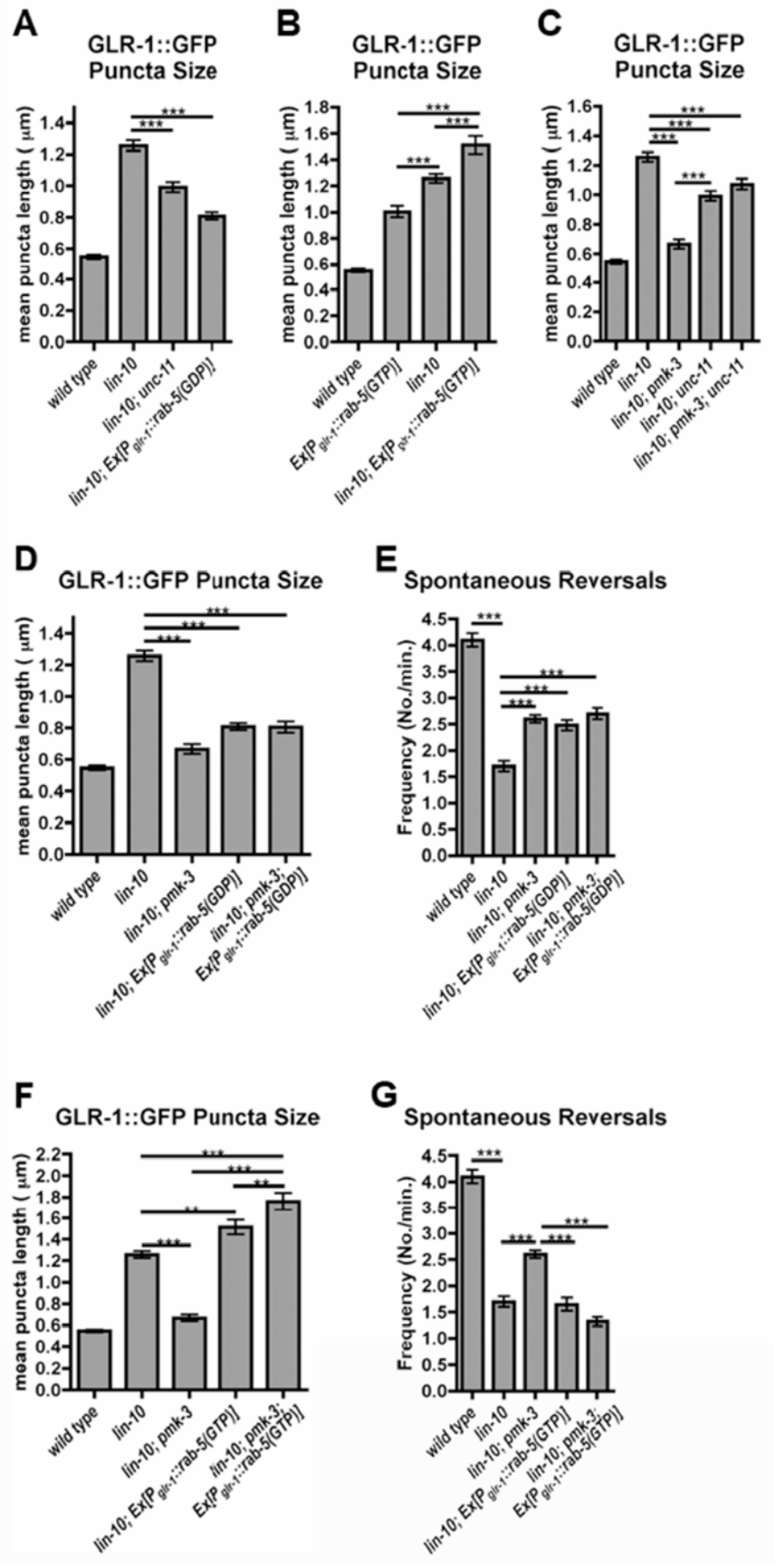
A
GLR-1::GFP Puncta Size
mean puncta length (μm)
wild type
lin-10
lin-10; unc-11
lin-10; Ex[Pglr-1::rab-5(GDP)]
B
GLR-1::GFP Puncta Size
mean puncta length (μm)
wild type
Ex[Pglr-1::rab-5(GTP)]
lin-10
lin-10; Ex[Pglr-1::rab-5(GTP)]
C
GLR-1::GFP Puncta Size
mean puncta length (μm)
wild type
lin-10
lin-10; pmk-3
lin-10; unc-11
lin-10; pmk-3; unc-11
D
GLR-1::GFP Puncta Size
mean puncta length (μm)
wild type
lin-10
lin-10; pmk-3
lin-10; Ex[Pglr-1::rab-5(GDP)]
lin-10; pmk-3; Ex[Pglr-1::rab-5(GDP)]
E
Spontaneous Reversals
Frequency (No./min.)
wild type
lin-10
lin-10; pmk-3
lin-10; Ex[Pglr-1::rab-5(GDP)]
lin-10; pmk-3; Ex[Pglr-1::rab-5(GDP)]
F
GLR-1::GFP Puncta Size
mean puncta length (μm)
wild type
lin-10
lin-10; pmk-3
lin-10; Ex[Pglr-1::rab-5(GTP)]
lin-10; pmk-3; Ex[Pglr-1::rab-5(GTP)]
G
Spontaneous Reversals
Frequency (No./min.)
wild type
lin-10
lin-10; pmk-3
lin-10; Ex[Pglr-1::rab-5(GTP)]
lin-10; pmk-3; Ex[Pglr-1::rab-5(GTP)]

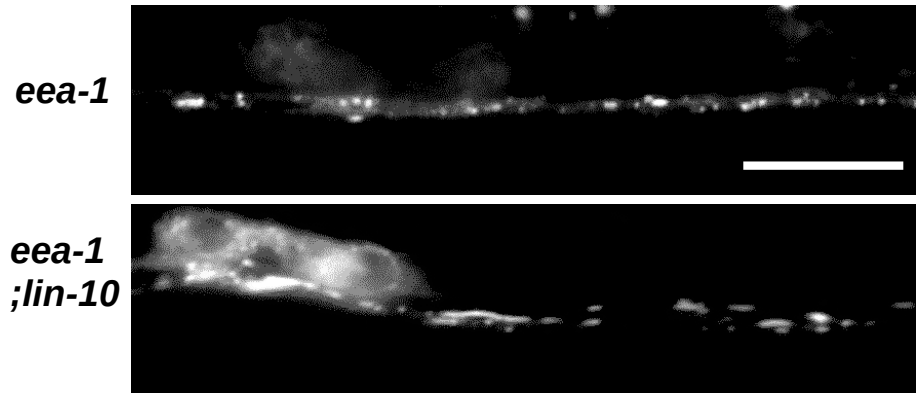

Figure 3-8. Mutation in EEA-1 does not affect GLR-1 localization.

GLR-1::GFP fluorescence was observed along ventral cord dendrites of *eea-1* and *eea-1 lin-10* double mutant background. Bar, 10 μm.

Figure 3-9. A model for the regulation of GLR-1 AMPAR trafficking by PMK-3 and RPM-1.

GLR-1 (gray channels) endocytosis can occur via clathrin (pit indicated to left of the synapse). Gray arrows indicate major trafficking steps, positively regulated by the factor(s) indicated next to the arrows. Black arrows indicate positive (stimulatory) genetic regulatory interactions between two factors. GLR-1 endocytosis is mediated by UNC-11/AP180 and RAB-5. Once endocytosed, receptors can either be recycled to the synapse in a step requiring LIN-10, or degraded. PMK-3/p38 MAPK stimulates GLR-1 endocytosis via RAB-5 activation. PMK-3 is activated by a MAP kinase cascade, which includes MKK-4 and DLK-1. RPM-1 and FSN-1, working as an E3 ligase, negatively regulate DLK-1 (and hence p38 MAPK signaling) by ubiquitin-mediated turnover.

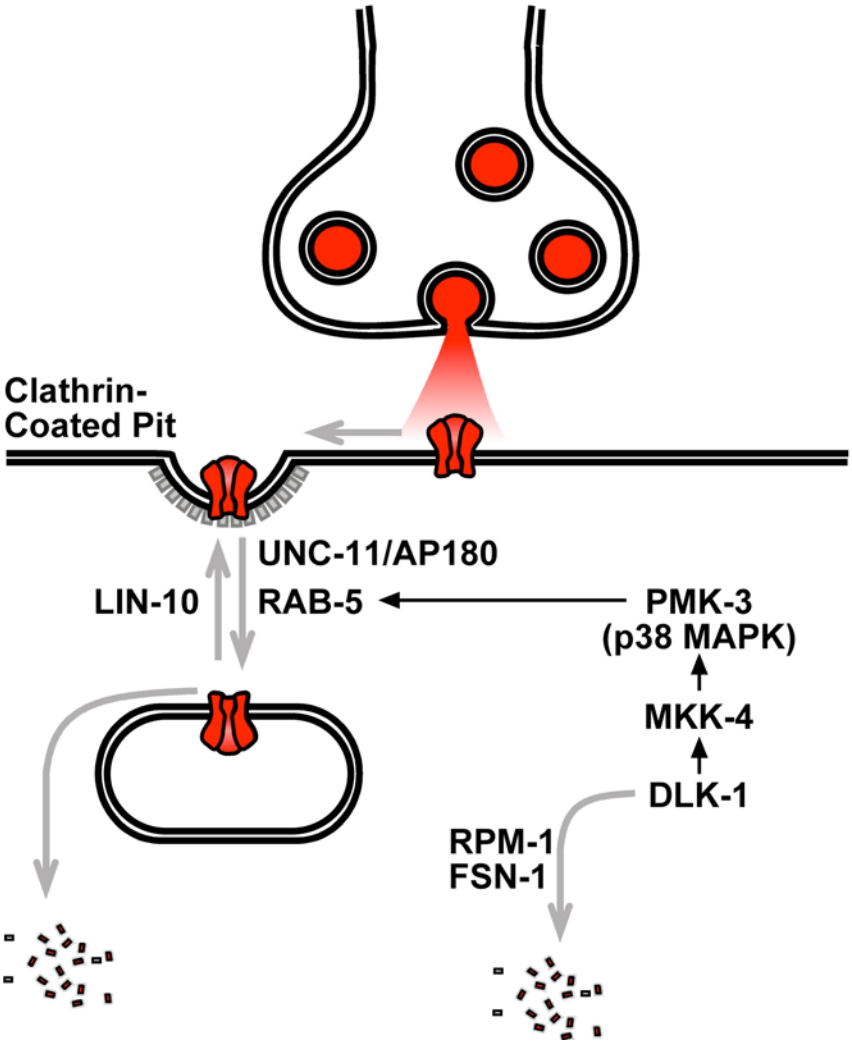
Clathrin-
Coated Pit
UNC-11/AP180
LIN-10
RAB-5
PMK-3
(p38 MAPK)
MKK-4
DLK-1
RPM-1
FSN-1

CHAPTER IV

OTHER COMPONENTS OF MAPK SIGNALING PATHWAYS IN GLR-1 TRAFFICKING

ABSTRACT

Regulated trafficking of AMPA receptors at synapses during synaptic plasticity requires the involvement of signaling cascades. In mammals, the Ras family small GTPases Ras, Rap1, and Rap2, as well as their downstream MAPK pathways, play a role in LTP, depotentiation, and LTD, respectively. The exact role of these factors remains to be elucidated. By the benefit of *C. elegans* genetics, we found that mutations in *rap-1* suppress the GLR-1 defects in *lin-10* mutants, suggesting that *rap-1* could play a role in the endocytosis pathway of GLR-1. We also found that the MAPKKs *jkk-1, sek-1,* and *mkk-4* are involved in GLR-1 trafficking. Mutants for *mkk-4* suppress the GLR-1 localization defects of *rpm-1,* but do not suppress *lin-10*. By contrast, *jkk-1* mutants suppress the GLR-1 localization defects of *lin-10*. Mutations in *sek-1* accumulate GLR-1 puncta like *rpm-1* mutants along their neurites; also, *sek-1* mutants additively increase the GLR-1 puncta size of *lin-10,* indicating that *sek-1* also regulates GLR-1 trafficking.

These results suggest that multiple MAPK pathways are involved in vivo for GLR-1 localization in *C. elegans*. In particular, suppression of the GLR-1 accretion of *lin-10* mutants by *jkk-1* or *rap-1* mutations might add more mechanistic explanations for the involvement of MAPK signaling in GLR-1 receptor endocytosis, recycling, or degradation.

INTRODUCTION

Considering the complex processes of regulated AMPA receptor trafficking, the issue of the signaling pathways that control the trafficking processes is beginning to emerge. The involvement of several MAPK signaling pathways in the activity dependent, NMDA receptor mediated AMPA receptor trafficking was already described briefly in Chapter I. However, questions still remain. For example, what are the upstream and downstream targets of MAPK pathways? How does a single synapse differentiate multiple signaling pathways for AMPA receptor trafficking? How much cross talk in signaling components exist in regulating AMPA receptor trafficking? To address several unsolved questions, *C. elegans*, with the advantages of the simple neural circuits and powerful genetics, is an attractive model organism.

Multiple MAPK signaling pathways have been identified in *C. elegans* (summarized in Figure 4-1). There is a single ERK1/2 ortholog in *C. elegans*, called *mpk-1*, which was originally characterized for its role in EGFR signaling and vulval induction (Lackner et al., 1994). There are two clear JNK orthologs in *C. elegans*, *jnk-1* and *kgb-1*, which were originally characterized for their roles in synaptic vesicle trafficking and stress response, respectively (Berman et al., 2001; Byrd et al., 2001; Kimble et al., 1982; Mizuno et al., 2004). There are three p38 MAPK orthologs in *C. elegans*: *pmk-1, pmk-2,* and *pmk-3* (Berman et al., 2001; Nakata et al., 2005; Wyszynski et al., 2002). All three genes are part of an operon regulated by a single promoter, showing expression in neurons and other tissues.

Five orthologs of MAPKKs have been identified in *C. elegans*: *mek-2, jkk-1, mek-1, sek-1*, and *mkk-4*. The MEK2 homolog MEK-2 activates the ERK1/2 homolog MPK-1 during vulval induction (Lackner and Kim, 1998; Lackner et al., 1994; Wu et al., 1995). JKK-1 and MEK-1 are homologs of mammalian MKK7 (Kawasaki et al., 1999b; Koga et al., 2000). JKK-1, an activator of JNK-1, is expressed in almost all neurons of *C. elegans*. Null mutants of *jkk-1* and *jnk-1* are defective in coordinated locomotion and mislocalize presynaptic vesicle markers in the DD motor neurons (Byrd et al., 2001; Kawasaki et al., 1999b; Villanueva et al., 2001). Interestingly, mutants for *unc-16*, a homolog of murine JNK-signaling scaffolding protein JIP3/JSAP, accumulate GLR-1, implicating involvement of JNK-signaling in AMPA receptor trafficking in *C. elegans* (Byrd et al., 2001). The other MKK7 homolog, MEK-1, is activated by MLK-1(MAPKKK), and activates KGB-1 (a JNK-like MAPK) in a stress response to cadmium and copper stress (Koga et al., 2000; Mizuno et al., 2004). Null mutants of *jnk-1* also show hypersensitivity to heavy metal stress, similar to *mek-1* mutants (Villanueva et al., 2001). MEK-1 also activates PMK-1 in pathogen-induced immune response (Kim et al., 2004). The MKK3/6 homolog SEK-1, which is activated by NSY-1 (a MAPKKK), activates PMK-1 (p38 MAPK) during innate immunity against pathogens *Pseudomonas aeruginosa* (Kim et al., 2002). Therefore, the activation of PMK-1 against pathogens includes two different upstream MAPKKs, MEK-1 and SEK-1. Also, the NSY-1–SEK-1 cascade is known to be activated by Ca^{2+} through CaMKII to control AWC cell fate decision for STR-2 (odorant receptor) expression (Tanaka-Hino et al., 2002). The MKK4/SEK1 homolog MKK-4, which is activated by DLK-1, is upstream of PMK-3 p38 MAPK, and is required for the proper localization of presynaptic components in

GABAergic motor neurons (Nakata et al., 2005). By yeast two–hybrid screening, JKK-1 was found to interact with PMK-2 p38 MAPK. Also, deletion mutants of *pmk-2* and *zak-1* (MAPKKK) show growth arrest at the L1 larval stage due to a severe feeding defect. Therefore, ZAK-1-JKK-1-PMK-2 is also a possible p38 MAPK cascade (Hisamoto et al., 2003 worm meeting).

Thus, there is cross talk at the level of MAPKKs in activating downstream targets, the MAPKs, which supports previous studies suggesting that at least two MAPKKs can function as activators of a MAPK (Kyriakis and Avruch, 2001).

As already reviewed in Chapter I, the small GTPases Ras and Rap work upstream of MAPK pathways in regulating AMPA receptor trafficking for LTP and LTD in mammals. *C. elegans* has three orthologs of Ras, *let-60(K-Ras), ras-1(R-Ras),* and *ras-2(M-Ras)*. *let-60* has been widely studied to function upstream of the *mpk-1* Erk1/2 pathway for vulval induction (Han et al., 1993; Lackner et al., 1994; Sternberg et al., 1993; Szewczyk et al., 2002; Wu et al., 1995). However, the function of *ras-1* and *ras-2* are enigmatic in *C. elegans*. There are three *C. elegans* orthologs of Rap, *rap-1(Rap1b), rap-2(Rap2a), and rap-3(Rap1a).* Null mutant animals of *rap-1* show slightly abnormal morphology and function of hypodermal cells, whereas *rap-2* mutants do not have any visible defects. However, the phenotypes of double mutants for *rap-1* and *rap-2* are similar to those of their upstream modulator, *pxf-1* (Ras-GEF) in terms viability and hypodermal morphology, implicating a functional redundancy of *rap-1* and *rap-2* in the hypodermis (Pellis-van Berkel et al., 2005). Interestingly, PXF-1 is expressed in head neurons and the ventral nerve cord, implicating its role in the *C. elegans* nervous system (Pellis-van Berkel et al., 2005). RAP-3 functions are so far unknown.

To further elucidate the MAPK pathways for AMPA receptor trafficking, we have investigated the mutants of MAPKKs, where lots of cross talk has been identified, for GLR-1 localization defects. In this chapter, we describe the results of our observation for GLR-1 localization in the MAPKK mutant animals in combination with *lin-10* and/or *rpm-1* mutant backgrounds. Furthermore, by observing the effect of mutations in Ras family proteins on GLR-1 localization in wild-type and *lin-10* mutant backgrounds, we show that *rap-1* suppresses the GLR-1 localization defects of *lin-10*, similar to the effect of *pmk-3* mutations, implicating that *rap-1* might function upstream of *pmk-3*.

MATERIAL AND METHODS

Standard methods were used to culture *C. elegans*. Animals were grown at 20^{o}C on standard NGM plates seeded with OP50 *E. coli*. Some strains were provided by the *Caenorhabditis* Genetics Center. The following strains were used: N2, *lin-10(e1439), nuIs25[GLR-1::GFP], mek-1(ks54), jkk-1(km2), sek-1(km4), mkk-4(ju91), dlk-1(ju476), rpm-1(od14), ras-1(gk237), ras-2(ok682), rap-1(pk2082), rap-2(gk11),* and *let-60(n1046).*

Confirming Mutant Strains

Animals were lysed in worm lysis buffer (50 mM KCl, 10 mM Tris-HCl pH8.3, 2.5 mM $MgCl_2$, 0.45% NP-40, 0.45% Tween 20, 0.01% gelatine, freshly added 60 μg/ml proteinase K) at 60 ^{o}C for 60 min, followed by 95 ^{o}C for 15 min. PCR was carried out by

adding 5 μl of the worm-lysed solution into total 50 μl of PCR reaction mixture. Takara *ExTaq*^{TM} polymerase was used for PCR. PCR conditions were as manufacture's protocol provided. Double or triple mutants have been generated to see the genetic interaction of interested genes. To confirm *dlk-1(ju476)*, an insertion mutation adding 5 tandem repeat nucleotides at glycine 631 position of the DNA, primers tcagaaatcctacgcaacgacg (DLK-1_5) and gtataaccctgactccgcccattt (DLK-1_3) were used. To confirm *mkk-4(ju91)*, a missense mutation altering glycine 265 to an arginine, primers gtcagccgtatcttgcagtaagtg (MKK-4_5') and cttagcctcttcaatttcgggtcc (MKK-4_3') were used. To confirm *rap-1(pk2082)*, a nonsense mutation converting glutamine 130 to amber stop codon, primers tcaggagcaattcacagcgatg (C27B7.8_F) and cacgggttcgagcatgacaaaa (C27B7.8_R) were used. Sequencing of the PCR products from the primers of *dlk-1*, *mkk-4*, and *rap-1* were sent to GENEWIZ Inc. (South Plainfield, NJ) for sequencing. For *jkk-1(km2)*, a deletion mutation deleting 970bp from the genomic DNA, primers tcgatagctgtgtgtgtcttgc (jkk-1_5) and gtgaactggaagcaaccgagaa (jkk-1_3) were used. To confirm *sek-1(km4)*, a deletion mutation deleting 2084bp from the genomic DNA, primers cgacacactgattgccttttgg (sek-1_5) and gtgggggatggttggtgtaatt (sek-1_3) were used. Size of PCR products from the primers for *jkk-1(km2)* and *sek-1(km4)* were examined by running on agarose gel (1%).

Fluorescence Microscopy

L4 to young adult stage of worms (n=30-50) were mounted on 2% agarose pads with 10 mM levamisole. Fluorescent images were observed using a Zeiss Axioplan II. A 100X

(Numerical Aperture = 1.4) PlanApo objective was used to detect GFP signal. Imaging was done with an ORCA charge-coupled device (CCD) camera (Hamamatsu, Bridgewater, NJ) using IPLab software (Scanalytics, Inc, Fairfax, VA). Exposure times were chosen to fill the 12-bit dynamic range without saturation. Maximum intensity projections of z-series stacks were obtained and out-of-focus light was removed with a constrained iterative deconvolution algorithm.

RESULTS

To further examine what components of MAPK signaling pathways are involved in GLR-1 trafficking, we observed GLR-1::GFP in the known mutant backgrounds for MAPKKs that activate JNK and P38 MAPK: *mek-1, jkk-1, sek-1, and mkk-4.* Also, to examine the genetic interaction of these genes with *lin-10* and *rpm-1,* we have generated each MAPKK mutant in combination with *lin-10* and/or *rpm-1* mutations (Table 4-1). Additionally, we examined the genetic interaction of *lin-10* and/or *rpm-1* with *dlk-1*(MAPKKK). From these mutants, although we failed to observe any phenotypic effect of *mek-1* mutations, we found interesting results as follows.

MKK-4 (or DLK-1) Loss of Function Mutants Suppress *rpm-1 lin-10* Double Mutants, But Not *lin-10* Single Mutants, for GLR-1 Localization Defects.

Previous studies suggested that the DLK-1(MAPKKK)-MKK-4(MAPKK)-PMK-3(P38 MAPK) signaling pathway regulates presynaptic morphology, and against this pathway

RPM-1, a ubiquitin ligase, functions as a negative regulator by ubiquitinating DLK-1 for degradation (Nakata et al., 2005). We found that the PMK-3 p38 MAPK pathway also regulates postsynaptic GLR-1 endocytosis as mutations in *pmk-3* suppress GLR-1 localization defects in *lin-10* mutants. Moreover, RPM-1 negatively regulates this pathway by regulating the abundance of DLK-1 (Chapter III). To know additionally the effect of genetic interactions of this pathway on GLR-1 localization, we examined *mkk-4* mutants, *mkk-4 lin-10* double mutants, and *mkk-4 rpm-1 lin-10* triple mutants. Also, we examined *dlk-1* mutants, *dlk-1 rpm-1* double mutants, *dlk-1 lin-10* double mutants, and *dlk-1 rpm-1 lin-10* triple mutants to test the effect of upstream of *mkk-4* on GLR-1 localization. Interestingly, we found that the mutants of *mkk-4* or *dlk-1*, by themselves, showed normal GLR-1 puncta phenotype (Figure 4-2A, 4-3A), and did not suppress GLR-1 internal accumulation in *lin-10* mutants, unlike *pmk-3* mutants (Figure 4-2B, 4-3B). However, the huge accumulation of GLR-1::GFP observed in *rpm-1 lin-10* double mutants was suppressed by *mkk-4* or *dlk-1* mutations (Figure 4-2C, 4-3D). We also observed that the GLR-1 accretions observed in *rpm-1* single mutants were suppressed by *dlk-1* mutations (Figure 4-3C). Interestingly, we found also that *mkk-4* or *dlk-1* mutations suppressed the neurite outgrowth defects of GLR-1 neurons observed in *rpm-1* mutants (Appendix III), supporting functional negative relationship between *mkk-4* (or *dlk-1) and rpm-1* in GLR-1 expressing neurons. These results indicate that, although PMK-3 p38 MAPK cascade regulates GLR-1 endocytosis and DLK-1 functions upstream of PMK-3 (Chapter III), other MAPK signaling components upstream of PMK-3 might function redundantly in *C. elegans* for GLR-1 endocytosis.

Loss of Function of JKK-1 Suppresses GLR-1 Localization Defects of *lin-10* Mutants

jkk-1 mutations did not affect GLR-1 localization (Figure 4-4A); however, *jkk-1* suppressed GLR-1 localization defects of *lin-10* (Figure 4-4B) similar to *pmk-3* mutations. Also, the GLR-1 defects of *rpm-1 lin-10* double mutants were suppressed by *jkk-1* mutations (Figure 4-4C), further supporting the suppression of the *lin-10* GLR-1 phenotype by *jkk-1* mutations. Because we didn't test whether GLR-1 accumulation observed in *rpm-1* mutants could be suppressed by *jkk-1* mutations, at this stage we don't know whether the MAPK cascade mediated by *jkk-1* also genetically interacts with *rpm-1*. However, our finding that *jkk-1* mutations suppress *lin-10* mutations, together with our observation that *mkk-4* mutations suppress *rpm-1* mutants but not *lin-10* mutations, and that *pmk-3* suppresses both *rpm-1* and *lin-10* mutations, implicates the involvement of another MAPK cascade component, JKK-1, on activating PMK-3 p38 MAPK for the regulation of GLR-1 endocytosis in postsynaptic neurons.

GLR-1 Accumulation by the Loss of Function Mutants of SEK-1

Previous studies suggest that the NSY-1/ASK-1(MAPKKK)-SEK-1(MAPKK)-PMK-1 (p38 MAPK) cascade functions against pathogen induced stress and for a neuronal cell fate decision(Kim et al., 2002; Tanaka-Hino et al., 2002). To investigate whether the same pathway has a role in GLR-1 trafficking, we have examined *sek-1* mutants as an initial approach for this pathway. Interestingly, GLR-1::GFP puncta in *sek-1* single mutants are larger than that of wild-type puncta (Figure 4-5A). *sek-1 lin-10* mutants additively increase the size of GLR-1 puncta (Figure 4-5B). The size and thickness of

GLR-1 patches in these double mutants were smaller than those of *rpm-1 lin-10* mutants (Chapter III). Therefore, we think that *sek-1* and *lin-10* might function separately in parallel fashion for GLR-1 localization. We also observed the triple mutants of *sek-1, lin-10,* and *rpm-1,* and found that the size and thickness of puncta are similar to that of *lin-10 rpm-1* double (Figure 4-5C). These data implicate that GLR-1 trafficking could also be regulated by a SEK-1 mediated MAPK pathway (possibly through PMK-1 p38 MAPK).

RAP-1 Loss of Function Suppresses the GLR-1 Accumulation of *lin-10* Mutants

To examine possible upstream regulators of MAPK pathways, we have observed GLR-1 localization in mutants for the *C. elegans* orthologs of Ras family members, *let-60(gf), ras-1,ras-2, rap-1,* and *rap-2,* by itself or in combination with *lin-10* mutations. Among them, only *rap-1* mutants suppressed the GLR-1 localization defects of *lin-10* mutants. Interestingly *rap-2* mutants on their own showed no visible difference with wild-type GLR-1 localization (Table 4-2; Figure 4-6A,B). Because the Rap1 activation of the p38 MAPK pathway for LTD in mammals has already been reported (Zhu et al., 2002), our observation that *rap-1* mutations, as for *pmk-3* mutations, suppress the GLR-1 phenotype of *lin-10* mutations could implicate the involvement of RAP-1 in regulating the PMK-3 (p38 MAPK) pathway in *C. elegans*.

DISCUSSION

By the benefit of *C. elegans* genetics, we have found that *C. elegans* MAPKKs orthologs, *mkk-4, jkk-1,* and *sek-1,* and the Rap1 ortholog, *rap-1,* regulate GLR-1 trafficking. First, *mkk-4 (or dlk-1)* mutations suppress *rpm-1* mutations but not *lin-10* mutations. Second, *jkk-1* mutations suppress *lin-10* mutations. Third, *sek-1* mutants accumulate GLR-1 and this accumulation is additive with *lin-10* mutations. Fourth, *rap-1* mutations suppress *lin-10* mutations (Table 4-1, 4-2).

The First observation was unexpected because we found that *pmk-3* mutations suppress the GLR-1 localization defects of both *lin-10* and *rpm-1* mutations, and is regulated by DLK-1 for GLR-1 endocytosis (Chapter III). The possible explanation of this intriguing result could be that in *C. elegans* the signal input from DLK-1-MKK-4 cascade to PMK-3 is kept null or low under normal conditions because RPM-1 negatively regulates DLK-1; therefore, the net effect of loss of function mutations in *dlk-1* and *mkk-4* might not contribute to GLR-1 endocytosis through PMK-3.

Could other upstream MAPKKs affect PMK-3 activity for GLR-1 endocytosis under normal conditions? JKK-1 could be one possible candidate for this based upon our result that *jkk-1* mutations suppress the GLR-1 localization defects of *lin-10* mutants. JKK-1 might activate PMK-3, the activity of which would be required for normal constitutive endocytosis of GLR-1. However, an alternative interpretation for the result might also be possible. Because JKK-1 has been known to activate JNK-1(Byrd et al., 2001; Kawasaki et al., 1999b; Villanueva et al., 2001) or PMK-2 (Hisamoto et al., 2003

worm meeting), another MAPK pathway, JKK-1 might function parallel with the PMK-3 mediated pathway for GLR-1 trafficking. To clarify this question further study will be required.

The third observation is that *sek-1* mutants accumulate GLR-1, and that this effect is additive with *lin-10* mutations. This result indicates that PMK-1 (p38 MAPK) might also regulate GLR-1 trafficking in combination with other p38 MAPKs (PMK-3 and/or PMK-2). Indeed, *sek-1* has been known to function upstream of *pmk-1* (Kim et al., 2002; Tanaka-Hino et al., 2002). Also, considering that *rab-10* mutations additively increase the size of GLR-1 puncta in *lin-10* mutants, and because RAB-10 is involved in clathrin independent endocytosis of GLR-1(Glodowski et al., 2007), the easiest explanation for this observation is that SEK-1 dependent MAPK signaling might function in the GLR-1 endocytosis pathway independent of clathrin mediated endocytosis pathway.

Suppression of the GLR-1 localization defects of *lin-10* mutants by *rap-1* mutations indicates that *rap-1* might function upstream of the PMK-3 MAPK cascade as *pmk-3* mutations suppress the *lin-10* phenotype. These results support previous study in mammals that Rap1 functions upstream of p38 MAPK in NMDA receptor mediated LTD (Zhu et al., 2002). We could not detect any effect of *rap-2* mutations on GLR-1 localization in a *lin-10* mutant background. However, previous studies suggest that *rap-1* and *rap-2* function redundantly as when *rap-2* mutations, which on their own give a wild type phenotype, are combined with *rap-1* mutations, there is an enhancement of the defects in hypodermal morphogenesis and function compared to *rap-1* mutants

(Pellis-van Berkel et al., 2005). Therefore, it might be interesting to test the effect of *rap-1 rap-2* double mutants on *lin-10* mutants for GLR-1 localization.

In our pioneering study to screen all of known *C. elegans* MAPKKs orthlogs and Ras family protein orthologs for GLR-1 localization defects, we did not examine the effect of MEK-2, a MAPKK upstream of MPK-1 (ERK), on GLR-1 localization because of our observation that the gain of function mutants of *let-60* (Table 4-2), which is known to function upstream of LIN-45-MEK-2-MPK-1 cascade, do not show any visible GLR-1 localization defects. However, further confirmation by checking the GLR-1 phenotype in MPK-1 cascade mutants is required. Also, we couldn't examine the *rap-3*, mammalian Rap1b ortholog, because mutants for this gene are currently unavailable. However, the experimental approach by RNAi experiments might be possible.

FIGURES

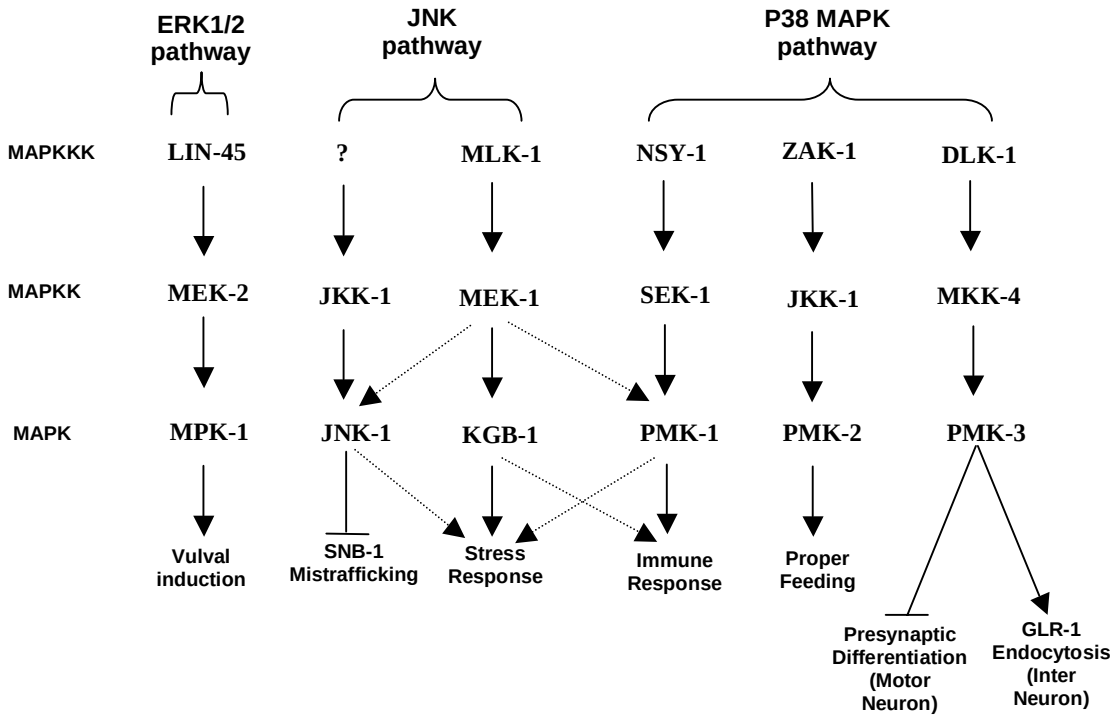

Figure 4-1. Multiple MAPK pathways and their known functions in *C. elegans*. Arrows indicate positive genetic interactions, whereas T bars indicate inhibitory genetic interactions.

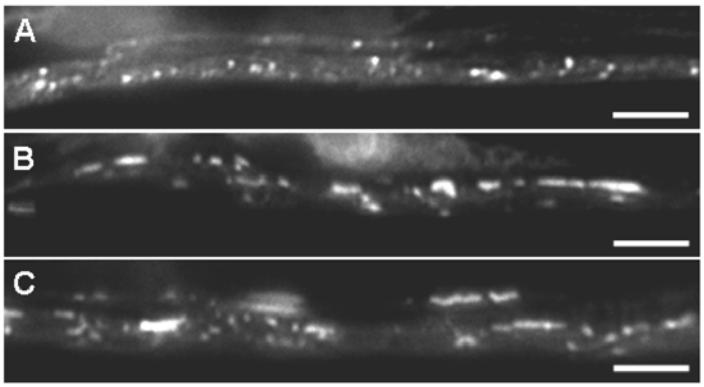

Figure 4-2. Phenotypic suppression of *rpm-1 lin-10* double mutants by MKK-4 loss of function. Microphotographs of GLR-1::GFP fluorescence along ventral cord dendrites of (A) *mkk-4* mutants, (B) *mkk-4 lin-10* double mutants, (C) *mkk-4 rpm-1 lin-10* triple mutants, Bar, 5 μm.

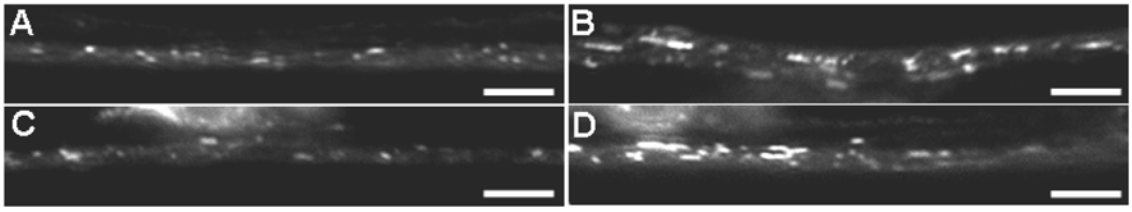

Figure 4-3. Phenotypic suppression of *rpm-1* and *rpm-1 lin-10* double by DLK-1 loss of function. Microphotographs of GLR-1::GFP fluorescence along ventral cord dendrites of (A) *dlk-1* mutants, (B) *dlk-1 lin-10* double mutants, (C) *dlk-1 rpm-1* double mutants, and (D) *dlk-1 rpm-1 lin-10* triple mutants, Bar, 5 μm.

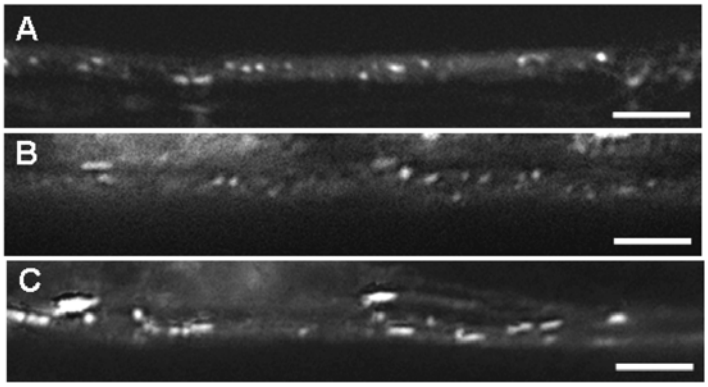

Figure 4-4. Phenotypic suppression of *lin-10* mutants by JKK-1 loss of function.

Microphotographs of GLR-1::GFP fluorescence along ventral cord dendrites of (A) *jkk-1* mutants, (B) *jkk-1 lin-10* double mutants, (C) *jkk-1 rpm-1 lin-10* triple mutants, Bar, 5μm.

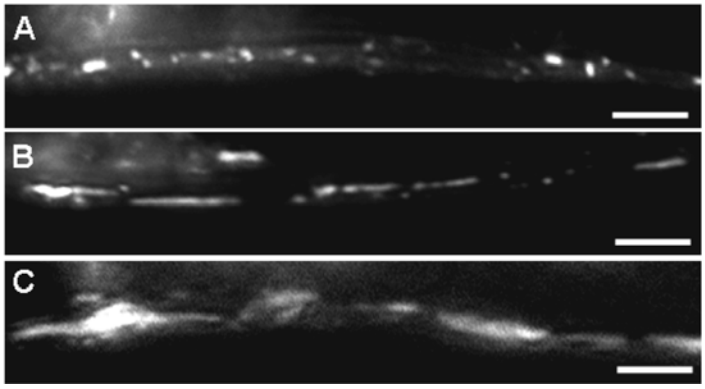

Figure 4-5. *sek-1* regulates GLR-1 localization in parallel with *lin-10*

Microphotographs of GLR-1::GFP fluorescence along ventral cord dendrites of (A) *sek-1* mutants, (B) s*ek-1 lin-10* double mutants, (C) *sek-1 rpm-1 lin-10* triple mutants, Bar,5μm.

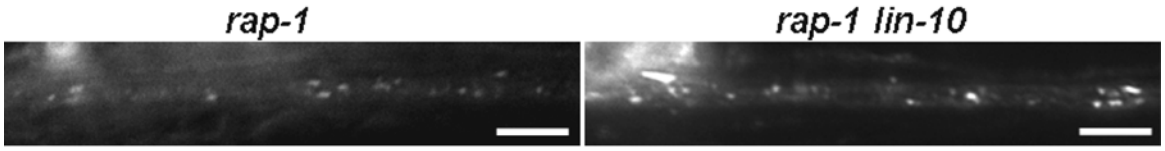

Figure 4-6. *rap-1* mutants suppress GLR-1 localization defects of *lin-10* mutants

Microphotographs of GLR-1::GFP fluorescence along ventral cord dendrites of (A) *rap-1* mutants and (B) *rap-1 lin-10* double mutants, Bar, 5 μm.

TABLES

MAPK pathwway	MAPKK	*mapkk* mutants in combination wih *lin-10* and/or *rpm-1*	GLR-1::GFP phenotypes [a] in mutants
ERK1/2	**MEK-2**	NA	NA
JNK	**MEK-1**	*mek-1*	*
		mek-1;lin-10	***
		mek-1;rpm-1;lin-10	**** ****
	JKK-1	*jkk-1*	*
		jkk-1;lin-10	*
		jkk-1;rpm-1;lin-10	**
p38 MAPK	**SEK-1**	*sek-1*	**
		sek-1;lin-10	*** **
		sek-1;rpm-1;lin-10	**** **** ***
	MKK-4	*mkk-4*	*
		mkk-4;lin-10	***
		mkk-4;rpm-1;lin-10	***

a. symbols used denote GLR-1::GFP puncta phenotype (size)

*	wild type
**	like *rpm-1* mutants (slight increase of size)
***	like *lin-10* mutants
*** **	larger than *lin-10* mutants but smaller than *rpm-1lin-10* double
**** ****	like *rpm-1 lin-10* double
**** **** ***	larger than *rpm-1 lin-10* double

Red symbols indicate the change of GLR-1 localization by MAPKK loss of function mutation

Table 4-1. The effect of MAPKK loss of function mutation alone or in combination with lin-10 single or lin-10 rpm-1 double mutants on GLR-1 localization.

Ras Family Proteins	*C. elegans* orthologs	Mutants with GRL-1::GFP fusion	GLR-1::GFP phenotypes [a] in mutants
Ras	LET-60	*let-60(gf)*	*
		let-60;lin-10	NA
	RAS-1	*ras-1*	*
		ras-1;lin-10	***
	RAS-2	*ras-2*	*
		ras-2;lin-10	***
Rap	RAP-1	*rap-1*	*
		rap-1;lin-10	*
	RAP-2	*rap-2*	*
		rap-2;lin-10	***
	RAP-3	*rap-3*	NA
		rap-3;lin-10	NA

a. symbols used denote GLR-1::GFP puncta phenotype (size)
* wild type
*** like *lin-10* mutants
Red symbols indicate the change of GLR-1 localization by MAPKK loss of function mutation

Table 4-2. The effect of *ras* family genes mutants alone or with *lin-10* mutants on GLR-1 localization.

CHAPTER V

CONCLUSIONS AND FUTURE DIRECTION

By the forward genetic approach with EMS mutagenesis, in which we screened approximately 20,000 haploid genomes, we have identified *rpm-1* as an enhancer mutation of the GLR-1 localization defects of *lin-10* mutants. With the conventional two- and three-point mapping methods and SNPs mapping strategies, we could identify the *rpm-1* mutation efficiently. Previously, LIN-10 was found to be involved in the recycling of GLR-1 from the endosome back to the synapse (Glodowski et al., 2007). Based upon this, we demonstrate that RPM-1, an E3 liagase, regulates GLR-1 trafficking by negatively regulating DLK-1 levels, thereby reduces PMK-3 (p38 MAPK) activity, which is implicated in clathrin-dependent and RAB-5-mediated endocytosis of GLR-1.

As discussed earlier (Chapter III), for the better understanding of the role of the p38 MAPK pathway in the AMPA receptor endocytosis, it is required to determine the targets of p38 MAPK. As EEA-1 is unlikely to be the target of the p38 MAPK for GLR-1 endocytosis (Figure 3-8), other RAB-5 effectors known to be regulated by the p38 MAPK pathway in mammals, such as *rabs-5* (Rabenosyn-5 ortholog) or *gdi-1*(GDI ortholog) gene product could be a target of PMK-3 for promoting GLR-1 endocytosis.

Why does the p38 MAPK cascade require negative regulation by RPM-1? One possibility is that p38 MAPK signaling has to be continually kept in check, with RPM-1 constitutively maintaining low levels of DLK-1 protein. Alternatively, RPM-1 might act as a feedback to shut off p38 MAPK signaling after the initial activation event. A connection between p38 MAPK activity and RPM-1 levels or ubiquitin-ligase activity would support this model. Finally, in a de-repression mechanism, external stimuli might

activate p38 by deactivating RPM-1. To address these questions, we will need a better understanding of both the extrinsic and intrinsic factors that signal via this pathway.

The activation of the PMK-3 pathway by specific extrinsic cues could explain why mutations in *pmk-3* in an otherwise wild-type animal yield little effect on GLR-1 trafficking or GLR-1-mediated behaviors: PMK-3 signaling might only be required under certain circumstances. Indeed, an environment-dependent requirement for p38 MAPK in the brain has been observed in knockout mouse strains reared under different environmental conditions (Flavell et al., 2006). Alternatively, PMK-3 might function redundantly with other pathways; indeed, there are two other p38 MAPK paralogs in the genome (Berman et al., 2001).

The p38 pathway clearly mediates extrinsic signals in the mammalian brain, including ones that induce both metabotropic glutamate receptor (mGluR)-dependent and NMDAR-dependent long-term depression (Bolshakov et al., 2000; Huang et al., 2004; Zhu et al., 2002). In both cases, p38 MAPK is activated by Rap1, which is activated by either $G_{\beta\gamma}$ (triggered by mGluRs) or calcium (from NR2B-containing NMDARs) (Huang et al., 2004; Zhu et al., 2005). The p38 MAPK pathway is also activated by reactive oxygen species (ROS) and helps mediate the oxidative stress response in many different tissues (McCubrey et al., 2006). Activated AMPARs can contribute to excitotoxic neuronal death by excessive calcium influx and ROS production (Kwak and Weiss, 2006; Sattler and Tymianski, 2001). Thus, in addition to the role of p38 MAPK in LTD, it is possible that p38 MAPK is activated by excess ROS, and in turn triggers AMPAR

endocytosis. Such negative feedback could protect neurons from excitotoxicity by minimizing oxidative stress. An exploration of AMPAR trafficking in *C. elegans* under conditions of stress or in different environments should help to fully elucidate p38 MAPK signaling in neurons.

GLR-1 accumulation visualized as patches in ventral cord neurites has been observed in several mutants. In particular, *rpm-1 lin-10* double mutants show especially large patches. Although the reversal frequency tests suggest that the accumulation in the *rpm-1 lin-10* double mutants might not occur on synaptic membranes, it is necessary to provide direct evidence as to whether the GLR-1 patches are on the surface membrane or endosomal compartments of the dendrites. One possible method is to stain the cell surface GLR-1 by microinjecting antibodies which recognize N-terminal domain of GLR-1. Also, it is possible to measure the glutamate gated current to determine the abundance of GLR-1 on synapses. If those methods are not successful in *C. elegans*, using primary neuronal cells from the Phr1 knock mice (Bloom et al., 2007) might be an alternative to address this issue. However, it should be determined whether the similar localization defects of AMPA receptors can be seen in mammalian neurons.

By the reverse genetic approach, we found that *C. elegans* MAPKK orthologs, *mkk-4, jkk-1,* and *sek-1,* and a Rap1 ortholog, *rap-1,* regulate GLR-1 trafficking. It is necessary to examine further to elucidate the interaction and relationship between these MAPK cascade components on GLR-1 trafficking. To accomplish this: First, it is required to observe the GLR-1 phenotype on the remaining mutants of MAPKs, including *mpk-1,*

jnk-1, *kgb-1*, *pmk-1*, and *pmk-2*. Null mutants for *mpk-1*, *jnk-1*, *kgb-1*, and *pmk-1* are viable, whereas *pmk-2* mutants are lethal; therefore, reducing *pmk-2* function in neurons by expressing, via the *glr-1* promoter, a dominant negative version of the kinase, thereby bypassing the problem of *pmk-2* mutant viability (Berman et al., 2001) is one possibility to test. Also it is necessary to examine the known *C. elegans* MAPKKKs, *mlk-1*, *nsy-1*, and *zak-1* by making combinatorial pair-wise mutants with MAPKKs.

APPENDIX I

Mapping and Cloning of a Suppressor Mutation, *od15.*

RESULTS AND DISCUSSION

We have isolated 18 suppressors and 2 enhancer mutations for the GLR-1 localization defects of *lin-10* mutants. As already described, two enhancer mutations are in the *rpm-1* gene. In parallel with *od14* and *od22* mapping, we also decided to map one suppressor mutation, called *od15*. *od15* mutant animals have a dorsal-coiler behavioral phenotype in response to a light head touch with platinum wire or tapping of the culture plate.

od15 is on Chromosome III

Two-factor crosses were conducted with the same set of markers used in *od14* mapping procedures (Figure 2-3). The *od15* mutation segregated from the *lon-1* (LG III) mutation, indicating that *od15* is on chromosome III. This result was further confirmed by SNP mapping using pkP3076 primers (map position -0.83 on LG III). *od15* mutations were separated from the background mutations (*lin-10 nuIs25)* by crossing *lin-10 nuIs25;od15* to *lon-1*. Separated mutants (*od15*) were confirmed by crossing *od15* males with *lin-10 nuIs25;lon-1* to regenerate *lin-10nuIs25;od15* mutants, which were scored by fluorescence compound microscopy. Consistent with our initial observation in the *lin-10* mutants background, *od15* mutants, on their own, showed a dorsal-coiler behavioral phenotype upon plate tapping and light head touch with platinum wire. Notably, *od15* showed egg laying defects (Egl) also. Further mapping and functional studies were conducted by following their phenotypes.

_od15_ reduces the expression of GFP fusion proteins driven by the _glr-1_ promoter

In parallel with mapping and cloning, we did several experiments to get an idea of the function of the *od15* gene product. We observed the GFP fusion proteins of GLR-1, SNB-1, and LIN-10 in *od15* mutants to see whether the *od15* mutation affects the localization of these proteins. *od15* mutants on their own reduced the intensity of GFP fluorescence of GLR-1 fusion proteins in head neuronal cell bodies, ventral nerve dendrites, and PVC neuronal cell bodies (Figure AI-1top panels); however, we could not detect differences in GLR-1::GFP localization patterns other than GFP intensities. Interestingly, GFP intensities of SNB-1 and LIN-10 were also reduced by *od15* mutations, but otherwise their GFP puncta seemed to be localized as in wild type animals (Figure AI-1middle and bottom panels, respectively). All these GFP fusion proteins were expressed by the *glr-1* promoter; therefore, the simplest possible explanation is that the *od15* gene product regulates the expression of GLR-1 transcriptionally.

Two-point Mapping

od15 mutant males were crossed to *dpy-17* (LGIII, -2.17) or *vab-7* (LGIII,+5.54) to make double mutants recombinants. For *od15 vab-7* recombinants, among the singled 29 F2 animals with *od15* mutant phenotypes, 2 animals exhibited *vab-7* phenotypes in their progeny (F3). This result suggests that the *od15* mutation is around 6.9 cM apart from *vab-7*. For *dpy-17od15* recombinants, among the singled 122 F2 animals with the Dpy-17 mutant phenotype, 3 animals exhibited *od15* in their progeny. This result implies that *od15* is around 2.5 cM from *dpy-17*. Taken together, these results suggest that *od15* might reside around 0 map position on chromosome III.

SNP Mapping

Double mutant recombinants for *dpy-17 od15* were crossed to CB4856 (Hawaiian, HA) males to let recombination happen in between the mutations. We obtained 64 recombinants (F2) containing *od15* mutants without the Dpy-17 mutant phenotype. From the next generation, we isolated homozygous recombinants for which the region containing *dpy-17* was replaced by HA, yet retained the *od15* mutation. We obtained the following SNP data:

pkP3076 (-0.83) → 13 (HA) /64

pkP3103 (-0.78) → 8 (HA)/13 (From pkP3076)

uCE3-1010 (-0.74) → 4 (HA)/8(From pkP3103)

snp_ H14A12[1] (-0.73) → 2 (HA)/4(From uCE3-1010)

uCE3-1016 (-0.72) → 0 (HA)/4(From uCE3-1010)

uCE3-1017 (-0.67) → 0 (HA)/4(From uCE3-1010)

uCE3-1019 (-0.66) → 0 (HA)/8(From pkP3103)

pkP3105 (-0.59) → 0 (HA)/13 (From pkP3076)

kP3048 (-0.55) → 0 (HA)/13 (From pkP3076)

pkP3049 (-0.31) → 0 (HA)/13 (From pkP3076)

pkP3050 (-0.20) →0 (HA)/13 (From pkP3076)

Therefore, the left side positional border of *od15* mutation decided by our SNP mapping strategies was -0.73~-0.72 map position on chromosome III.

***od15* Mutants Contain A Mutation in the *egl-5* Gene**

Using nearby gene search functions in the *C. elegans* database (Wormbase), genes on the chromosome from -0.72 map position were scanned. The *egl-5* gene (map position -0.57 on chromosome III) was picked as a candidate because the mutants exhibit exactly the same phenotype with *od15* mutants (Egl, coiler). Using primers for *egl-5* genomic DNA, we identified that an *od15* mutation falls into the first splicing acceptor signal on *egl-5* mRNA. The mutation is at the junction of splicing between the first exon and intron (Figure AI-2). EGL-5 is a homeodomain transcription factor, orthologous to Drosophila Abd-B and the vertebrate Hox9-13 proteins, that is expressed in the posterior of the animal and is necessary for the specification of the HSN cell fate and of cell fates within the tail region (Chisholm, 1991; Ferreira et al., 1999; Salser et al., 1993).

To test whether known *egl-5* mutants also exhibit the same GLR-1 phenotype, we observed GLR-1 phenotypes of both *egl-5(n945)* and *egl-5(n486)*, a nonsense mutation in the third exon and a missense mutation in the fourth exon, respectively (Figure AI-2). To our surprise, both *egl-5*mutants not only did not reduce the GFP intensity of *nuIs25*, but also did not suppress the GLR-1 localization defects of *lin-10* mutants, which are suppressed by *od15* mutations. Also, we did complementation experiments with *od15* and *egl-5* mutations. *egl-5* did not complement the behavioral defects of *od15*, but did complement for the GLR-1 phenotype. These intriguing results could be interpreted in two ways: First, as we couldn't segregate the behavioral defects from the GLR-1 defects in *od15* mutants, based on an assumption that those two phenotypes are derived from separate mutations, *od15* mutants might contain another mutation in a second gene which is near to the *egl-5* gene. Second, alternatively, if the phenotypes are due to the same *od15* molecular lesion, then we might consider that the

od15 mutation is a recessive gain of function for GLR-1 localization. To test the first hypothesis, we might need to try again to segregate the *od15* mutation from *egl-5,* and we need to narrow-down the right side border of *od15* using the GLR-1::GFP phenotype to follow the gene. To test the second hypothesis, we need to do a microinjection experiment of the *glr-1* promoter driving *egl-5* cDNA construct to see whether the phenotype is rescued. We might also need to examine the mRNA transcript for the *egl-5* gene in *od15* mutants by RT-PCR to see whether the mutation generates a different splicing variant of mRNA.

METHODS AND MATERIALS

Standard methods were used to culture *C. elegans*. Animals were grown at 20^{o}C on standard NGM plates seeded with OP50 *E. coli*. Some strains were provided by the *Caenorhabditis* Genetics Center. Methods for PCR, sequencing, microscopic observation, and mapping (SNP mapping, two-factor cross) are described in Chapter II.

Strains

N2, *nuIs25[GLR-1::GFP], lin-10(e1439)nuIs25, dpy-10(e128), lon-1(e185), dpy-20(e1282ts), dpy-11(e224), lon-2(e678), dpy-17(e164), vab-7(e1562), egl-5(n945),egl-5(n486),* and the CB4856 Hawaiian strain.

Primers

SNP Primers On chromosome III for SNP Mapping

List of primers, position (in parenthesis), sequences, and corresponding enzymes (for some SNP sequencing primers were used for identification) are as follows:

pkP3050 (-0.20)	atccgacgagtcaaatgtgg	cttgttttcagacgcttcgc	NsiI
pkP3049 (-0.31)	agcagatgaaagttccgacg	ccccgctgtggttattatac	AccI
pkP3048 (-0.55)	gtaaatttcgggctcccatg	aaaagtgagctcatgctccg	ApoI
pkP3105 (-0.59)	tagccataactgcttccatcc	cgacttccaaagaaattccaag	Sau3A/MboI
pkP3103 (-0.78)	aattccacgagttccatgtctg	gcggtgtatcgtccatttc	BamHI
pkP3076 (-0.83)	cattaggaagtgatgcaagtgg	tggatttgagaggtgtccatag	AvaII
uCE3-1019 (-0.66)	atgctggcacagaagacgtag	gattccattggagcttgtgcc	
	(sequencing primer : tgcgctacttcttctacactg)		
uCE3-1017 (-0.67)	aagtttcaaaccagtgggagg	gcaagagttggagcgttatagt	
	(sequencing primer : actaattgtctctgagcacctg)		
uCE3-1016 (-0.72)	tcgctgaaacgggagcttaac	ctgccccgttcacttcattct	
	(sequencing primer : tcagatcagtggcttcgatac)		
snp_ H14A12[1] (-0.73)	tgcgggagaagagaaaagctg	gaacagtggtgcgcgaaaa	
	(sequencing primer : ccatgccgagtttgatttgc)		
uCE3-1010 (-0.74)	gcgagaaacgccgaatacaatc	gcttcgtcaatgtccctct	
	(sequencing primer : gcgaagtcagaagaagcaagtc)		

Primers to Amplify *egl-5* Genomic DNA

C08C3.1F	ttccggttagccagtcactttg	C08C3.1R	ggagcatcgtttgggagttt

Primers for the sequencing of *egl-5* Genomic DNA

C08C3.1_1S **tctctcttcgactctctccaac : mutation is observed by this primer**

C08C3.1_2S gtgagtccaacttcaaaagtgc

C08C3.1_3S gctctaaaccccatccgaaaac

FIGURES

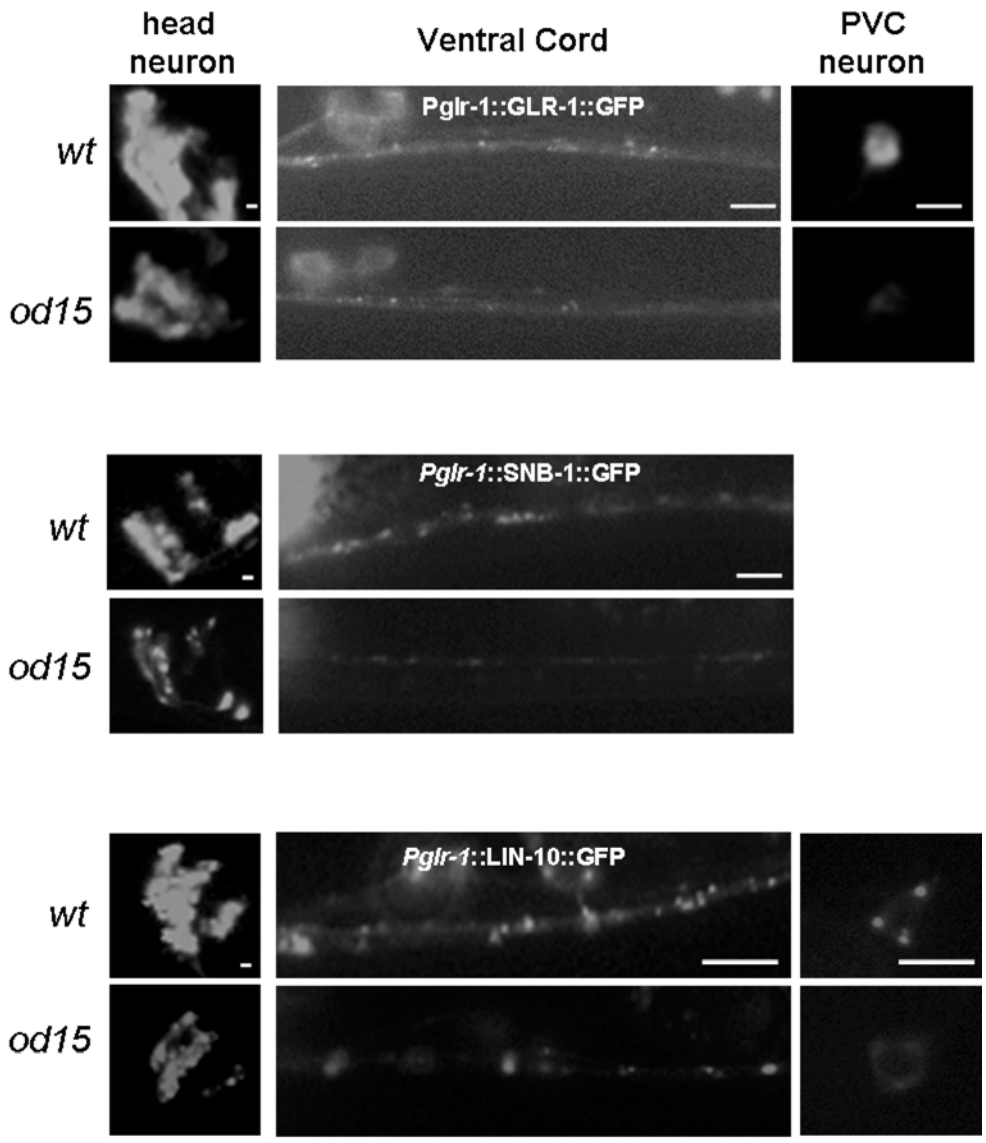

Figure AI-1. Low level expression of the *glr-1* promoter driven GFP fusion proteins in *od15* mutants. GLR-1::GFP (top panels), SNB-1::GFP (middle panels), and LIN-10::GFP(bottom panels) fluorescence were observed along head neuronal cell bodies (left), ventral cord dendrites (middle), and tail PVC neuronal cell body (right). Bar, 5 μm.

5'ATGAACACTTCGACGAGTGCATTCGATTTTGGCTCGTCGACAGCTTCATCAGCTGCCACGT
CGACAACATCTTCACAACCAGATGCCAATGATCATTTATCG**g(→a)t**gagattattaaatttaaaaagtttttg
agcatgcaaatttttatccagtattttatttaaaacattctggatattcaagtttataaaaagtttggcttaacaaaaaaaatgatccttttcta
gtctatggagtagaattcaaaactttcaatttaacttctaaccaacttcatttgagtttcagtcaactgttgctatacatttcttaaatattaaggat
gcatttttcttacgttaggttttcagctagatacctcaagtttataatattcaatcatgcagatatatttaataccttgaagtgagtccaacttcaa
aagtgcacaaaatctagctacaacatgcacctggtttctttcttctttggaatattatgaaacttttagtcggcaaaatttcaaacaacaaaaa
taccttaaatggggagggagatcacgttaaataatattgtttttttaataactcttaatttgc**ag**AGACTTGCCGCCATGACGCA
AGGAGTTGGAAAAGAAGATCCAGAAACATCATCAACTCCATCCACAGAAGCCAGTCTTTACC
CAGGTA**gt**tagtggctcctcccctttccaccgaattctaaccacaccattttc**ag**TCTCGGCTGCGTACATGCAGAGC
TACGGCTGGCCACAGAACTACAACTACTTTGGTCAACCATTGGGCCCTGCCACGTTTCCCG
GAT**(G→A)**GCCTCAGTGCTATCCGAATACGGCGTGGCCCAACTACG**gt**gagttgttcggtcagttacttttc
attattttgtgtgcttaaaactattgaaattaaatattttgaactgaaattcaagcagagatctagtatagaatataattaaattagtctcctaga
aattcatttaaattttctaaataatttttttgttaaaagtcagcttataggattctttttttttaacgttttcaataaattaacgccaccttcacgcctcct
ctcttgccctcgtctgaccctatatgctatcttacgttagatgagtcgagtgtgagttgcgccccgtagaccgtttgatactcagatattcatac
atgatatttttatttttataaaggggtttcacattataaaccgacacaacttattttccctgcaatttctgttaattattagaattcttgagaacttggc
attttccgggggaatttatggtcacttttcgctctaaaccccatccgaaaactcaaaagatatataataacaatacatatgaagatagaga
aatataagtaacttcactaaaatcttcaagtgctcaagaaagtgaatgaagaggtggggataagcactcacagcaagcttctgcaagg
aatgcctagtcaaattttaaaaaaatctcataaataaaaatcaataaattctattaaaccaattatattttatatttc**ag**CATCATCAAA
GAAAGGCCGTCAAACGTATCAACGCTATCAAACATCAGTTCTTGAAGCGAAATTCCAACAGT
CATCATACGTGTCAAAGAAACAACGTGAAGAGCTCCGCCTGCAGACTCAATTGACAGATCGT
CAAATCAAAATCTGGTTCCAAAAT**(C→T)**GTCGAATGAAGGCGAAAAAAGAGAAGCAAAGAGT
AGATGATCACACGGAACATACTCCACTTCTACCGGCAAATCCACCAAAAGGAATGGGAATGG
ATATGGATGATGAGAAAAAATGGCAAATGGCTCATTGGCCACCAGCAGCTGCACACAATCCA
TATCAATACCCGTTGTGTCCACCGTAA3'

Figure AI-2. *od15* mutants contain a mutation in the *egl-5* gene.

The *egl-5* gene sequences. The o*d15* mutation changes the first splicing junctional donor sequence G to A (red color). The *egl-5 (n945)* mutation alters the conceptual translation of EGL-5 protein from tryptophan to an Amber stop codon at amino acid 93 (blue color). The *egl-5(n486)* mutation is a missense mutation that alters arginine to cysteine at amino acid 159 (green color). Shaded capital letters represent exons, small characters represent introns. All three introns in the *egl-5* gene contain the donor (gt) and acceptor (ag) splicing sequences common to *C. elegans* genes.

APPENDIX II

RAB-10 Mediated GLR-1 Trafficking Is Not Mediated

By The p38 MAPK Pathway

INTRODUCTION

Rab proteins, members of small GTPases of the the Ras superfamily, have been studied intensively for the regulation of vesicular cargo protein trafficking pathways, including recycling of endocytic proteins to the target plasma membrane (Zerial and McBride, 2001). In the *C. elegans* intestine, RAB-10 has been identified to function in a recycling pathway from early endosomes to recycling endosomes (Chen et al., 2006). Recently, our lab has characterized the role of RAB-10 in the recycling pathway of GLR-1 (Glodowski et al., 2007): Similar to *lin-10* mutants, loss of function mutant animals for *rab-10* accumulate GLR-1 (Figure AII-1A,C,I) and show a decreased reversal frequency in locomotion, indicating the reduction of synaptic GLR-1 levels. However, unlike *lin-10* mutants, accumulation of GLR-1 in *rab-10* mutants is not suppressed by blocking of the clathrin-dependent endocytosis of GLR-1 with *unc-11* (AP180) or *itsn-1* (Intersectin 1) mutants, but suppressed by impairing clathrin-independent endocytosis by depleting cholesterol from the culture environment. Double mutants for both genes show additive GLR-1 localization defects (Figure AII-1B,C,D,I), suggesting the separate, parallel mechanism of RAB-10 and LIN-10 function in GLR-1 trafficking.

RESULTS AND DISCUSSION

Mutations in *rab-10* are additive to *rpm-1,* and are not suppressed by *pmk-3* mutations for GLR-1 localization defects

To explore whether RAB-10-mediated endocytic recycling of GLR-1 is also regulated by PMK-3 p38 MAPK pathway, which we identified to regulate the clathrin-dependent and the LIN-10-involved endocytosis of GLR-1 (Chapter III), we have examined the effect of *rpm-1* and *pmk-3* mutations on GLR-1 trafficking defects of *rab-10* mutants. We found that *rpm-1 rab-10* double mutants additively increase GLR-1 puncta size (Figure AII-1E,I), Also, *rpm-1 lin-10 rab-10* triple mutants show a huge accumulation of GLR-1, even larger than in *rpm-1 lin-10* double mutants, appearing as one continuous accumulation through the ventral nerve cord (Figure AII-1F,I). These results suggest that *rab-10* functions in parallel with *rpm-1* in GLR-1 trafficking. Because RPM-1 negatively regulates the PMK-3 pathway for GLR-1 localization (Chapter III), we hypothesize that *pmk-3* mutations, which suppress the GLR-1 phenotypes of *lin-10* mutants, might not suppress the GLR-1 accumulation of *rab-10* mutants. Consistent with our hypothesis, we find that *pmk-3* mutations do not affect the GLR-1 localization defects of *rab-10* mutants: the GLR-1 phenotypes of *pmk-3 rab-10* double mutants and *rab-10* single mutants are similar (Figure AII-1C,G,I). In addition, *pmk-3 rab-10 lin-10* triple mutants show a similar accumulation of GLR-1 as *rab-10* single mutants (Figure AII-1C,H,I). Taken together, these results suggest that RAB-10 mediated GLR-1 trafficking is not mediated by the PMK-3 p38 MAPK pathway. Also, conversely, these results show that the regulated trafficking of GLR-1 by PMK-3 pathways is not happening through clathrin-independent endocytosis.

Lipid rafts are microdomains on the plasma membrane that consist of cholesterol, glycosphingolipids, sphingomyelin, and long-chain unsaturated phospholipids. Hydrophobic interactions between sphingomyelin and glycosphingolipids hold lipid rafts

together, and the stability of the rafts is further enhanced by intercalated cholesterol molecules (Brown and London, 1998; Brown and London, 2000). Lipid rafts are abundant in dendrites, where they are associated with postsynaptic proteins, including AMPA receptors(Hering et al., 2003; Wong and Schlichter, 2004). Clathrin-independent internalization of proteins is mostly found in lipid rafts (Nichols, 2003). Although there is evidence in mammals for chlathrin-independent endocytosis of mGluR5, a metabotropic glutamate receptor (Fourgeaud et al., 2003), our understanding of the functional requirements and mechanisms of this unconventional endocytosis is still poor. Therefore, further studies using *C. elegans*, including screening to find gentic modifiers of *rab-10*, will shed light on the enigmatic questions on clathrin-independent endocytosis.

MATERIALS AND METHODS

Standard methods were used to culture *C. elegans*. Animals were grown at 20^{o}C on standard NGM plates seeded with OP50 *E. coli*. The following strains were used: *nuIs25 [GLR-1::GFP], lin-10(e1439)nuIs25, rpm-1(od14), pmk-3(ok169),* and *rab-10(q373).* *lin-10 rab-10 nuIs25* triple, *rab-10 nuIs25* double recombinants (they are all on the same chromosome, I) were generated by Glodowski, D (Rongo Lab). Methods for microscopic observations are described in Chapter II.

FIGURES

Figure AII-1. GLR-1 endocytosis mediated by RAB-10 is not dependent on PMK-3 p38 MAPK pathways. GLR-1::GFP fluorescence was observed along ventral cord dendrites of (A) wild-type animals, (B) *lin-10* mutants, (C) *rab-10* mutants, (D) *rab-10 lin-10* double mutants, (E) *rab-10 rpm-1* double mutants, (F) *rab-10 rpm-1 lin-10* triple mutants, (G) *rab-10 pmk-3* double mutants, or (H) *rab-10 pmk-3 lin-10 triple* mutants. The mean size of fluorescent structures (including puncta and accretions) are plotted for adult nematodes of the given genotype (I). Bar, 10 μm. Error bars are SEM. N=15-20 animals for each genotype. ***P<0.001 by ANOVA followed by Bonferroni's Multiple Comparison to wild-type (open bars, left) or *lin-10* mutants (shaded bars, right).

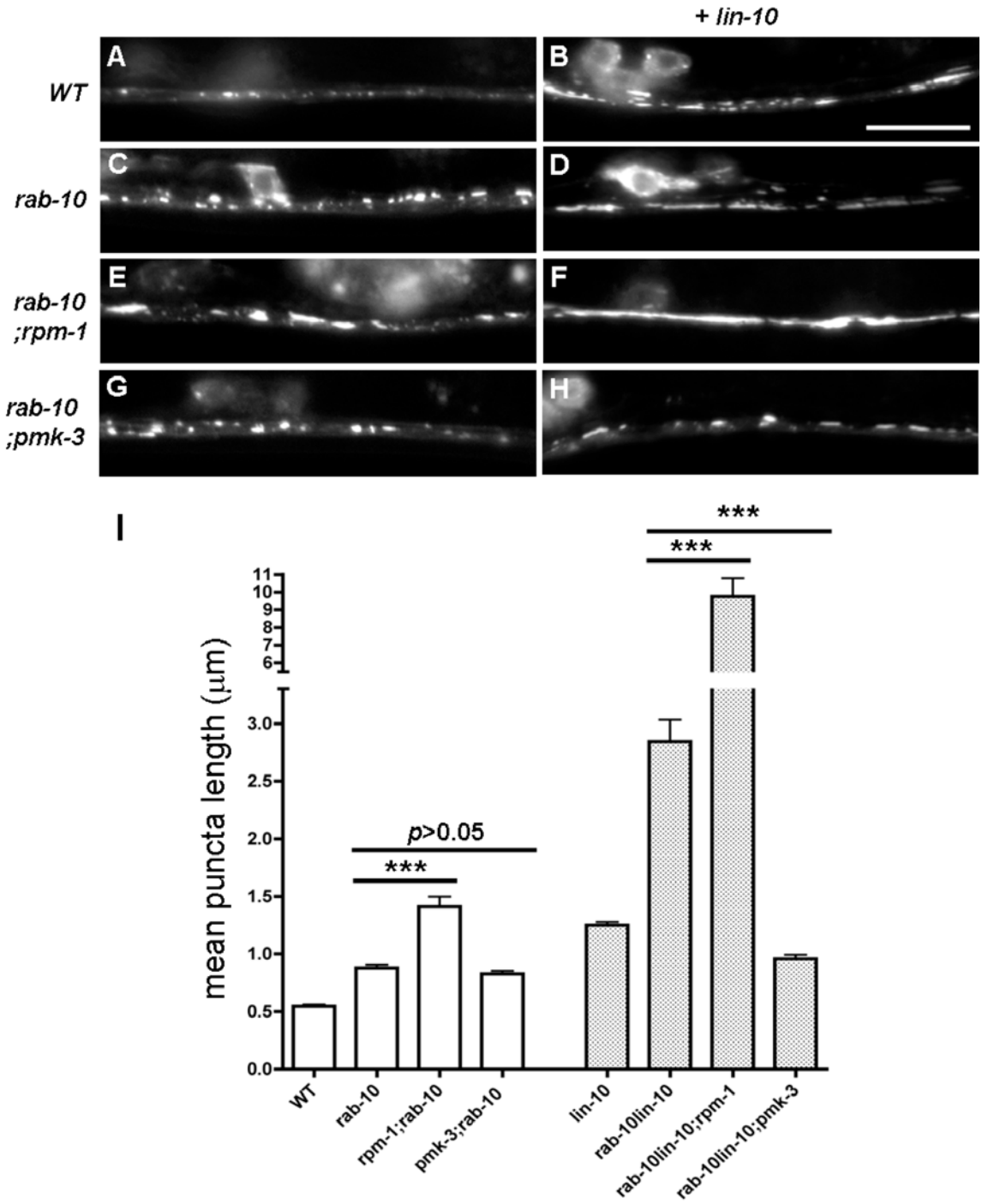
+ lin-10
A
B
WT
C
D
rab-10
E
F
rab-10
;rpm-1
G
H
rab-10
;pmk-3
I
mean puncta length (μm)
p>0.05
***
***
***
WT
rab-10
rpm-1;rab-10
pmk-3;rab-10
lin-10
rab-10lin-10
rab-10lin-10;rpm-1
rab-10lin-10;pmk-3

APPENDIX III

Neurite Overgrowth In MAPK Pathway Mutants

In addition to synaptic defects, the loss of function mutation in *rpm-1* and *fsn-1* cause neurite growth defects (overgrowth), extending the neurites of mechanosensory neurons (ALM and PLM) (Liao et al., 2004; Schaefer et al., 2000). Such neurite overgrowth has also been observed from the loss of function mutants of the RPM-1 homologs, *Drosophila highwire*, mice *phr1*, and zebrafish *esrom* (Bloom et al., 2007; Burgess et al., 2004; Collins et al., 2006; D'Souza et al., 2005; Karlstrom et al., 1996; Wan et al., 2000).

Recently, two different signaling pathways have been implicated in the neurite overgrowth in different species. In *Drosophila*, Highwire targets Wallenda, which encodes a MAPKKK homologous to the vertebrate dual leucine zipper-bearing kinases DLK and LZK, that reside upstream of JNK to regulate the Fos transcription factor (Collins et al., 2006). In contrast, in mice, Phr1 targets DLK, thereby negatively regulating p38 MAPK pathways that function to regulate microtubule stability (Lewcock et al., 2007). We have also observed neurite overgrowth in GLR-1 expressing neuron in several mutants described below.

RESULTS AND DISCUSSION

The Tail Regional Neurites Morphology of GLR-1 Expressing Neuron

In wild type animals, the neurites terminate around 10 to 15 μm away from the PVC neuronal cell bodies (Figure AIII-2, Left Panels). Some GLR-1 expressing neurons in *rpm-1* mutants, presumably AVG and AVA, extend neurites that pass over the region where the PVC neuronal cell bodies reside, and into the tail region (Figure AIII-1).

The p38 MAPK Pathway Positively Regulates Neurite Growth

In Chapter III and IV, we examined mutations of *rpm*-1 and related genes, several of the MAPK pathway molecules, and their putative upstream *ras* family genes for GLR-1 localization. Among the mutants of these genes, we also found that *rpm-1* and *fsn-1* mutants exhibit overgrowth of neurites in the tail region. That is, neurites do not terminate properly and overgrow (as in Figure AIII-2, Right Panels). This is consistent with previous observations in the mechanosensory neurons in terms of neurite overgrowth extending to abnormal positions (Liao et al., 2004; Schaefer et al., 2000). We have also found that overexpression of DLK-1 mimics the *rpm-1* loss- of- function mutation, and the *dlk-1*, *mkk-4*, and *pmk-3* mutation suppress the neurite overgrowth of the *rpm-1* mutation (Table AIII-1), suggesting that p38 MAPK-mediated signaling pathways regulate the neurites overgrowth as observed in Phr1 mutant mice (Lewcock et al., 2007).

The JNK Pathway Negatively Regulates Neurite Growth

Interestingly, we have found that loss of function mutations in *jkk-1* and *rap-2* also show the neurite overgrowth defects seen in *rpm-1*. Loss- of -function mutations in *jkk-1*, and its effector, *jnk-1*, cause the mislocalization of presynaptic vesicle markers in the DD motor neurons (Byrd et al., 2001; Kawasaki et al., 1999b). Rap-2 has been implicated as an upstream component of the of JNK pathway in mammals (Machida et al., 2004; Taira et al., 2004; Zhu et al., 2005). Therefore, these results indicate that the activity of the Rap-2/JNK pathway is critical for guiding neurite growth.

The positive effect of the p38 MAPK pathways and the negative effect of the JNK pathways neurite overgrowth suggest that these pathways genetically antagonize one another for neurite growth. However, based on our previous results that *jkk-1* mutations, like pmk-3 mutations, suppress the GLR-1 localization defects of *lin-10* mutants (in Chapter IV), we suggest that the regulation of the MAPK pathways for AMPA receptor localization and neuronal morphology might be through disparate mechanisms. It will be interesting to follow the neurite growth phenotype in several double or triple mutants as suggested in Chapter V for the further study of MAPK pathways to understand whether the MAPK signaling components act in concert to regulate neurite growth.

FIGURES

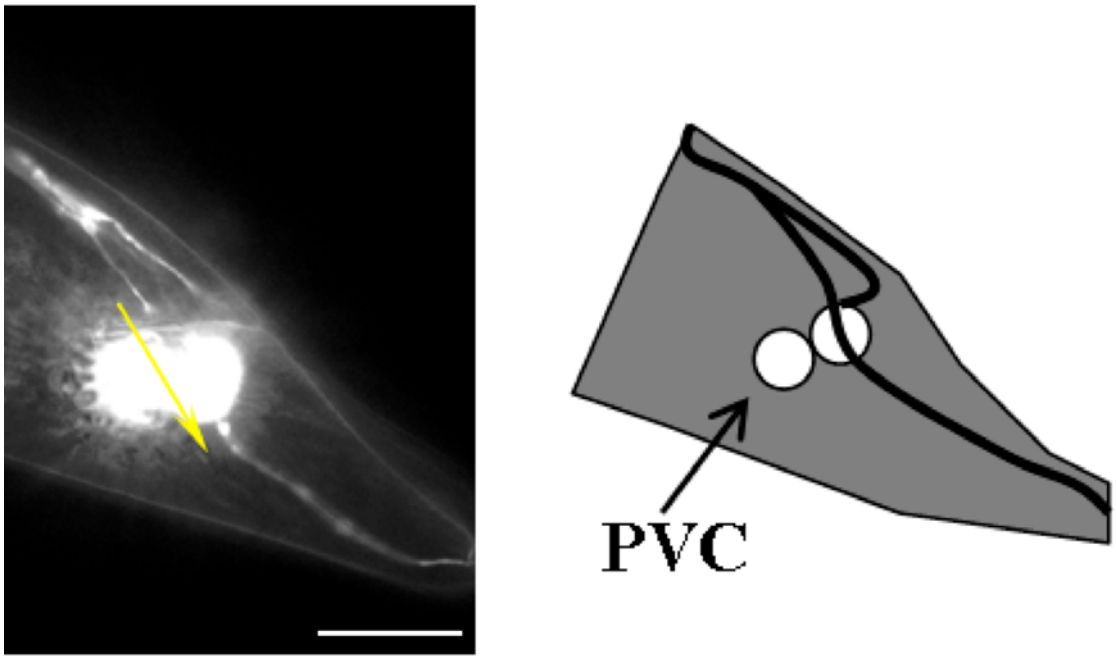

Figure AIII-1. Phenotype of the tail regional neurites that extend over PVC neuronal cell bodies toward tail. *Left panel*, fluorescence photomicrograph (63X objective) of the GLR-1::GFP-expressing neurites that passing (yellow arrow) the PVC neuronal cell bodies at tail region. *Right*, the recapitulating drawing. Bar, 10 μm.

Figure AIII-2. Phenotypes of the tail regional neurite observed in wild-type and the defective mutants. Fluorescence photomicrograph (63X objective) of the GLR-1::GFP-expressing neurites in the wild-type animals (Left Panels) and the defective mutants (Right Panels). Arrows denote the end point of the neurites and an arrow head on the top right panel indicates abnormal morphology of the neurites, a node like structure, that sometimes appear in the mutants animals. Bars, 10μm.

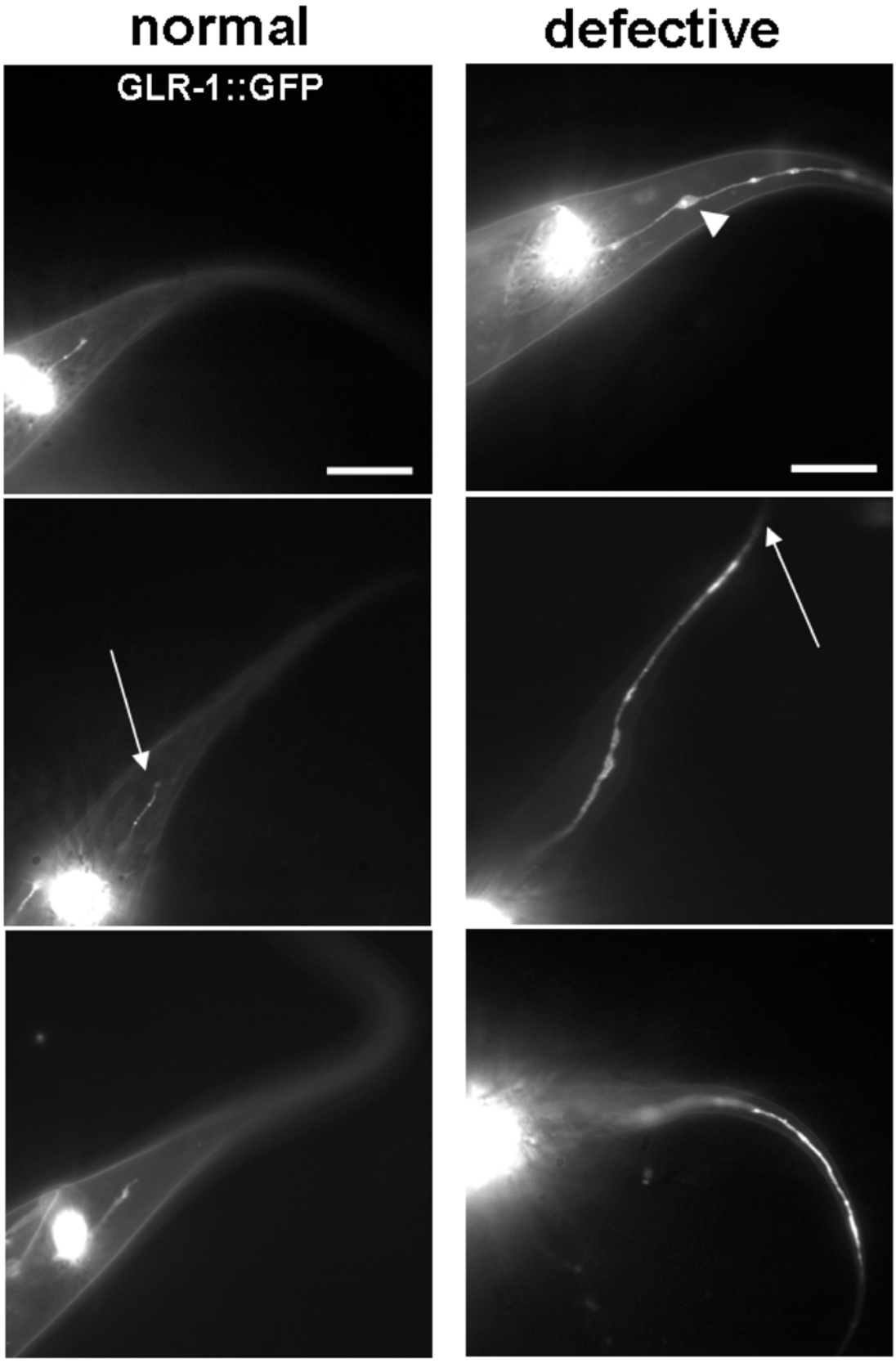
normal
defective
GLR-1::GFP

TABLE

mutants with the tail regional neurites overgrowth	GLR-1 phenotypes of the mutants	Suppressors of the neurites overgrowth defects
rpm-1	slightly accumulate of their own and enhance the GLR-1 defects of *lin-10* mutants	*dlk-1, mkk-4, pmk-3*
fsn-1		NA
overexpression of P_{glr-1}*:: dlk-1*		*pmk-3*
jkk-1	normal of its own suppress the GLR-1 defects of *lin-10* mutants	NA
rap-2	normal	NA

Table AIII-1. Mutations that regulate the neurites growth.

REFERENCES

Abraham, W. C., and Tate, W. P. (1997). Metaplasticity: a new vista across the field of synaptic plasticity. Prog Neurobiol *52*, 303-323.

Alberi, S., Boda, B., Steiner, P., Nikonenko, I., Hirling, H., and Muller, D. (2005). The endosomal protein NEEP21 regulates AMPA receptor-mediated synaptic transmission and plasticity in the hippocampus. Mol Cell Neurosci *29*, 313-319.

Baran, R., Aronoff, R., and Garriga, G. (1999). The C. elegans homeodomain gene unc-42 regulates chemosensory and glutamate receptor expression. Development *126*, 2241-2251.

Barbieri, M. A., Li, G., Colombo, M. I., and Stahl, P. D. (1994). Rab5, an early acting endosomal GTPase, supports in vitro endosome fusion without GTP hydrolysis. J Biol Chem *269*, 18720-18722.

Barria, A., Derkach, V., and Soderling, T. (1997). Identification of the Ca2+/calmodulin-dependent protein kinase II regulatory phosphorylation site in the alpha-amino-3-hydroxyl-5-methyl-4-isoxazole-propionate-type glutamate receptor. J Biol Chem *272*, 32727-32730.

Beattie, E. C., Carroll, R. C., Yu, X., Morishita, W., Yasuda, H., von Zastrow, M., and Malenka, R. C. (2000). Regulation of AMPA receptor endocytosis by a signaling mechanism shared with LTD. Nat Neurosci *3*, 1291-1300.

Berger, A. J., Hart, A. C., and Kaplan, J. M. (1998). G alphas-induced neurodegeneration in Caenorhabditis elegans. J Neurosci *18*, 2871-2880.

Berman, K., McKay, J., Avery, L., and Cobb, M. (2001). Isolation and characterization of pmk-(1-3): three p38 homologs in Caenorhabditis elegans. Mol Cell Biol Res Commun *4*, 337-344.

Bingol, B., and Schuman, E. M. (2004). A proteasome-sensitive connection between PSD-95 and GluR1 endocytosis. Neuropharmacology *47*, 755-763.

Bloom, A. J., Miller, B. R., Sanes, J. R., and DiAntonio, A. (2007). The requirement for Phr1 in CNS axon tract formation reveals the corticostriatal boundary as a choice point for cortical axons. Genes Dev *21*, 2593-2606.

Bolshakov, V. Y., Carboni, L., Cobb, M. H., Siegelbaum, S. A., and Belardetti, F. (2000). Dual MAP kinase pathways mediate opposing forms of long-term plasticity at CA3-CA1 synapses. Nat Neurosci *3*, 1107-1112.

Borg, J. P., Straight, S. W., Kaech, S. M., de Taddeo-Borg, M., Kroon, D. E., Karnak, D., Turner, R. S., Kim, S. K., and Margolis, B. (1998). Identification of an evolutionarily conserved heterotrimeric protein complex involved in protein targeting. J Biol Chem *273*, 31633-31636.

Bredt, D. S., and Nicoll, R. A. (2003). AMPA receptor trafficking at excitatory synapses. Neuron *40*, 361-379.

Brockie, P. J., Madsen, D. M., Zheng, Y., Mellem, J., and Maricq, A. V. (2001). Differential expression of glutamate receptor subunits in the nervous system of Caenorhabditis elegans and their regulation by the homeodomain protein UNC-42. J Neurosci *21*, 1510-1522.

Brown, D. A., and London, E. (1998). Functions of lipid rafts in biological membranes. Annu Rev Cell Dev Biol *14*, 111-136.

Brown, D. A., and London, E. (2000). Structure and function of sphingolipid- and cholesterol-rich membrane rafts. J Biol Chem *275*, 17221-17224.

Brown, T. C., Tran, I. C., Backos, D. S., and Esteban, J. A. (2005). NMDA receptor-dependent activation of the small GTPase Rab5 drives the removal of synaptic AMPA receptors during hippocampal LTD. Neuron *45*, 81-94.

Bucci, C., Parton, R. G., Mather, I. H., Stunnenberg, H., Simons, K., Hoflack, B., and Zerial, M. (1992). The small GTPase rab5 functions as a regulatory factor in the early endocytic pathway. Cell *70*, 715-728.

Burbea, M., Dreier, L., Dittman, J. S., Grunwald, M. E., and Kaplan, J. M. (2002). Ubiquitin and AP180 regulate the abundance of GLR-1 glutamate receptors at postsynaptic elements in C. elegans. Neuron *35*, 107-120.

Burgess, R. W., Peterson, K. A., Johnson, M. J., Roix, J. J., Welsh, I. C., and O'Brien, T. P. (2004). Evidence for a conserved function in synapse formation reveals Phr1 as a candidate gene for respiratory failure in newborn mice. Mol Cell Biol *24*, 1096-1105.

Butz, S., Okamoto, M., and Sudhof, T. C. (1998). A tripartite protein complex with the potential to couple synaptic vesicle exocytosis to cell adhesion in brain. Cell *94*, 773-782.

Byrd, D. T., Kawasaki, M., Walcoff, M., Hisamoto, N., Matsumoto, K., and Jin, Y. (2001). UNC-16, a JNK-signaling scaffold protein, regulates vesicle transport in C. elegans. Neuron *32*, 787-800.

Campbell, R. E., Tour, O., Palmer, A. E., Steinbach, P. A., Baird, G. S., Zacharias, D. A., and Tsien, R. Y. (2002). A monomeric red fluorescent protein. Proc Natl Acad Sci U S A *99*, 7877-7882.

Carvalho, A. L., Kameyama, K., and Huganir, R. L. (1999). Characterization of phosphorylation sites on the glutamate receptor 4 subunit of the AMPA receptors. J Neurosci *19*, 4748-4754.

Cavalli, V., Vilbois, F., Corti, M., Marcote, M. J., Tamura, K., Karin, M., Arkinstall, S., and Gruenberg, J. (2001). The stress-induced MAP kinase p38 regulates endocytic trafficking via the GDI:Rab5 complex. Mol Cell *7*, 421-432.

Chalfie, M., Sulston, J. E., White, J. G., Southgate, E., Thomson, J. N., and Brenner, S. (1985). The neural circuit for touch sensitivity in Caenorhabditis elegans. J Neurosci *5*, 956-964.

Chang, H. C., and Rongo, C. (2005). Cytosolic tail sequences and subunit interactions are critical for synaptic localization of glutamate receptors. J Cell Sci *118*, 1945-1956.

Chen, C. C., Schweinsberg, P. J., Vashist, S., Mareiniss, D. P., Lambie, E. J., and Grant, B. D. (2006). RAB-10 is required for endocytic recycling in the Caenorhabditis elegans intestine. Mol Biol Cell *17*, 1286-1297.

Chisholm, A. (1991). Control of cell fate in the tail region of C. elegans by the gene egl-5. Development *111*, 921-932.

Chung, H. J., Xia, J., Scannevin, R. H., Zhang, X., and Huganir, R. L. (2000). Phosphorylation of the AMPA receptor subunit GluR2 differentially regulates its interaction with PDZ domain-containing proteins. J Neurosci *20*, 7258-7267.

Coleman, S. K., Cai, C., Mottershead, D. G., Haapalahti, J. P., and Keinanen, K. (2003). Surface expression of GluR-D AMPA receptor is dependent on an interaction between its C-terminal domain and a 4.1 protein. J Neurosci *23*, 798-806.

Colledge, M., Snyder, E. M., Crozier, R. A., Soderling, J. A., Jin, Y., Langeberg, L. K., Lu, H., Bear, M. F., and Scott, J. D. (2003). Ubiquitination regulates PSD-95 degradation and AMPA receptor surface expression. Neuron *40*, 595-607.

Collins, C. A., Wairkar, Y. P., Johnson, S. L., and DiAntonio, A. (2006). Highwire restrains synaptic growth by attenuating a MAP kinase signal. Neuron *51*, 57-69.

D'Souza, J., Hendricks, M., Le Guyader, S., Subburaju, S., Grunewald, B., Scholich, K., and Jesuthasan, S. (2005). Formation of the retinotectal projection requires Esrom, an ortholog of PAM (protein associated with Myc). Development *132*, 247-256.

Dev, K. K., Nishimune, A., Henley, J. M., and Nakanishi, S. (1999). The protein kinase C alpha binding protein PICK1 interacts with short but not long form alternative splice variants of AMPA receptor subunits. Neuropharmacology *38*, 635-644.

DiAntonio, A., and Hicke, L. (2004). Ubiquitin-dependent regulation of the synapse. Annu Rev Neurosci *27*, 223-246.

Dingledine, R., Borges, K., Bowie, D., and Traynelis, S. F. (1999). The glutamate receptor ion channels. Pharmacol Rev *51*, 7-61.

Dreier, L., Burbea, M., and Kaplan, J. M. (2005). LIN-23-mediated degradation of beta-catenin regulates the abundance of GLR-1 glutamate receptors in the ventral nerve cord of C. elegans. Neuron *46*, 51-64.

Ehlers, M. D. (2000a). Reinsertion or degradation of AMPA receptors determined by activity- dependent endocytic sorting. Neuron *28*, 511-525.

Ehlers, M. D. (2000b). Reinsertion or degradation of AMPA receptors determined by activity-dependent endocytic sorting. Neuron *28*, 511-525.

Esteban, J. A., Shi, S. H., Wilson, C., Nuriya, M., Huganir, R. L., and Malinow, R. (2003). PKA phosphorylation of AMPA receptor subunits controls synaptic trafficking underlying plasticity. Nat Neurosci *6*, 136-143.

Ferreira, H. B., Zhang, Y., Zhao, C., and Emmons, S. W. (1999). Patterning of Caenorhabditis elegans posterior structures by the Abdominal-B homolog, egl-5. Dev Biol *207*, 215-228.

Flavell, S. W., Cowan, C. W., Kim, T. K., Greer, P. L., Lin, Y., Paradis, S., Griffith, E. C., Hu, L. S., Chen, C., and Greenberg, M. E. (2006). Activity-dependent regulation of MEF2 transcription factors suppresses excitatory synapse number. Science *311*, 1008-1012.

Fourgeaud, L., Bessis, A. S., Rossignol, F., Pin, J. P., Olivo-Marin, J. C., and Hemar, A. (2003). The metabotropic glutamate receptor mGluR5 is endocytosed by a clathrin-independent pathway. J Biol Chem *278*, 12222-12230.

Gallagher, S. M., Daly, C. A., Bear, M. F., and Huber, K. M. (2004). Extracellular signal-regulated protein kinase activation is required for metabotropic glutamate receptor-dependent long-term depression in hippocampal area CA1. J Neurosci *24*, 4859-4864.

Gerges, N. Z., Backos, D. S., and Esteban, J. A. (2004). Local control of AMPA receptor trafficking at the postsynaptic terminal by a small GTPase of the Rab family. J Biol Chem *279*, 43870-43878.

Gerges, N. Z., Brown, T. C., Correia, S. S., and Esteban, J. A. (2005). Analysis of Rab protein function in neurotransmitter receptor trafficking at hippocampal synapses. Methods Enzymol *403*, 153-166.

Glickman, M. H., and Ciechanover, A. (2002). The ubiquitin-proteasome proteolytic pathway: destruction for the sake of construction. Physiol Rev *82*, 373-428.

Glodowski, D. R., Chen, C. C., Schaefer, H., Grant, B. D., and Rongo, C. (2007). RAB-10 Regulates Glutamate Receptor Recycling in a Cholesterol-dependent Endocytosis Pathway. Mol Biol Cell.

Glodowski, D. R., Wright, T., Martinowich, K., Chang, H. C., Beach, D., and Rongo, C. (2005). Distinct LIN-10 domains are required for its neuronal function, its epithelial function, and its synaptic localization. Mol Biol Cell *16*, 1417-1426.

Greger, I. H., Khatri, L., and Ziff, E. B. (2002). RNA editing at arg607 controls AMPA receptor exit from the endoplasmic reticulum. Neuron *34*, 759-772.

Grill, B., Bienvenut, W. V., Brown, H. M., Ackley, B. D., Quadroni, M., and Jin, Y. (2007). C. elegans RPM-1 regulates axon termination and synaptogenesis through the Rab GEF GLO-4 and the Rab GTPase GLO-1. Neuron *55*, 587-601.

Grunwald, M. E., and Kaplan, J. M. (2003). Mutations in the ligand-binding and pore domains control exit of glutamate receptors from the endoplasmic reticulum in C. elegans. Neuropharmacology *45*, 768-776.

Grunwald, M. E., Mellem, J. E., Strutz, N., Maricq, A. V., and Kaplan, J. M. (2004). Clathrin-mediated endocytosis is required for compensatory regulation of GLR-1 glutamate receptors after activity blockade. Proc Natl Acad Sci U S A *101*, 3190-3195.

Gu, Y., and Stornetta, R. L. (2007). Synaptic plasticity, AMPA-R trafficking, and Ras-MAPK signaling. Acta Pharmacol Sin *28*, 928-936.

Guo, Q., Xie, J., Dang, C. V., Liu, E. T., and Bishop, J. M. (1998). Identification of a large Myc-binding protein that contains RCC1-like repeats. Proc Natl Acad Sci U S A *95*, 9172-9177.

Haddad, J. J. (2005). N-methyl-D-aspartate (NMDA) and the regulation of mitogen-activated protein kinase (MAPK) signaling pathways: a revolving neurochemical axis for therapeutic intervention? Prog Neurobiol *77*, 252-282.

Han, M., Golden, A., Han, Y., and Sternberg, P. W. (1993). C. elegans lin-45 raf gene participates in let-60 ras-stimulated vulval differentiation. Nature *363*, 133-140.

Hanley, J. G., and Henley, J. M. (2005). PICK1 is a calcium-sensor for NMDA-induced AMPA receptor trafficking. Embo J *24*, 3266-3278.

Hart, A. C., Sims, S., and Kaplan, J. M. (1995). Synaptic code for sensory modalities revealed by C. elegans GLR-1 glutamate receptor. Nature *378*, 82-85.

Hayashi, Y., Shi, S. H., Esteban, J. A., Piccini, A., Poncer, J. C., and Malinow, R. (2000). Driving AMPA receptors into synapses by LTP and CaMKII: requirement for GluR1 and PDZ domain interaction. Science *287*, 2262-2267.

Hering, H., Lin, C. C., and Sheng, M. (2003). Lipid rafts in the maintenance of synapses, dendritic spines, and surface AMPA receptor stability. J Neurosci *23*, 3262-3271.

Hicke, L., and Dunn, R. (2003). Regulation of membrane protein transport by ubiquitin and ubiquitin-binding proteins. Annu Rev Cell Dev Biol *19*, 141-172.

Hodgkin, J., Papp, A., Pulak, R., Ambros, V., and Anderson, P. (1989). A new kind of informational suppression in the nematode Caenorhabditis elegans. Genetics *123*, 301-313.

Hoege, C., Pfander, B., Moldovan, G. L., Pyrowolakis, G., and Jentsch, S. (2002). RAD6-dependent DNA repair is linked to modification of PCNA by ubiquitin and SUMO. Nature *419*, 135-141.

Horiuchi, H., Giner, A., Hoflack, B., and Zerial, M. (1995). A GDP/GTP exchange-stimulatory activity for the Rab5-RabGDI complex on clathrin-coated vesicles from bovine brain. J Biol Chem *270*, 11257-11262.

Huang, C. C., You, J. L., Wu, M. Y., and Hsu, K. S. (2004). Rap1-induced p38 mitogen-activated protein kinase activation facilitates AMPA receptor trafficking via the GDI.Rab5 complex. Potential role in (S)-3,5-dihydroxyphenylglycene-induced long term depression. J Biol Chem *279*, 12286-12292.

Huang, L., Kinnucan, E., Wang, G., Beaudenon, S., Howley, P. M., Huibregtse, J. M., and Pavletich, N. P. (1999). Structure of an E6AP-UbcH7 complex: insights into ubiquitination by the E2-E3 enzyme cascade. Science *286*, 1321-1326.

Huibregtse, J. M., Scheffner, M., Beaudenon, S., and Howley, P. M. (1995). A family of proteins structurally and functionally related to the E6-AP ubiquitin-protein ligase. Proc Natl Acad Sci U S A *92*, 2563-2567.

Isaac, J. T., Nicoll, R. A., and Malenka, R. C. (1995). Evidence for silent synapses: implications for the expression of LTP. Neuron *15*, 427-434.

Joazeiro, C. A., and Weissman, A. M. (2000). RING finger proteins: mediators of ubiquitin ligase activity. Cell *102*, 549-552.

Juo, P., and Kaplan, J. M. (2004). The anaphase-promoting complex regulates the abundance of GLR-1 glutamate receptors in the ventral nerve cord of C. elegans. Curr Biol *14*, 2057-2062.

Kaech, S. M., Whitfield, C. W., and Kim, S. K. (1998). The LIN-2/LIN-7/LIN-10 complex mediates basolateral membrane localization of the C. elegans EGF receptor LET-23 in vulval epithelial cells. Cell *94*, 761-771.

Karlstrom, R. O., Trowe, T., Klostermann, S., Baier, H., Brand, M., Crawford, A. D., Grunewald, B., Haffter, P., Hoffmann, H., Meyer, S. U., *et al.* (1996). Zebrafish mutations affecting retinotectal axon pathfinding. Development *123*, 427-438.

Kawasaki, H., Fujii, H., Gotoh, Y., Morooka, T., Shimohama, S., Nishida, E., and Hirano, T. (1999a). Requirement for mitogen-activated protein kinase in cerebellar long term depression. J Biol Chem *274*, 13498-13502.

Kawasaki, M., Hisamoto, N., Iino, Y., Yamamoto, M., Ninomiya-Tsuji, J., and Matsumoto, K. (1999b). A Caenorhabditis elegans JNK signal transduction pathway regulates coordinated movement via type-D GABAergic motor neurons. Embo J *18*, 3604-3615.

Kennedy, M. J., and Ehlers, M. D. (2006). Organelles and Trafficking Machinery for Postsynaptic Plasticity. Annu Rev Neurosci.

Kim, C. H., Chung, H. J., Lee, H. K., and Huganir, R. L. (2001). Interaction of the AMPA receptor subunit GluR2/3 with PDZ domains regulates hippocampal long-term depression. Proc Natl Acad Sci U S A *98*, 11725-11730.

Kim, D. H., Feinbaum, R., Alloing, G., Emerson, F. E., Garsin, D. A., Inoue, H., Tanaka-Hino, M., Hisamoto, N., Matsumoto, K., Tan, M. W., and Ausubel, F. M. (2002). A conserved p38 MAP kinase pathway in Caenorhabditis elegans innate immunity. Science *297*, 623-626.

Kim, D. H., Liberati, N. T., Mizuno, T., Inoue, H., Hisamoto, N., Matsumoto, K., and Ausubel, F. M. (2004). Integration of Caenorhabditis elegans MAPK pathways mediating immunity and stress resistance by MEK-1 MAPK kinase and VHP-1 MAPK phosphatase. Proc Natl Acad Sci U S A *101*, 10990-10994.

Kim, M. J., Dunah, A. W., Wang, Y. T., and Sheng, M. (2005). Differential roles of NR2A- and NR2B-containing NMDA receptors in Ras-ERK signaling and AMPA receptor trafficking. Neuron *46*, 745-760.

Kim, S., Ko, J., Shin, H., Lee, J. R., Lim, C., Han, J. H., Altrock, W. D., Garner, C. C., Gundelfinger, E. D., Premont, R. T., *et al.* (2003). The GIT family of proteins forms

multimers and associates with the presynaptic cytomatrix protein Piccolo. J Biol Chem *278*, 6291-6300.

Kimble, J., Hodgkin, J., Smith, T., and Smith, J. (1982). Suppression of an amber mutation by microinjection of suppressor tRNA in C. elegans. Nature *299*, 456-458.

Ko, J., Kim, S., Valtschanoff, J. G., Shin, H., Lee, J. R., Sheng, M., Premont, R. T., Weinberg, R. J., and Kim, E. (2003). Interaction between liprin-alpha and GIT1 is required for AMPA receptor targeting. J Neurosci *23*, 1667-1677.

Koga, M., Zwaal, R., Guan, K. L., Avery, L., and Ohshima, Y. (2000). A Caenorhabditis elegans MAP kinase kinase, MEK-1, is involved in stress responses. Embo J *19*, 5148-5156.

Kondo, K., Hodgkin, J., and Waterston, R. H. (1988). Differential expression of five tRNA(UAGTrp) amber suppressors in Caenorhabditis elegans. Mol Cell Biol *8*, 3627-3635.

Kondo, K., Makovec, B., Waterston, R. H., and Hodgkin, J. (1990). Genetic and molecular analysis of eight tRNA(Trp) amber suppressors in Caenorhabditis elegans. J Mol Biol *215*, 7-19.

Kwak, S., and Weiss, J. H. (2006). Calcium-permeable AMPA channels in neurodegenerative disease and ischemia. Curr Opin Neurobiol *16*, 281-287.

Kyriakis, J. M., and Avruch, J. (2001). Mammalian mitogen-activated protein kinase signal transduction pathways activated by stress and inflammation. Physiol Rev *81*, 807-869.

Lackner, M. R., and Kim, S. K. (1998). Genetic analysis of the Caenorhabditis elegans MAP kinase gene mpk-1. Genetics *150*, 103-117.

Lackner, M. R., Kornfeld, K., Miller, L. M., Horvitz, H. R., and Kim, S. K. (1994). A MAP kinase homolog, mpk-1, is involved in ras-mediated induction of vulval cell fates in Caenorhabditis elegans. Genes Dev *8*, 160-173.

Lee, H. K., Barbarosie, M., Kameyama, K., Bear, M. F., and Huganir, R. L. (2000). Regulation of distinct AMPA receptor phosphorylation sites during bidirectional synaptic plasticity. Nature *405*, 955-959.

Lee, S. H., Liu, L., Wang, Y. T., and Sheng, M. (2002). Clathrin adaptor AP2 and NSF interact with overlapping sites of GluR2 and play distinct roles in AMPA receptor trafficking and hippocampal LTD. Neuron *36*, 661-674.

Lewcock, J. W., Genoud, N., Lettieri, K., and Pfaff, S. L. (2007). The Ubiquitin Ligase Phr1 Regulates Axon Outgrowth through Modulation of Microtubule Dynamics. Neuron *56*, 604-620.

Li, L., Linning, R. M., Kondo, K., and Honda, B. M. (1998). Differential expression of individual suppressor tRNA(Trp) gene gene family members in vitro and in vivo in the nematode Caenorhabditis elegans. Mol Cell Biol *18*, 703-709.

Li, S., Tian, X., Hartley, D. M., and Feig, L. A. (2006a). Distinct roles for Ras-guanine nucleotide-releasing factor 1 (Ras-GRF1) and Ras-GRF2 in the induction of long-term potentiation and long-term depression. J Neurosci *26*, 1721-1729.

Li, S., Tian, X., Hartley, D. M., and Feig, L. A. (2006b). The environment versus genetics in controlling the contribution of MAP kinases to synaptic plasticity. Curr Biol *16*, 2303-2313.

Liao, D., Hessler, N. A., and Malinow, R. (1995). Activation of postsynaptically silent synapses during pairing-induced LTP in CA1 region of hippocampal slice. Nature *375*, 400-404.

Liao, E. H., Hung, W., Abrams, B., and Zhen, M. (2004). An SCF-like ubiquitin ligase complex that controls presynaptic differentiation. Nature *430*, 345-350.

Lin, J. W., Ju, W., Foster, K., Lee, S. H., Ahmadian, G., Wyszynski, M., Wang, Y. T., and Sheng, M. (2000). Distinct molecular mechanisms and divergent endocytotic pathways of AMPA receptor internalization. Nat Neurosci *3*, 1282-1290.

Lu, J., Helton, T. D., Blanpied, T. A., Racz, B., Newpher, T. M., Weinberg, R. J., and Ehlers, M. D. (2007). Postsynaptic positioning of endocytic zones and AMPA receptor cycling by physical coupling of dynamin-3 to homer. Neuron *55*, 874-889.

Mace, G., Miaczynska, M., Zerial, M., and Nebreda, A. R. (2005). Phosphorylation of EEA1 by p38 MAP kinase regulates mu opioid receptor endocytosis. Embo J *24*, 3235-3246.

Machida, N., Umikawa, M., Takei, K., Sakima, N., Myagmar, B. E., Taira, K., Uezato, H., Ogawa, Y., and Kariya, K. (2004). Mitogen-activated protein kinase kinase kinase kinase 4 as a putative effector of Rap2 to activate the c-Jun N-terminal kinase. J Biol Chem *279*, 15711-15714.

Malenka, R. C., and Bear, M. F. (2004). LTP and LTD: an embarrassment of riches. Neuron *44*, 5-21.

Malinow, R., and Malenka, R. C. (2002). AMPA receptor trafficking and synaptic plasticity. Annu Rev Neurosci *25*, 103-126.

Mammen, A. L., Kameyama, K., Roche, K. W., and Huganir, R. L. (1997). Phosphorylation of the alpha-amino-3-hydroxy-5-methylisoxazole4-propionic acid receptor GluR1 subunit by calcium/calmodulin-dependent kinase II. J Biol Chem *272*, 32528-32533.

Man, H. Y., Sekine-Aizawa, Y., and Huganir, R. L. (2007). Regulation of {alpha}-amino-3-hydroxy-5-methyl-4-isoxazolepropionic acid receptor trafficking through PKA phosphorylation of the Glu receptor 1 subunit. Proc Natl Acad Sci U S A *104*, 3579-3584.

Maricq, A. V., Peckol, E., Driscoll, M., and Bargmann, C. I. (1995). Mechanosensory signalling in *C. elegans* mediated by the GLR-1 glutamate receptor. Nature *378*, 78-81.

Matsuda, S., Mikawa, S., and Hirai, H. (1999). Phosphorylation of serine-880 in GluR2 by protein kinase C prevents its C terminus from binding with glutamate receptor-interacting protein. J Neurochem *73*, 1765-1768.

McCabe, B. D., Hom, S., Aberle, H., Fetter, R. D., Marques, G., Haerry, T. E., Wan, H., O'Connor, M. B., Goodman, C. S., and Haghighi, A. P. (2004). Highwire regulates presynaptic BMP signaling essential for synaptic growth. Neuron *41*, 891-905.

McCubrey, J. A., Lahair, M. M., and Franklin, R. A. (2006). Reactive oxygen species-induced activation of the MAP kinase signaling pathways. Antioxid Redox Signal *8*, 1775-1789.

Mellem, J. E., Brockie, P. J., Zheng, Y., Madsen, D. M., and Maricq, A. V. (2002). Decoding of polymodal sensory stimuli by postsynaptic glutamate receptors in C. elegans. Neuron *36*, 933-944.

Mitrovich, Q. M., and Anderson, P. (2000). Unproductively spliced ribosomal protein mRNAs are natural targets of mRNA surveillance in C. elegans. Genes Dev *14*, 2173-2184.

Mizuno, T., Hisamoto, N., Terada, T., Kondo, T., Adachi, M., Nishida, E., Kim, D. H., Ausubel, F. M., and Matsumoto, K. (2004). The Caenorhabditis elegans MAPK phosphatase VHP-1 mediates a novel JNK-like signaling pathway in stress response. Embo J *23*, 2226-2234.

Moser, E. I., Krobert, K. A., Moser, M. B., and Morris, R. G. (1998). Impaired spatial learning after saturation of long-term potentiation. Science *281*, 2038-2042.

Muratani, M., and Tansey, W. P. (2003). How the ubiquitin-proteasome system controls transcription. Nat Rev Mol Cell Biol *4*, 192-201.

Murthy, V., Han, S., Beauchamp, R. L., Smith, N., Haddad, L. A., Ito, N., and Ramesh, V. (2004). Pam and its ortholog highwire interact with and may negatively regulate the TSC1.TSC2 complex. J Biol Chem *279*, 1351-1358.

Nakata, K., Abrams, B., Grill, B., Goncharov, A., Huang, X., Chisholm, A. D., and Jin, Y. (2005). Regulation of a DLK-1 and p38 MAP kinase pathway by the ubiquitin ligase RPM-1 is required for presynaptic development. Cell *120*, 407-420.

Nichols, B. J. (2003). GM1-containing lipid rafts are depleted within clathrin-coated pits. Curr Biol *13*, 686-690.

Nonet, M. L., Holgado, A. M., Brewer, F., Serpe, C. J., Norbeck, B. A., Holleran, J., Wei, L., Hartwieg, E., Jorgensen, E. M., and Alfonso, A. (1999). UNC-11, a Caenorhabditis elegans AP180 homologue, regulates the size and protein composition of synaptic vesicles. Mol Biol Cell *10*, 2343-2360.

Osten, P., Srivastava, S., Inman, G. J., Vilim, F. S., Khatri, L., Lee, L. M., States, B. A., Einheber, S., Milner, T. A., Hanson, P. I., and Ziff, E. B. (1998). The AMPA receptor GluR2 C terminus can mediate a reversible, ATP-dependent interaction with NSF and alpha- and beta-SNAPs. Neuron *21*, 99-110.

Palmer, C. L., Lim, W., Hastie, P. G., Toward, M., Korolchuk, V. I., Burbidge, S. A., Banting, G., Collingridge, G. L., Isaac, J. T., and Henley, J. M. (2005). Hippocalcin functions as a calcium sensor in hippocampal LTD. Neuron *47*, 487-494.

Park, M., Penick, E. C., Edwards, J. G., Kauer, J. A., and Ehlers, M. D. (2004). Recycling endosomes supply AMPA receptors for LTP. Science *305*, 1972-1975.

Passafaro, M., Piech, V., and Sheng, M. (2001). Subunit-specific temporal and spatial patterns of AMPA receptor exocytosis in hippocampal neurons. Nat Neurosci *4*, 917-926.

Patrick, G. N., Bingol, B., Weld, H. A., and Schuman, E. M. (2003). Ubiquitin-mediated proteasome activity is required for agonist-induced endocytosis of GluRs. Curr Biol *13*, 2073-2081.

Pellis-van Berkel, W., Verheijen, M. H., Cuppen, E., Asahina, M., de Rooij, J., Jansen, G., Plasterk, R. H., Bos, J. L., and Zwartkruis, F. J. (2005). Requirement of the Caenorhabditis elegans RapGEF pxf-1 and rap-1 for epithelial integrity. Mol Biol Cell *16*, 106-116.

Perez-Otano, I., and Ehlers, M. D. (2005). Homeostatic plasticity and NMDA receptor trafficking. Trends Neurosci *28*, 229-238.

Perez, J. L., Khatri, L., Chang, C., Srivastava, S., Osten, P., and Ziff, E. B. (2001). PICK1 targets activated protein kinase Calpha to AMPA receptor clusters in spines of hippocampal neurons and reduces surface levels of the AMPA-type glutamate receptor subunit 2. J Neurosci *21*, 5417-5428.

Pfaffl, M. W. (2001). A new mathematical model for relative quantification in real-time RT-PCR. Nucleic Acids Res *29*, e45.

Pickart, C. M. (2001). Mechanisms underlying ubiquitination. Annu Rev Biochem *70*, 503-533.

Qin, Y., Zhu, Y., Baumgart, J. P., Stornetta, R. L., Seidenman, K., Mack, V., van Aelst, L., and Zhu, J. J. (2005). State-dependent Ras signaling and AMPA receptor trafficking. Genes Dev *19*, 2000-2015.

Roche, K. W., O'Brien, R. J., Mammen, A. L., Bernhardt, J., and Huganir, R. L. (1996). Characterization of multiple phosphorylation sites on the AMPA receptor GluR1 subunit. Neuron *16*, 1179-1188.

Rongo, C., and Kaplan, J. M. (1999). CaMKII regulates the density of central glutamatergic synapses in vivo. Nature *402*, 195-199.

Rongo, C., Whitfield, C. W., Rodal, A., Kim, S. K., and Kaplan, J. M. (1998). LIN-10 is a shared component of the polarized protein localization pathways in neurons and epithelia. Cell *94*, 751-759.

Rumbaugh, G., Adams, J. P., Kim, J. H., and Huganir, R. L. (2006). SynGAP regulates synaptic strength and mitogen-activated protein kinases in cultured neurons. Proc Natl Acad Sci U S A *103*, 4344-4351.

Rush, A. M., Wu, J., Rowan, M. J., and Anwyl, R. (2002). Group I metabotropic glutamate receptor (mGluR)-dependent long-term depression mediated via p38 mitogen-activated protein kinase is inhibited by previous high-frequency stimulation and activation of mGluRs and protein kinase C in the rat dentate gyrus in vitro. J Neurosci *22*, 6121-6128.

Salser, S. J., Loer, C. M., and Kenyon, C. (1993). Multiple HOM-C gene interactions specify cell fates in the nematode central nervous system. Genes Dev *7*, 1714-1724.

Sattler, R., and Tymianski, M. (2001). Molecular mechanisms of glutamate receptor-mediated excitotoxic neuronal cell death. Mol Neurobiol *24*, 107-129.

Schaefer, A. M., Hadwiger, G. D., and Nonet, M. L. (2000). rpm-1, a conserved neuronal gene that regulates targeting and synaptogenesis in C. elegans. Neuron *26*, 345-356.

Schaefer, H., and Rongo, C. (2006). KEL-8 is a substrate receptor for CUL3-dependent ubiquitin ligase that regulates synaptic glutamate receptor turnover. Mol Biol Cell *17*, 1250-1260.

Schnell, J. D., and Hicke, L. (2003). Non-traditional functions of ubiquitin and ubiquitin-binding proteins. J Biol Chem *278*, 35857-35860.

Setou, M., Seog, D. H., Tanaka, Y., Kanai, Y., Takei, Y., Kawagishi, M., and Hirokawa, N. (2002). Glutamate-receptor-interacting protein GRIP1 directly steers kinesin to dendrites. Nature *417*, 83-87.

Shen, L., Liang, F., Walensky, L. D., and Huganir, R. L. (2000). Regulation of AMPA receptor GluR1 subunit surface expression by a 4. 1N-linked actin cytoskeletal association. J Neurosci *20*, 7932-7940.

Shepherd, J. D., Rumbaugh, G., Wu, J., Chowdhury, S., Plath, N., Kuhl, D., Huganir, R. L., and Worley, P. F. (2006). Arc/Arg3.1 mediates homeostatic synaptic scaling of AMPA receptors. Neuron *52*, 475-484.

Shi, S., Hayashi, Y., Esteban, J. A., and Malinow, R. (2001). Subunit-specific rules governing AMPA receptor trafficking to synapses in hippocampal pyramidal neurons. Cell *105*, 331-343.

Shim, J., Umemura, T., Nothstein, E., and Rongo, C. (2004). The unfolded protein response regulates glutamate receptor export from the endoplasmic reticulum. Mol Biol Cell *15*, 4818-4828.

Shin, H., Wyszynski, M., Huh, K. H., Valtschanoff, J. G., Lee, J. R., Ko, J., Streuli, M., Weinberg, R. J., Sheng, M., and Kim, E. (2003). Association of the kinesin motor KIF1A with the multimodular protein liprin-alpha. J Biol Chem *278*, 11393-11401.

Simske, J. S., Kaech, S. M., Harp, S. A., and Kim, S. K. (1996). LET-23 receptor localization by the cell junction protein LIN-7 during C. elegans vulval induction. Cell *85*, 195-204.

Song, I., and Huganir, R. L. (2002). Regulation of AMPA receptors during synaptic plasticity. Trends Neurosci *25*, 578-588.

Song, I., Kamboj, S., Xia, J., Dong, H., Liao, D., and Huganir, R. L. (1998). Interaction of the N-ethylmaleimide-sensitive factor with AMPA receptors. Neuron *21*, 393-400.

Steiner, P., Alberi, S., Kulangara, K., Yersin, A., Sarria, J. C., Regulier, E., Kasas, S., Dietler, G., Muller, D., Catsicas, S., and Hirling, H. (2005). Interactions between NEEP21, GRIP1 and GluR2 regulate sorting and recycling of the glutamate receptor subunit GluR2. Embo J *24*, 2873-2884.

Steiner, P., Sarria, J. C., Glauser, L., Magnin, S., Catsicas, S., and Hirling, H. (2002). Modulation of receptor cycling by neuron-enriched endosomal protein of 21 kD. J Cell Biol *157*, 1197-1209.

Sternberg, P. W., Golden, A., and Han, M. (1993). Role of a raf proto-oncogene during Caenorhabditis elegans vulval development. Philos Trans R Soc Lond B Biol Sci *340*, 259-265.

Szewczyk, N. J., Peterson, B. K., and Jacobson, L. A. (2002). Activation of Ras and the mitogen-activated protein kinase pathway promotes protein degradation in muscle cells of Caenorhabditis elegans. Mol Cell Biol *22*, 4181-4188.

Taira, K., Umikawa, M., Takei, K., Myagmar, B. E., Shinzato, M., Machida, N., Uezato, H., Nonaka, S., and Kariya, K. (2004). The Traf2- and Nck-interacting kinase as a putative effector of Rap2 to regulate actin cytoskeleton. J Biol Chem *279*, 49488-49496.

Tanaka-Hino, M., Sagasti, A., Hisamoto, N., Kawasaki, M., Nakano, S., Ninomiya-Tsuji, J., Bargmann, C. I., and Matsumoto, K. (2002). SEK-1 MAPKK mediates Ca2+ signaling to determine neuronal asymmetric development in Caenorhabditis elegans. EMBO Rep *3*, 56-62.

Thomas, G. M., and Huganir, R. L. (2004). MAPK cascade signalling and synaptic plasticity. Nat Rev Neurosci *5*, 173-183.

Turrigiano, G. G., Leslie, K. R., Desai, N. S., Rutherford, L. C., and Nelson, S. B. (1998). Activity-dependent scaling of quantal amplitude in neocortical neurons. Nature *391*, 892-896.

Turrigiano, G. G., and Nelson, S. B. (2004). Homeostatic plasticity in the developing nervous system. Nat Rev Neurosci *5*, 97-107.

Ullrich, O., Reinsch, S., Urbe, S., Zerial, M., and Parton, R. G. (1996). Rab11 regulates recycling through the pericentriolar recycling endosome. J Cell Biol *135*, 913-924.

Updike, D. L., and Mango, S. E. (2007). Genetic Suppressors of Caenorhabditis elegans pha-4/FoxA Identify the Predicted AAA Helicase ruvb-1/RuvB. Genetics *177*, 819-833.

van Delft, S., Schumacher, C., Hage, W., Verkleij, A. J., and van Bergen en Henegouwen, P. M. (1997). Association and colocalization of Eps15 with adaptor protein-2 and clathrin. J Cell Biol *136*, 811-821.

Villanueva, A., Lozano, J., Morales, A., Lin, X., Deng, X., Hengartner, M. O., and Kolesnick, R. N. (2001). jkk-1 and mek-1 regulate body movement coordination and response to heavy metals through jnk-1 in Caenorhabditis elegans. Embo J *20*, 5114-5128.

Wan, H. I., DiAntonio, A., Fetter, R. D., Bergstrom, K., Strauss, R., and Goodman, C. S. (2000). Highwire regulates synaptic growth in Drosophila. Neuron *26*, 313-329.

Wenthold, R. J., Petralia, R. S., Blahos, J., II, and Niedzielski, A. S. (1996). Evidence for multiple AMPA receptor complexes in hippocampal CA1/CA2 neurons. J Neurosci *16*, 1982-1989.

White JG, Southgate E, Thomson JN, Brenner S (1986). The structure of the nervous system of the nematode *Caenorhabditis elegans*. Philos Trans R Soc Lond [Biol] 314:1-340.

Whitfield, C. W., Benard, C., Barnes, T., Hekimi, S., and Kim, S. K. (1999). Basolateral localization of the *Caenorhabditis elegans* epidermal growth factor receptor in epithelial cells by the PDZ protein LIN-10. Mol Biol Cell *10*, 2087-2100.

Wicks, S. R., Yeh, R. T., Gish, W. R., Waterston, R. H., and Plasterk, R. H. (2001). Rapid gene mapping in Caenorhabditis elegans using a high density polymorphism map. Nat Genet *28*, 160-164.

Wierenga, C. J., Ibata, K., and Turrigiano, G. G. (2005). Postsynaptic expression of homeostatic plasticity at neocortical synapses. J Neurosci *25*, 2895-2905.

Wong, W., and Schlichter, L. C. (2004). Differential recruitment of Kv1.4 and Kv4.2 to lipid rafts by PSD-95. J Biol Chem *279*, 444-452.

Wu, Y., Han, M., and Guan, K. L. (1995). MEK-2, a Caenorhabditis elegans MAP kinase kinase, functions in Ras-mediated vulval induction and other developmental events. Genes Dev *9*, 742-755.

Wyszynski, M., Kim, E., Dunah, A. W., Passafaro, M., Valtschanoff, J. G., Serra-Pages, C., Streuli, M., Weinberg, R. J., and Sheng, M. (2002). Interaction between GRIP and liprin-alpha/SYD2 is required for AMPA receptor targeting. Neuron *34*, 39-52.

Xia, J., Zhang, X., Staudinger, J., and Huganir, R. L. (1999). Clustering of AMPA receptors by the synaptic PDZ domain-containing protein PICK1. Neuron *22*, 179-187.

Zerial, M., and McBride, H. (2001). Rab proteins as membrane organizers. Nat Rev Mol Cell Biol *2*, 107-117.

Zheng, Y., Brockie, P. J., Mellem, J. E., Madsen, D. M., and Maricq, A. V. (1999a). Neuronal control of locomotion in C. elegans is modified by a dominant mutation in the GLR-1 ionotropic glutamate receptor. Neuron *24*, 347-361.

Zheng, Y., Brockie, P. J., Mellem, J. E., Madsen, D. M., and Maricq, A. V. (1999b). Neuronal control of locomotion in C. elegans is modified by a dominant mutation in the GLR-1 ionotropic glutamate receptor. Neuron *24*, 347-361.

Zheng, Y., Mellem, J. E., Brockie, P. J., Madsen, D. M., and Maricq, A. V. (2004). SOL-1 is a CUB-domain protein required for GLR-1 glutamate receptor function in C. elegans. Nature *427*, 451-457.

Zhu, J. J., Esteban, J. A., Hayashi, Y., and Malinow, R. (2000). Postnatal synaptic potentiation: delivery of GluR4-containing AMPA receptors by spontaneous activity. Nat Neurosci *3*, 1098-1106.

Zhu, J. J., Qin, Y., Zhao, M., Van Aelst, L., and Malinow, R. (2002). Ras and Rap control AMPA receptor trafficking during synaptic plasticity. Cell *110*, 443-455.

Zhu, Y., Pak, D., Qin, Y., McCormack, S. G., Kim, M. J., Baumgart, J. P., Velamoor, V., Auberson, Y. P., Osten, P., van Aelst, L., *et al.* (2005). Rap2-JNK removes synaptic AMPA receptors during depotentiation. Neuron *46*, 905-916.

Zwang, Y., and Yarden, Y. (2006). p38 MAP kinase mediates stress-induced internalization of EGFR: implications for cancer chemotherapy. Embo J *25*, 4195-4206.

CURRICULUM VITAE

EUNCHAN PARK

EDUCATION

01. 2008 Ph.D. Graduate Program in Neuroscience, Rutgers/UMDNJ
02. 1997 M.S. Neuropharmacology, Ajou University School of Medicine, Suwon, South Korea
Thesis title : Modulation of Neuronal Apoptosis and Necrosis by Nerve Growth Factor (NGF) in Rat Striatal Cell Cultures
02. 1995 B.S. Biochemistry, Yonsei University , Seoul, South Korea

EXPERIENCES/ HONORS

06.2007- 01.2008 New Jersey Commission on Spinal Cord Research Fellow
07.2006- 06.2007 Charles and Johanna Busch Predoctoral Fellow
09.2003- 06.2006 Graduate Assistant, Waksman Institute, Rutgers University
02.2001- 08.2002 Manager of Research & Development Team
Neurotech Pharmaceuticals Co. Ltd.
10.1997- 01.2001 First Lieutenant, The Republic of Korea Air Force
02.1997- 10.1997 Research Scientist, Dept. of Pharmacol. Ajou Univ. Sch. of Med.
03.1995- 02.1997 Teaching Assistant, Dept. of Pharmacol. Ajou Univ. Sch. of Med.
03.1995- 02.1997 Full scholarship graduate student, Ajou Univ. Sch. of Med.

PUBLICATIONS

1. Won SJ, Park EC, Ryu BR, Ko HW, Sohn S, Kwon HJ, and Gwag BJ. NT-4/5 Exace -rbates Free Radical-Induced Neuronal Necrosis in vitro and in vivo. Neurobiology of Disease 7(4):251-9, 2000.
2. Won SJ, Ko HW, Kim EY, Park EC, Huh K, Jung NP, Choi I, Oh YK, Shin HC and B. J. Gwag. Nuclear factor kappa B-mediated kainate neurotoxicity in the rat and hamster hippocampus. Neuroscience 94:83-91, 1999.
3. Park EC, Jou I and Gwag BJ. Nerve growth factor potentiates the oxidative necrosis of striatal cholinergic neurons. Neuroreport, 9(4): 687-690, 1998.
4. Park EC, Jou Ilo, Joe EH, Sohn SH, and Gwag BJ. Attenuation and potentiation of ne -uronal deaths by nerve growth factor in rat striatal cell cultures. Korean Experimental Neurobiology 5: 67-73, 1996.

PATENT

Gwag, Byoung-Joo; Yoon, Sung-Hwa; Moon, Ho-Sang; Park, Eun-Chan; Won, Seok-Joon; Lee, Young-Ae; and Lee, Hae-Un. Tetrafluorobenzyl Derivatives And Pharmaceutical Composition For Preventing And Treating Acute And Chronic Neurodegenerative Diseases In Central Nervous System Containing The Same. Aug. 9th, 2005. USPTO, Cl. 560-136. PCT Pub. No. WO04/000786, PCT Pub. Date Dec. 31, 2003.